(1)

National Defence / Défense nationale

DESIGN OF A BOUNDED WAVE EMP SIMULATOR
(Intended as second stage simulator for DREO)

by

P.A.A. Sevat

DEFENCE RESEARCH ESTABLISHMENT OTTAWA
REPORT NO. 1003

Canada

June 1989
Ottawa

National Defence / Défense nationale

DESIGN OF A BOUNDED WAVE EMP SIMULATOR (Intended as second stage simulator for DREO)

by

P.A.A. Sevat
Nuclear Effects Section
Electronics Division

DEFENCE RESEARCH ESTABLISHMENT OTTAWA
REPORT NO. 1006

PCN
041LT

June 1989
Ottawa

ABSTRACT

This report is concerned with the design of a bounded wave Electromagnetic Pulse (EMP) simulator. Different types of simulators are described and their pros and cons are discussed. A detailed design is given for a wire grid parallel plate type simulator. The fields inside the simulator as well as the radiated fields around the simulator are also computed.

RÉSUMÉ

Ce rapport traite de la conception d'un simulateur d'impulsions électro-magnétiques (IEM) de type à onde guidée. Différents types de simulateurs sont revus, ainsi que leurs avantages et leurs inconvénients. Les plans détaillés d'un simulateur de type à grille parallèle y sont décris. Les champs électro-magnétiques à l'intérieur et à l'extérieur du simulateur sont aussi calculés.

EXECUTIVE SUMMARY

Electromagnetic Pulse (EMP) simulators are used to simulate the EMP generated by a nuclear weapon and to harden equipment against the effects of EMP.

At present, DREO has a 1 m EMP simulator for testing computer terminal size equipment. In order to develop the R&D capability for testing larger objects such as a helicopter, a much bigger threat level facility is required.

This report concerns the design of a bounded wave EMP simulator suitable for testing large size equipment. Different types of simulators are described and their pros and cons are discussed. A bounded wave parallel plate type simulator is chosen for it's efficiency and the least environmental impact.

Detailed designs are given for 6 m and 10 m parallel plate type wire grid simulators. Electromagnetics fields inside and outside the simulators are computed. Preliminary specifications for a pulse generator required for the simulator are also given. Finally, the electromagnetic fields radiated from the simulator are computed and discussed.

TABLE OF CONTENTS

DESIGN OF A BOUNDED WAVE EMP SIMULATOR

Intended as second stage simulator for DREO

1.0 INTRODUCTION

The Phase I simulator in the EMP Project of Defence Research Establishment Ottawa, started in October 1987, is installed and is now being tested. It is a small laboratory simulator (height 1 metre), installed in building 39 and intended for experiments which are expected to continue through FY 89/90.

In Phase II a larger EMP simulator with a larger test volume is needed. This second stage simulator, intended as a R&D tool for EMP Protection Studies, will be built in the field behind building 39. Some of the components of the Phase I simulator will be used for the second stage simulator, such as the shielded room, the sensors and the data acquisition and processing instruments. New equipment will include the criterion level pulse generator, the transmission line with its support structure and a fibre-optic data transmission system. If possible the 100 kV pulser from the small simulator will also be used for low level survey studies until the larger pulser is available.

Previous DREO proposals for a second stage simulator specified a 6 m bounded-wave simulator. This height is sufficient to accept vehicle-sized systems. Larger bounded-wave simulators were considered too expensive.

Free-field simulators are expected to have unacceptable radiation for the proposed site. Therefore a choice has to be made among the different types of bounded-wave simulators. The dimensions should be limited to an acceptable size and the shape adapted to the available site.

In this report the general rules for designing a bounded-wave simulator are given, with two examples, one with a height of 6m and another with a

height of 10m, respectively called a 6m and 10m line. The calculations of the expected radiation are given in Appendix A.

The work has been performed as a part of the Consulting Service Contract mentioned in the agreement attached to letter DREO 3743A-GE (ED) of 9 May 1988.

2.0 SIMULATOR REQUIREMENTS

As starting point for the design the following restrictions are made:

- Only the exo-atmospheric EMP has to be simulated.
- The time history of this pulse should be as described in appropriate NATO documents.
- The working volume should have a length of about 20m, a maximum width of 20m and a height not more than 10m.
- If possible the dimensions of the working volume should be flexible.
- The maximum field strength should be 50-65 kV/m.
- The radiation should be as low as possible.

3.0 SELECTION OF SIMULATOR TYPE

Since the available site does not permit a high radiation level the bounded-wave (or transmission line) EMP simulator is the most suitable type for this purpose. An advantage is that this type of simulator can also be used for endo-atmospheric EMP simulation, perhaps important in a later stage.

It should be kept in mind that it is impossible to completely duplicate the EMP threat fields by simulation. Each type of simulator has its limitations. For the bounded-wave simulator they are:

- vertical polarization and horizontal propagation
- no ground interactions (a limitation for ground-based systems, an advantage for air born systems)
- potential interaction of simulator and object under test
- limited working volume

Special features are the high threat level at relatively low cost and the proper wave impedance. EMP simulation with horizontal polarization has been left out of consideration here, because of the high cost.

A selection can be made among the following types of bounded-wave simulators, see fig. 1:

- parallel plate simulator (PPS)
- conical plate simulator (CPS)
- triangular plate simulator (TPS)
- rhombic wire simulator (RWS)

3.1 Parallel Plate Simulator

This type of simulator operates by guiding an electromagnetic wave across a test object situated between two metallic surfaces of a transmission line, operating in the transverse electromagnetic (TEM) propagation mode. That

is a traveling wave with a vertical electric field and a horizontal magnetic field. The transmission line is driven at one end by a generator and loaded at the other end by a termination. The generator and termination are connected to the horizontal transmission line section by transition sections (tapers). The characteristic impedance of the transmission line is determined by the width-to-height ratio, a/h, and can be made constant from generator to termination by tapering the transitions. When the transmission line is correctly terminated, $R = Z_o$, all energy delivered by the generator should be dissipated by the terminating resistor R. Without reflections there will be only traveling waves and no standing waves.

However the TEM mode, launched in the input taper, experiences reflections before reaching the termination. At the junction of the tapers with the horizontal section, energy is converted to other propagating modes. Moreover, for frequencies higher than the frequency at which plate spacing h is a half wavelength, it is possible to maintain higher order modes in the transmission line. In the literature deep notches in the frequency spectrum of the field in the working volume are reported (2 to 9).

3.2 Conical Plate Simulator

To prevent reflections caused by local deviations of Z_o at the junctions of the horizontal section of the PPS and to avoid radiation generated in this section the idea was born to eliminate this horizontal part of the simulator and to use the input taper as working volume. The question is then how to prevent reflections at the end of the input taper. The second step was to eliminate the output taper as well and to leave the end of the generator taper open. The wave launched by the generator in the taper should then be radiated in free space. In this case the taper behaves like a horn antenna. Since the dimensions of the horn antenna are too small for radiating low frequencies, some kind of termination is needed at the end. This type of simulator is called conical plate simulator (CPS).

3.3 Triangular Plate Simulator

In the TPS only the horizontal parallel plate section of the PPS is eliminated. The input taper is directly connected to the output taper in the middle of the simulator. It is obvious that the discontinuity between the tapers is larger than in the PPS, with larger reflections as result.

3.4 Rhombic Wire Simulator

Since a major part of the current is concentrated near the edges of the plates King and others replaced the tapers of the TPS by a wire or tube at the two edges of the tapers, thus forming a rhombic antenna above the ground (4 to 7). This structure is mainly used for R&D purposes since the radiated electromagnetic fields of such antennae can accurately be determined. With this model the analysis of phenomena can be used for other EMP simulators.

3.5 Examination of the Pros and Cons

Let us go back to the PPS. The reflections, standing wave ratios (SWR's) and notches reported in the literature were calculated and measured with continuous wave (CW) excitation (2,3). CW excitation, however, is different from a single shot, pulse excitation. With CW excitation the discontinuities experienced by the traveling waves cause reflections and since the excitation is continuous, standing waves are formed. The SWR is dependent on the mismatch.

With a single pulse excitation no standing waves will exist and there is no SWR. Radiation of the resonant structure, existing with CW exitation at frequencies related to the simulator height h, causing notches inside the waveguide, cannot build up large magnitudes with a single pulse excitation.

For pulse excitation the time-space concept can better be used for describing the electromagnetic properties of EMP Simulators (See fig. 2). The clear-time, defined as the time from the initial observation of the wave to

the time of arrival of the first interference wave (reflection) at the point of observation, is a more useful parameter. It may be that at frequencies where notches are observed with CW excitation, some energy will be radiated with pulse excitation, however the guided wave travelling between the parallel plates will not be influenced by that. The reflections at the discontinuities of the PPS can be reduced by designing relatively long tapers (low elevating angle) and by "smoothing" the angle of the junctions.

A small elevation angle has more advantages. One of them is that the wave front launched in the taper is less spherical, causing less distortion of the field orientation near the top plate of the horizontal section. The spherical wave in the transistion section tries to transform into a plane wave in the working volume to establish the TEM propagating wave in the horizontal wave guide. For that reason it is recommendable to design a minimum length of this section equal to 3h. With a good design the reflections at the terminating resistor of the PPS can be made very small as has been shown in the past (10).

The advantages claimed for the CPS are:

- no reflections
- no typical radiation frequencies
- no distortion of the field orientation

Since the horn antenna is not ideally matched to the impedance of free space ($Z_o = 120\pi\ \Omega$) - the low frequencies cannot be radiated and have to be terminated - and even when this large terminating network is made very sparce will be seen by the launched wavefront - reflections will exist. These reflections arrive in the working volume with a delay related to the clear time. For frequencies with wavelength comparable to the height of the large terminating network, resonances exist with consequent resonant radiation. This can be reduced by decreasing the inductance of the network (11). Disadvantages of the CPS compared to the PPS are the larger radiation and the geometrical 1/R attenuation of the launched wave amplitude with distance from the generator.

Comparing the characteristics of the PPS and CPS it can be concluded that the PPS is the best choice as second stage EMP simulator for DREO.

4.0 THREAT ENVIRONMENT (17)

A commonly accepted worst-case model for the exo-atmospheric EMP is:

$$E(t) = E_o \left(e^{-\alpha t} - e^{-\beta t}\right) \qquad (1)$$

with:

$$E_o = 5.3 \cdot 10^4 \text{ V/m}$$

$$\alpha = 3.7 \cdot 10^6 \text{ s}^{-1}$$

$$\beta = 3.9 \cdot 10^8 \text{ s}^{-1}$$

The spectrum of (1) can be calculated with:

$$E(\omega) = E_o \left(\frac{1}{\alpha + j\omega} - \frac{1}{\beta + j\omega} \right) \qquad (2)$$

With $\omega = 0$ the constant spectral amplitude at low frequencies and with $\omega = \alpha$ and $\omega = \beta$, the -3 dB cut-off frequencies can be calculated. Figs. 3 and 4 show the time history and amplitude spectrum. The rise time t_r (10% - 90%) = 5 ns, the half width time t_h (50% - 50%) = 200 ns, the peak field strength is 50 kV/m. The incident field at the earth surface can be considered as a plane wave:

$$E/H = 120\pi\ \Omega \qquad (3)$$

The polarization north and south of ground zero (GZ) is horizontal and at a large distance east or west from GZ almost vertical.

The analytical model presented in (1) has a discontinuity at $t = 0$ that physically cannot exist and that the EMP will not have. Moreover this phenomenon cannot be simulated too.

Therefore the following expression can better be used:

$$E(t) = \left(1 + \frac{\alpha}{\beta}\right) \frac{A\, e^{\alpha t}}{1 + \frac{\alpha}{\beta} e^{(\alpha+\beta)t}} \qquad (4)$$

with:

$$A = 5 \cdot 10^4 \text{ V/m} = E_{pk} \text{ at } t = 0$$

$$\alpha = 7.8 \cdot 10^8 \text{ s}^{-1}$$

$$\beta = 3.45 \cdot 10^6 \text{ s}^{-1}$$

The rise time, half width time and E_{pk} are the same as in model (1), however the field has a more gradual rise. The dashed lines in fig. 3 and 4 show the difference. This time history looks more like that of the EMP simulator. The relaxed high frequency end of the spectrum has important consequences for the exposed equipment in the simulator because most of the responses are related to the first derivative of the field. This effect can be shown in fig. 5, the first derivative of the spectrum. Fig. 6 shows the cumulative energy density of (1).

5.0 ELECTROMAGNETIC FIELD IN THE SIMULATOR

The field in the parallel-plate waveguide of the simulator is composed of TEM, TE and TM modes. If the elevation angle θ of the input taper is small, the dominant mode is a TEM mode. This mode of propagation is indistinguishable from free space propagation.

5.1 Field Magnitude

The field strength in the simulator is given by the expressions:

$$E_z \sim \frac{V}{b} \quad V/m \tag{5}$$

$$H_x \sim \frac{V}{b \cdot Z_o} \quad A/m \tag{6}$$

where V is the peak pulse amplitude, b the plate separation in metres and Z_o the wave impedance of free space.

5.2 Field Distortion

The dimensions of the transmission line are determined by the size of the objects placed in the working volume. The vertical electric field component is short-circuited by the vertical conductive parts of the object. The height of the parallel plate section should be chosen such that the largest object is not unduly overstressed by the increased field strength. For field changes of 20% or less a simulator height of 5 to 10 times the largest object is suggested. In practical cases, with large objects, heights between 2 and 3 times are satisfactory. The transverse dimensions will be related to the number and width of the objects and to the tolerable field variations across the working area. Conductors exposed to the simulated field reradiate their induced energy. The major field component is the quasi electrostatic field, that falls off inversely with D^3. D is the distance from the radiating conductor. At distances equal to the height of the object, the field distortion is ca 50% and at 2, 3 and 4 times the object height respectively

6, 2 and 1%.

5.3 Field Orientation

The electromagnetic field orientation and relative magnitude for a TEM wave in a parallel-plate wave guide can be displayed by a plot of equipotential lines and field lines as shown in fig. 7. The equipotential lines, given by constant v, show the magnetic field orientation, their spacing relates to the electric field magnitude (volts per metre). The field lines, given by constant u, show the electric field orientation, their spacing relates to the magnetic field magnitude (amperes per metre).

5.4 Field Uniformity

The field uniformity for the TEM wave in the transmission line depends on the ratio of b/a and the location within the line (2b is the separation and 2a the width of a parallel two plate transmission line, see fig. 8a). In fig. 9 through 20 the field and potential distribution is given for b/a ranging from 0.2 to 5. Since the plots are symmetric, reflection across the x and y axes will extend the graphs to all four quadrants.

Since we can place a conductor along any equipotential line we can convert the system to an asymmetric two-plate transmission line with an infinite ground plane at y = 0. As can be seen from the plots a low value b/a results in a minimum fringing effect at the edges of the upper plate.

5.5 Field Variation

The field variation across an asymmetrical two-plate transmission line is illustrated in fig. 22. The values are normalized to that of a semi-infinite system and the dimension x is measured from the edge of the upper plate. As may be seen the field strength drops to 50% at the plate edge. Longitudinal fringing will mainly be found at the taper junctions. For

instance, a taper ratio of 3:1 results in a 4% rise in field strength at the junction.

5.6 Summary

If one is prepared to tolerate field variations within a factor of two, it is possible to utilize a line twice the object height with objects separated by a distance equal to their height and work to the edge of the line.

For 30% variations the line height needs to be 3 times the object height and objects should be spaced apart by 1½ times their height and kept 1 object height away from the line edge.

6.0 DESIGN OF A 6M TRANSMISSION LINE

6.1 Dimensions

The dimensions of the simulator depend on the size of the objects in the working volume. Typical large objects for the Army are vehicles, tanks, etc. and for the Air Force small aircraft and helicopters. The height of these large metal objects is assessed as 3 and 5m respectively. If field variations of 50% can be tolerated the height of the horizontal part of the simulator should be at least 6m and 10m respectively.

Let us start with the 6m transmission line. From the graphs in fig. 9 to 20 it can be seen that simulators with a low b/a ratio have the best field uniformity (low impedance lines). Let us look for a width 2a of 6 m, 8 m, 10 m and 12 m. The ratio b/a is then 2, 1.5, 1.2 and 1. The electromagnetic field orientation and relative magnitude up to half height and to the edge of the working volume can be read from the corresponding figures. A width of 10m appears to be a reasonable compromise, see the dashed line in fig. 16. If smaller objects are expected a width of 8 m is a good choice as well and it reduces the apex angle ϕ of the input taper (shorter rise time). The useful length of the mid-section is limited by the reflection at the junction between input taper and mid-section, see fig. 23.

As mentioned earlier the input taper launches a TEM type wave with a spherical wavefront. When this wave enters the simulator working volume a reflection occurs. This reflection in area B adds to the wave launched by the taper sections at a time corresponding to the clear time and causes a distortion of the wave onset and amplitude. The field in the A portion of the working volume shown in figure 23, is not distorted by the reflected wave. This means that the length of an undistorted working volume depends on the length of the input taper. The input taper plays an important role in the simulator performance. A larger taper length results in a less spherical wavefront, a shorter rise time, a larger clear time for reflections in the direction of the generator and in less radiation.

6.2 Rise Time

For a length of the working volume of 20 m at a working height of 3 m a taper length of 40 m is needed to be outside the reflection area. The spherical wave launched in the input taper must be converted to a plane wave in the working volume to establish the waveguide TEM propagating wave. This conversion takes place in a time that is equivalent to the propagation time corresponding to the spherical wave distance $\Delta\iota$, see fig. 23:

$$\Delta\iota = h\ (\csc\theta - \cot\theta) \qquad (7)$$

The time associated with propagation over this distance is representative of the TEM wave rise time. With a taper length of 40 m and a simulator height of 6 m, $\theta = 8.53°$ and $\Delta\iota = 0.45$ m. The corresponding rise time $t_\iota = \Delta\iota/c = 1.5$ ns. The clear time of the taper is $2\times40/c = 267$ ns.

The total rise time of the simulator + pulser is:

$$t_t \sim \sqrt{t_\iota^2 + t_p^2} \qquad (8)$$

For a total rise time $t_t = 5$ ns the rise time of the pulser should be $t_p \leq 4.77$ ns.

If desired the input taper can be used as working volume with the restrictions mentioned earlier. The horizontal wave-guide acts then as a perfect termination for the taper, much better than in the case of the conical plate simulator. Moreover the radiation level is lower than with the CPS.

The input taper can be made shorter at the sacrifice of some working height at the end of the working volume. With a taper length of 30 m the rise time of the line $t_\iota = 2$ ns. The clear time is 200 ns and the rise time for the pulser should be $t_p \leq 4.58$ ns. The rise time measured in practical situations at the input of the working volume is smaller than the calculated value. That is because $\Delta\iota$ in fig 23 with a working height of h/2 is smaller. The effective rise time of the wavefront should be considered in two planes,

in azimuth as well as in elevation. For the calculation of the path difference Δl in azimuth only half of the width of the line should be used. With a taper length of 30 m and a width of 10m, Δl = 0.41 m and t_1 = 1.4 ns.

Since the rise time of the taper in both azimuth and elevation will not contribute significantly to the overall rise time within the facility a taper length of 30 m will be applied in the further design.

6.3 Reflections

An abrupt change at the junctions between taper and line will introduce a capacitive mis-match and result in the mentioned reflections. A radius introduced at these points will minimize this effect and improve the design. The reflection at the junction of the parallel-plate section and the termination (output) taper can be reduced in the same way as with the input taper. A smaller length of the output taper results in larger reflections and shorter clear times of the multiple reflections, see fig. 2. The parallel-plate section is given the same length as the two tapers to make optimum use of the undistorted area at the ground plate (experiments with cables upon the ground). This section does not contribute to the radiation of the line, see appendix A.

6.4 Impedance

The design aim of a simulator transmission line is to keep the characteristic impedance Z_1 as constant as possible from the beginning to the end of the line to prevent reflections. This is a kind of an art, since many factors are influencing the impedance, some of which are not very well understood. The design can be started with calculating the approximate values of the impedance. Afterwards the impedance can be measured with TDR methods. Where necessary, corrections can be made in the structure.

The derivation of the line impedance has been extensively treated by Baum in his Sensor and Simulator Note SSN 21 (12). Brown et al used this note

to produce a set of graphs and tables to simplify the design, see tables 1 to 5 and figs. 9 to 20 (13). The impedance can be defined as:

$$Z = f_g \cdot Z_o \ \Omega \qquad (9)$$

where f_g is a geometric factor of the particular line and Z_o is the wave impedance of free space. Factor f_g can be read from the tables 1 to 5. Parameter b/a is for asymmetric two plate lines as defined in fig. 8B, a = 1/2 width and b = h (height). In our case b/a = 6/5 = 1.2 and $Z = 0.5 \cdot f_g \cdot Z_o$ = 98.5 Ω.

Fig 21 gives a quick view of Z versus b/a. The generator and termination dimensions are matched to those of the line by gradual tapers. The ratio b/a applies for the tapers as well.

It should be noted from the figs. 9 to 20 that the field falls off slowly with increasing distance from the edge of the upper plate. Therefore the ground plane should extend significantly beyond the edges of the upper plate and intercept most of the field for the calculations to be valid. When the width of the lower plate is decreased from infinity to the same width as the upper plate, the impedance will increase. This is shown in fig 24. The asymptote given at each curve is the impedance for infinite width (14). In practice the lover plate may be in contact with the earth, which is also a conductor. This will increase the effective width of the lower plate and thus decrease the line impedance. The effect of the earth on the impedance is negligible if factor a_1/a is greater than three to four. However that is a rather large ratio. Therefore the earth is an uncertain factor in determining the line impedance in many practical cases. In our case with b/a = 1.2, a/h = 0.83. Take a ratio $a_1/a = 2$. The increase in line impedance is about 14 Ω. Dependent on the conductivity of the earth this varies from 14 Ω to 0 Ω.

6.5 Wire Grids

Up to this point, solid conducting plates were considered to form a transmission line. For large transmission lines, like this one, the solid

plates should be replaced with wires installed parallel to the direction of propagation to avoid mechanical or structural problems (weight, wind, snow, rain, etc.).

Wire grids will distort the field near the wires and will increase the line impedance. The field in the vicinity of a wire is illustrated in fig. 25 (12). The leakage of the field through the grid has the effect of shifting the grid to give an increase in the effective plate spacing. This will have a corresponding effect on the line impedance. This shift of the grid is given by:

$$\Delta h = \frac{s}{2\pi} \ln \left(\frac{s}{2\pi r}\right) \qquad (10)$$

where s is the wire spacing and r is the wire radius.

If the transmission line is removed from the effects of the conducting earth, a Δh factor will also be required when the lower plate consists of parallel wires.

The wire spacing must be small compared with the wavelength of the highest frequency to be propagated down the line. With wider wire spacing, the high frequencies will radiate energy between the wires. This radiation will cause a loss of high frequency content in the wave and will maintain a spherical wavefront for high frequencies within the working volume (15).

With a wire spacing s = 40 cm and wire radius r = 4 mm, Δh = 17.6 cm for the upper plate, and 0 to 17.6 cm for the lower plate, dependent on the conductivity of the earth. Assume the effect of the earth is negligible, then the effective plate spacing is $h + 2 \cdot \Delta h = 6 + 0.352 = 6.352$ m. Factor b/a = 6.352/5 = 1.27, and $f_g = 0.5383$, $Z = 0.5 \cdot f_g \cdot Z_o = 101.5\ \Omega$. With a lower plate width two times the upper plate width 14 Ω has to be added: $Z = 101.5 + 14 = 115.5\ \Omega$. The wire spacing s = 40 cm corresponds with a frequency c/0.4 = 750 MHz which is high compared to the highest frequency to be propagated, see fig. 4.

The accuracy of impedance suggested in the tables is partly cancelled

by the unknown effect of the earth upon the impedance. This uncertainty can be decreased by connecting the perimeter of the lower plate to ground rods. The impedance of the line can be measured with a reflectometer, an instrument which measures the pulse impedance by reflection techniques. It shows the level and the location of the reflection.

6.6 Field Enhancement

The replacement of solid plates by a grid of wires has a second consequence; a field enhancement around the wires, see fig. 25. Shannon has derived an expression for the field enhancement (16). For a grid of parallel wires with the field applied to one side the field enhancement factor is:

$$f \sim 1/2 + 1/12 \cdot \left(\frac{\pi\, d}{s}\right) + \left[1 - e^{-\left(\frac{\pi\, d}{s}\right)}\right]^{-1} \qquad (11)$$

for $d/s \ll 0.1$, where d is the wire diameter and s the wire spacing. Fig. 26 shows f versus d/s.

Another field enhancement exists at the edge of the upper plate or wire grid. In our case, with $b/a = 1.3$, see fig. 17. For the geometry of a semi-infinite plate with a radiused edge Shannon gives as field enhancement factor:

$$f = \sqrt{\frac{h}{\pi\, r}} \quad \text{for } r/h \ll 1 \qquad (12)$$

where r is the edge radius and h the height of the line. Fig. 27 shows f versus r/h. In both cases the local field is clearly well in excess of the general field and may in fact exceed the breakdown strength of air. A discharge in the air, or a spark to a conductor may be the result.

6.6.1 Breakdown of the Air

The breakdown strength of the atmosphere is generally given as

25 kV/cm. The DC breakdown strength of a spark gap with air in a uniform field is given as:

$$E = 24.6p + 6.7 \frac{\sqrt{p}}{\sqrt{d}} \text{ kV/cm} \qquad (13)$$

where p is the pressure in atmospheres and d the gap spacing in cm. With p = 1 and d = 1, E = 31.3 kV/cm.

For short pulses the breakdown field strength can be larger, as a result of the time-lag to initiate a Townsend avalanche and to form a spark channel. It takes time to form a streamer. For instance, with a streamer velocity $v = 10^5$ m/s a pulse length of at least 10 µs is needed to cause a spark-over at a distance of 1 m (18).

Let us look to the design of our grid of wires. It has advantage to construct this grid as light and as strong as possible, for instance apply not too many, small diameter, stranded wires. With a diameter d = 3 mm and spacing s = 1 m, $d/s = 3 \cdot 10^{-3}$. From fig. 26 it can be read that the field enhancement factor f = 110. With a main field of 0.5 kV/cm the local field at the wires is 110 x 0.5 = 55 kV/cm. That is too large. Assuming a breakdown field strength of air of 25 kV/cm and applying a safety factor of 2, the maximum allovable field enhancement factor is:

$$f_m = \frac{12.5 \text{ kV/cm}}{0.5 \text{ kV/cm}} = 25$$

This value corresponds in fig. 26 with a ratio $d/s = 1.3 \cdot 10^{-2}$. When choosing a wire spacing s = 40 cm, to prevent radiation, it follows that d = 5.2 mm. It is recommended to choose a field strength in the facility that is a little larger than the required 50 or 65 kV/m, say E_f = 75 kV/m. With an E_f = 75 kV/m, f_m = 17 and the diameter d = 8 mm.

The field enhancement at the edge of the grid of wires can be approximated with fig 27 (valid for solid plates). With a wire radius r = 4 mm the ratio $r/h = 6.7 \cdot 10^{-4}$, and f = 22. The enhanced field at the edge is 22 x 0.75 = 16.5 kV/cm. This means the wire radius should not be less than 4 mm.

In the taper, the height h is decreasing, causing a lower field enhancement factor f and a larger field strength E_f in the taper. Table 6 shows the edge enhanced field E_e of the taper with a facility field strength E_f = 75 kV/m or 0.75 kV/cm and a wire radius r = 4 mm. It appears that E_e is rather large, particularly in the lower height regions.

6.6.2 Larger Edge Radius

To be sure that no breakdown of the air will occur the edge radius should be increased. With a factor f = 3 the field strength E_e is 13.5 kV/m, the ratio $r/h = 4.5 \cdot 10^{-2}$ and r = 45 mm. This can be simulated by some thinner wires placed at the circumference of a half circle with radius r = 4.5 cm, see fig. 28.

An advantage of this construction is that later on, the transmission line can also be used for endo-atmospheric simulations. A disadvantage is that the transmission line is less flexible. However, if a reinforced concrete pad is needed to allow heavy objects upon the ground plate the facility is more or less stationary as it is. In this case aluminum wires with a diameter of 8 mm are recommended.

6.7 Detailed Design

Now that the dimensions and the construction of the facility regarding the given boundary conditions are outlined, a more detailed design of the transmission line can be started.

6.7.1 Horizontal Section

The separation of the upper and lower grid of wires is 6 m. The upper grid has a width of 10 m and the lower 20 m, see figs. 29 and 30. They are constructed of aluminum wires with diameter d = 8 mm passed through plywood

spreaders which stiffen and shape the line. The spacing between the wires is 40 cm. The upper grid has 26 wires and the lower 51 wires. At the edges of the upper grid 5 extra wires with diameter d = 3 mm are forming a rounded edge with a radius r = 5 cm. The lower grid is at the periphery connected to small ground rods to minimize variations in the influence of the ground and to decrease the impedance.

The effect of the rounded edges upon the line impedance has to be compensated. Suppose the rounded edges can be replaced by flat plates with a width of approximately $1/4\pi d \sim 8$ cm. To keep the same impedance the flat part of the upper grid should have a width of 10 m - (2 x 8 cm). The wire spacing s = 40 cm is then a little smaller.

6.7.2 Input Taper

It is assumed that the height of the generator output is about 1 m and the peak output voltage is 450 kV. Table 7 shows the enhanced field at the edges and between the wires at several heights of the taper. The maximum values at the generator connection are 13 kV/cm and 17 kV/cm respectively. The field strength between the wires can be reduced by constructing the first part of the taper of solid plate. The connection to the generator should be given round edges in all directions to prevent additional field enhancements. The remaining maximum edge field strength is then 13 kV/cm, a factor 2 below the atmospheric breakdown level. This safety factor is a minimum, since an incorrect adjustment of the generator can double the output voltage, see section 6.8.2.

With these precautions complex structures with gas tight compartments filled with sulphur hexafluoride gas (SF_6) can be avoided. To close the generator housing and to electrically isolate the taper from the housing a perspex interface can be used with a thickness of about 15 mm. The minimum distance from conductive parts of the construction should be at least 1 m.

In table 8 the impedance of the taper at several places is given, see fig. 31. In the calculations an effective height is assumed of $h' = h + 2\Delta h$.

If a part of the upper or lower grid is made of solid plate the correction with Δh or $2\Delta h$ is not needed. The impedance of the taper is decreasing a little with decreasing height. This can be corrected by increasing the height. The correction in fig. 31 is given in centimetres.

In practice the impedance is a few ohms larger because of the limited width of the groundplate. The interface between the solid part and the wire part of the taper should be made gradual, e.g. with wire-mesh. At the top of the taper the reflections can be reduced by using a small elevation angle $\theta = 11.31°$ and by rounding of the shape of the junction.

6.7.3 Output Taper

The output taper has the same dimensions and construction as the input taper. The effective rise time is 2 ns in elevation and 1.4 ns in azimuth. The main task of the output taper is gradually connecting the horizontal parallel-plate section to its load. The transmission line is distributed loaded with a construction that forms an integral part with the taper. The dimensions of the connection to the load are determined by the terminating construction.

6.7.4 Termination

The aim of a good design is to prevent reflection of the guided wave back into the working volume. The output taper guides the wave to a relatively small resistive load, whose impedance is equal to the characteristic impedance of the transmission line structure and is "invisible" for the arriving wave front. The best way to prevent reflections is to make the transmission line infinitly long. This can be simulated by distributing the load over a finite length and make it a part of the taper.

Other design aims are:

- the termination should be resistive for all frequencies of interest, see Fig 4
- the termination should be able to handle a peak voltage of 450 kV
- the resistance should be adjustable between 100 and 110 Ω

A good choice for the resistive material is the carbon type resistor. It consists of a ceramic tube with a thin carbon layer on the outside. A suitable choice is Morganite, type 701 with a low inductance and anti-track bands to avoid spark-overs. The length is 250 mm, the diameter 25 mm.

With the anti-track bands the maximum allowable voltage per resistor is 30 kV. To handle 450 kV, 15 resistors in series are needed. With 20 resistors in series a safety factor of 1.3 is created and the total length is in agreement with the minimum height of 1 m, see Fig. 32. The inductance of 20 resistors in series can be reduced and the termination can be distributed over the whole width by connecting a number of resistor-strings in parallel.

With 16 resistor-strings in parallel and 82 Ω per resister, the total value is:

$$R_t = \frac{20 \times 82}{16} = 102.5\ \Omega$$

By disconnecting one of the strings the total value $R_t = 109.3\ \Omega$.

Damage by over-voltage across one of the resistors can be prevented by connecting the 16 strings not only at the two ends but also at each resistor station; thus forming equipotential lines, see fig. 33. By removing one or more resistors fine adjustments can be made (don't overstress the other resistors).

Since the resistive network forms a part of the taper and has a space dependent resistive value, the impedance of that part of the taper (formed by the terminating network) should be matched to the resistive value. This can be done by increasing the width of the network to infinity at zero height. In

practice a width two times that at 1 m height is sufficient. The ground plate is made of solid material. The rounded edges of the taper continue in the terminating network by two resistor strings at each side. Fig. 34 shows some construction details of the edges and in figs. 35 and 36 a suggestion for the wooden frame work is given. A detailed field enhancement plot of the edges can be made with the "resistive paper and silver paint" method. With the proposed dimensions of the terminating network the enhancement is up to the breakdown limit.

The peak voltage across the resistive network V = 450 kV. With a value R ~ 100 Ω the peak current i_{pk} = 4.5 kA. For a half width time $t_h = 0.7\tau$ = 200 ns, C = 2.86 nF and W = $1/2 \cdot CV^2$ = 290 J. The t_h of an endo-atmospheric EMP is about 190 µs (exponential decay) and W = 27.5 kJ. In both cases the dissipated energy is far below the maximum rating.

6.8 Pulse Generator

The pulse generator (also called pulser) loaded with about 100 Ω, should have a peak output voltage of 450 kV and a time history similar to that of the exo-atmospheric EMP, see fig. 3. The field strength E(t) has the same shape versus time as the output voltage of the pulser. The peak value is 450 kV/6m = 75 kV/m.

High voltage generators have relatively large dimensions, even when they generate this voltage for a short time. As a consequence they contain too much inductance to deliver high output voltages with a rise time in the ns range. High voltages together with short rise times car be obtained by a combination of a Marx generator and a pulse forming network like a peaking capacitor or a transfer capacitor. In this case the Marx generator should have an output voltage of about 450 kV + 20% = 540 kV. Ask for a 600 kV Marx to prevent an unpleasant surprise during the acceptance test.

6.8.1 Peaking Capacitor

The basic peaking capacitor circuit is schematically given in fig. 37. C_m is the total capacitance of the Marx generator and L_m is its inductance lumped together. C_p is the peaking capacitance and R_l is the load resistance.

Initially C_m is charged to V_o volts, the Marx voltage. After switch S_1 is closed the peaking capacitor C_p will be charged. The value of C_p is chosen so that when the voltage across it reaches V_o, the current through it is V_o/R_l. At this time S_2 is closed and the voltage across R_l and the current through R_l become immediately V_o and V_o/R_l respectively. In practice the rise time of the voltage and current are greater than zero because C_p, R_l and the interconnecting conductors contain some inductance.

The peaking capacitor is a relatively small, high-voltage, low-inductance capacitor. The capacitance is large enough to build up the current from the Marx generator to a level required by the load. When the generator current has build up, the load is connected and the current is transferred to the load, see fig. 38.

S1 is closed at t = 0

$$i_L(t) = \frac{V_o \sin(\omega_o t)}{\omega_o L_m} \qquad (14)$$

$$V_p(t) = V_o (1 - \cos(\omega_o t)) \qquad (15)$$

where

$$\omega_o = \frac{1}{\sqrt{L_m \cdot C_p}} \quad \text{and} \quad C_p \ll C_m$$

$i_L(t)$ is the current through L_m and $V_p(t)$ is the voltage across C_p

$$\text{At } t = \frac{\pi}{2\omega_o} \qquad i_L = \frac{V_o}{\omega_o L_m}$$

This value should be equal to $\frac{V_o}{R_l}$

This means $R_l = \omega_o L_m = \sqrt{L_m/C_p}$

or $C_p = \frac{L_m}{R_l^2}$ (16)

The decay of the pulse, after S_2 is closed, is determined by the capacitance $(C_m + C_p)$ and R_l. The required half width time 0.7τ = 200 ns,

$$(C_m + C_p) = \frac{200 \cdot 10^{-9}}{0.7 \cdot R_l} = 2.86 \text{ nF.}$$

For $C_p = 0.1 \cdot C_m$, $C_p \sim 290$ pF and $L_m = 2.9$ µH.

The calculation of C_p is an approximation, since some stray inductance and parasitic capacitance is neglected. The peaking capacitor can be made fairly small, with a low inductance. With a good design of C_p the rise time of the pulser (Marx generator + peaking circuit) is mainly defined by the series inductance of the spark-gap S_2.

6.8.2 Spark Gap

Spark gap S_1 in fig. 37 is the spark gap in one of the stages of the Marx generator when they are switched into series. It is a low voltage (50 kV) switch that does not play an important role in the total circuit. The main spark gap S_2 should ideally have no inductance, however the rise time is controlled by two factors: the inductance of the spark channel and the rate of current growth during the resistive phase, so called because of the energy used to heat and expand the plasma channel. The inductance is related to the gap distance and the resistive phase to the density of the applied gas.

The gap distance can be reduced by applying a gas with a larger electric strength than air, e.g. SF_6 with a factor 2 to 2.5 related to air and

by increasing the gas pressure. To further decrease the inductance of the spark gap the dimensions should be made as small as possible.

In our case the voltage across the spark gap is 450 kV. To prevent sparkovers upon the outside of the spark gap housing, field enhancements should be avoided and the spark gap can be placed in oil, together with the peaking capacitor.

The time the main spark gap fires determines the shape of the output voltage of the pulser, see fig. 39 (20). In extreme cases the output voltage can be two times the desired value ($2 \cdot V_o$ in fig. 38). The firing of the spark gap can be triggered. The time for self firing can be adjusted with the gap distance and the gas pressure.

6.8.3 Voltage Divider

When the peaking capacitor and the spark gap with trigger capacitor are placed in oil to keep the dimensions small, also a coaxial voltage divider can be combined with it to monitor the input voltage of the transmission line.

6.9 Electrical Specifications of the Pulser

When ordering a pulser the following specifications are important:

- maximum output peak voltage: 500 kV
- minimum output peak voltage: 100 kV
- rise time: 5 ns or less
- load: resistive, 100-110 Ω
- fall time: e-fold time 286 ns
- prepulse: < 2% of peak
- oscillations: < 5% of momentary amplitude
- pulse-to-pulse repeatability: ≤ 2% deviation
- output polarity: positive and negative
- charging time: 1 PPM at 500 kV
- lifetime
- spare parts
- definitions

(19)

In this report only the electrical properties of the simulator have been considered. Mechanical specifications such as the matching of the pulser output to the transmission line are also very important.

7.0 DESIGN OF A 10m TRANSMISSION LINE

If larger objects have to be investigated or the simulator should not have a fixed base, it is worth while to look at which of the properties can be sacrificed for larger dimensions and more flexibility.

7.1 Dimensions

Let us use a helicopter as an example. The largest height is assessed as 5.2 m and the length as 19 m. For exposing the helicopter in all directions a working volume is needed of about $l \times w \times h = 20 \times 20 \times 10$ m^3. If field variations of 50% are acceptable the simulator height can be limited to 10 m and the width to 20 m. When the same pulser of the 6 m - line is applied with an output peak voltage of 450 kV the peak field strength is 450 kV/10m = 45 kV/m. With a height of 10 m and width of 20 m, the ratio of b/a = 1. The uniformity and orientation of the field can be read from fig. 14. They are better than from the 6 m-line.

7.2 Rise Time

To have the same performance as the 6 m line the input taper should have a length of 5h that means 5 x 10 = 50 m. That is too long to be flexible and there is not always place for a simulator with large tapers. Therefore some distortion caused by reflections should be accepted.

Let us try a length of 20 or 30 m. In this case the rise time in horizontal and vertical direction is the same. With 20 m length t_r = 13 ns and with 30 m t_r = 5.4 ns. Since the responses of exposed equipment are directly proportional to the rise time (the first derivative of the field) no further concession should be made in this direction. We make a choice for the 30 m taper. Another advantage is a larger undistorted working volume.

7.3 Impedance

The impedance of the line with infinite width of the ground plate is 89.1 Ω. Some of the fine uniformity of the field in fig. 14 has to be sacrificed for more flexibility. We give the ground plate the same width as the upper plate. With a ratio $a_1/a = 1$ in fig. 24 the impedance will increase to about 115 Ω. The impedance can be made smaller by making the ground more conductive and/or to connect the ground plate to the ground via ground rods.

Instead of changing the resistive value of the termination, the impedance of the line can be adjusted by changing the width or the height of the upper plate, e.g. with a height of 9 m the impedance is 115 Ω - (89.1 - 83.9) = 109.8 Ω and the field strength is 50 kV/m. The line should be flexible!

7.4 Wire Grids

The replacement of plates by wires has the additional advantage that the height and width of the upper grid can be changed easier. We choose stranded steel wires with a diameter d = 3 mm and a spacing s = 1 m. A wavelength $\lambda = 1$ m corresponds with a frequency of $f = c/\lambda = 300$ MHz. Some radiation of high frequencies can be expected, with a little more spherical wavefront compared to the 6 m line. Since also the rise time is increased from 2 ns to 5.4 ns it is not too bad.

The effective height of the line is increased by the wires with $\Delta h = 74$ cm for the upper grid and 74 cm for the lower grid. This $2 \cdot \Delta h$ can be limited to 74 cm by applying chicken wire at the ground. This has the additional advantage that it is more flexible and can be extended to a larger area (lower impedance).

7.5 Field Enhancement

7.5.1 Horizontal Section

Between the wires: $d/s = 3 \cdot 10^{-3}$ and $f = 110$. With a facility field $E_f = 0.5$ kV/cm the local field is $110 \times 0.5 = 55$ kV/cm. That is too large! The breakdown voltage of the atmosphere is about 25 kV/cm. Let us try a spacing $s = 50$ cm, $d/s = 6 \cdot 10^{-3}$, $f = 55$ and $Ew = 55 \times 0.45 = 25$ kV/cm.

At the edges: $r/h = 1.5 \cdot 10^{-4}$, $f = 46$, $E_e = 23$ kV/cm. In this case the enhanced field between the wires and at the edges is about the same as the breakdown voltage of the air. For a breakdown a minimum pulse length is needed. If we use the half width time of the EMP, $t_h = 200$ ns and assume a streamer velocity $v = 10$ cm/µs a breakdown can be expected at a distance of 2 cm. Therefore a minimum distance of at least 5 cm should be used. Also corona should be avoided. Corona is dependent on factors such as humidity, air pressure, polarity, etc. If only the exo-atmospheric EMP is simulated with a short pulse length and any other field enhancement can be avoided, it may be possible to go to the limits. Another possibility is applying a lower output voltage of the pulser.

7.5.2 The Input Taper

Assume that the height of the pulser output is 1 m. Let us look at the field enhancement at this point because the normal local field strength is here 450 kV/m = 4.5 kV/cm.

Between the wires: the spacing $s = 5$ cm, $d/s = 6 \cdot 10^{-2}$, $f = 6.3$ and the local field $E_w = 6.3 \times 4.5 = 28.4$ kV/cm.

At the edges: $r/h = 1.5 \cdot 10^{-3}$, $f = 14.5$ and $E_e = 14.5 \times 4.5 = 65.3$ kV/cm.

Table 9 shows the enhanced field between the wires and at the edges for

a facility field strength E_f = 50 kV/m. The wire spacing s = 50 cm and the wire diameter d = 3 mm. From a taper height of 4 m down to 1 m the local field E_e increases from 36 to 72 kV/cm. This can be reduced by increasing the radius of the edges, for instance with thin wire mesh (chicken wire). A radius of 1 cm is enough, gradually decreasing with height. The same wire mesh can be used to short circuit the wires in the lower part of the taper, thus reducing E_w. It is also possible to use thicker wires at the edges, also for mechanical reasons. With no further field enhancements the local field is everywhere around 25 kV/cm. And that is the limit!

7.6 Detailed Design

7.6.1 Horizontal Section

The upper grid has a width of 20 m at a height of 10 m. The wires are spaced at 50 cm and have a diameter of 3 mm. The grid has 20/0.5 + 1 = 41 wires. The length is dependent on the dimensions of the object under test and the length of the input taper. In fig. 40, a maximum length of 30 m has been chosen. The lower plate can be made of wire-mesh, connected to earth at the periphery for lower impedance and better field uniformity.

7.6.2 Input Taper

The field enhancement shown in table 9 can be reduced by applying solid metal plate or wire-mesh at the taper end, near the pulser. To reduce E_e at 1 m height from 72.5 to 30 kV/cm, the field enhancement factor f should be made smaller, e.g. 30/72.5 x 14.5 = 6. In fig. 27, a ratio r/h = $9 \cdot 10^{-3}$ can be read, which results in a radius of 9 mm. The effective width is increased by this radius with $2 \cdot \Delta a$, approximated by $1/4\pi d$ = 1.57 cm for each edge.

Table 10 shows the fine adjustment for a constant impedance $Z_1 \sim 91\ \Omega$. The taper can be lifted up a few centimeters at the pulser end.

The exact value of Z_l is not so important, only the constant value. When the lower plate of wire mesh is in contact with a good conductive ground the impedance Z_l of the line is estimated to be 91 + 13 = 104 Ω.

7.6.3 Output Taper

A width of 20 m is relatively large for one taper. Therefore two tapers are designed to terminate the line. Advantages are: a shorter rise time in azimuth, less fringing at the junctions, better uniformity of the field and a simpler construction of the terminating network.

7.6.4 Termination

The minimum height for 450 kV should be 1 m. The length of the terminating networks is then about 1/10 × 30 = 3 m. The network is forming a part of the taper. The width is 1/10 × 10 = 1 m at the taper-network junction, see fig. 42. To match the impedance of the line to the local resistive value of the network, the width is increasing towards the ground connection. The connection to ground should have a low impedance. In fig. 41 the resistors are connected via a metal profile to the reinforcement of the concrete block. The resistors are confined in fibre glass reinforced tubes. The impedance of the line Z_l = 104 Ω. Each network should therefore have a value of 208 Ω, or 3 × 208 = 624 Ω per resistor string. Using the same type of resistors as in the 6 m line a total of 12 resistors of 52 Ω in series are needed. With a maximum voltage per resistor of 30 kV, the total voltage that can be handled is 360 kV. With a short pulse length a voltage overstress with 25% to 450 kV can be tried. Otherwise the fibre glass tubes can be filled with SF_6.

8.0 CONCLUSIONS

The choice between a parallel plate and a conical plate simulator has been made in favour of the first one. The advantages of both are more or less combined by applying a long input taper.

Two designs for a bounded wave simulator have been made, one with a fixed 6 m, and another with a more flexible, 10 m transmission line. For the first one a conservative design has been used. The larger working volume and the better flexibility of the second, more relaxed design have been obtained at the cost of a larger rise time, lover field strength and a higher radiation level (see table 11 and Appendix A). With the procedure given in this report any design in between these two can be made.

No efforts have been made for the design of a complete simulator (pulser and transmission line) since that was out of the scope of this task. However the electrical and mechanical matching of a future pulser to the transmission line can be made in a flexible way.

ACKNOWLEDGEMENTS

I like to thank Dr. Bev G. Young and Dr. Satish Kashyap for their encouragement and help in preparing this report and M.A. O'Keefe for typing the manuscript.

9.0 REFERENCES

1. NATO Documents on Nuclear Survivability Criteria for Armed Forces Material and Installations.

2. The Electromagnetic Field in an EMP Simulator at a High Frequency, R.W.P. King, D.J. Blejer. IEEE-EMC-21, no.3, Aug 1979.

3. Standing Waves and Notches in an EMP Simulator and Their Reduction, R.W.P. King, D.J. Blejer, T.T. Wu, IEEE, EMC-23, no. 2, May 1981.

4. The Rhombic EMP Simulator, H.M. Shen, R.W.P. King, IEEE, EMC-24, no. 2, May 1982.

5. Experimental Investigation of the Rhombic EMP Simulator: Comparison with Theory and Parallel-Plate Simulator, H.M. Shen, R.W.P. King, IEEE, EMC-24, no. 3, Aug 1982.

6. An experimental Investigation of the Rhombic EMP Simulator Under Pulse Excitation, H.M. Shen, R.W.P. King, T.T. Wu, IEEE, EMC-25, no. 1, Feb 1983.

7. Theoretical Analysis of the Rhombic Simulator Under Pulse Excitation, H.M. Shen, R.W.P. King, T.T. Wu, IEEE, EMC-25, no. 1, Feb 1983.

8. An Experimental Investigation of the Parallel-Plate EMP Simulator with Single-Pulse Excitation, H.M. Shen, R.W.P. King, T.T. Wu, IEEE, EMC-25, no. 3, Aug 1983.

9. The Exciting Mechanism of the Parallel-Plate EMP Simulator, H.M. Shen, R.W.P. King, T.T. Wu, IEEE, EMC-29, no. 1, Feb 1987.

10. Private communication FEL-TNO, The Haque, The Netherlands.

11. Sapiens Memo 11, Electromagnetic characteristics of the conical transmission-line EMP simulator SAPIENS, S. Garmland, FOA Report C 30415-A3, Feb 1986.

12. SSN 21, Impedances and field distributions for parallel plate transmission line simulators. C.E. Baum, AFWL, 6 June 1966.

13. SSN 52, A parameter study of two parallel plate transmission line simulators of EMP SSN 21, T.L. Brown, K.D. Granzow, Dikewood Corporation, 19 April 1968.

14. Engineering Techniques for Electromagnetic Pulse Hardness Testing. A.L. Whitson, SRI, Menlo Park, CA, Sept 1974, AD-786 722

15. Time-Domain Analysis of a Large EMP Simulator, C. Bardet, O. Dafif, B. Jecko, IEEE-EMC-29, no. 1, Feb 1987.

16. AFWL Technical Report No. AFWL-TR-69-80

17. De effecten van EMP op electronische systemen, P.A.A. Sevat, NERG, deel 48, nr.2, 1983.

18. Selleck, B., AWRE, Aldermaston, UK, Private Communication, 1970.

19. Pulspak 8080, A transportable all weather 500 kV EMP generator, Pulsar PATP 80-5-1, Oct 1980.

20. Pulspaks for EMP, Radiating Pulse Generator Systems, Phys. Int. Co, PTP 82-131, Sept 1982.

21. I.A.D. Lewis and F.H. Wells, Millimicrosecond Pulse Techniques, Pergamon Press, 1959.

22. Radiation from idealized shock excitation currents in a straight conductor rising from a perfect earth at an arbitrary angle, E.A. Lewis, Electromagnetic Wave Propagation, Academic Press, 1960.

APPENDIX A

ELECTROMAGNETIC RADIATION

A.1 Introduction

The electromagnetic radiation from parallel-plate simulators can roughly be approximated by the following method (18). When a step function voltage V is applied at the source end, a voltage wave of amplitude V and current V/Z_1 starts up the structure with a velocity v, close to the velocity c of light. The propagation of this transient current along the wires sets up radiation fields.

At time ι/v the wave reaches the horizontal section, at $2\cdot\iota/v$ the output taper and at $3\cdot\iota/v$ the termination (see Fig A1). The radiation of transients by straight conductors inclined at an arbitrary angle α from the zenith above a perfectly conducting ground plane has been described by Levis (21,22). Therefore consider first the input taper only.

In fig. A2 the conductor is in the plane YOZ and the observation point P has the spherical co-ordinates R, θ and ϕ. Levis derived the following expressions for the E field at a distance R from the source:

$$E_\theta = \frac{2k\beta\cdot\cos\alpha}{1 - \beta\cdot\sin\phi\cdot\sin\alpha} \qquad (A1)$$

$$E_\phi = \frac{-k\beta^2\cdot\sin(2\alpha)\cdot\cos\theta}{1 - \beta^2\cdot\cos^2\theta\cdot\cos^2\alpha} \qquad (A2)$$

$$E_R = 0$$

where

$$k = \frac{V}{4\pi\varepsilon_0\cdot R\cdot Z_1\cdot c} \qquad (A3)$$

β is the ratio of v/c

v is the velocity of the wave along the conductor

c is the velocity of light

$\varepsilon_o = 8.85 \cdot 10^{-12}$ F/m

The radiation in the E_R plane = 0 in all directions. As we are primarily concerned with fields at ground level, i.e. when $\theta = 90°$, E_ϕ becomes equal to zero and only the vertically polarized field E_θ is left.

Assume the worst case, that v = c, then $\beta = 1$ and (A1) can be written as:

$$E_\theta = \frac{A}{(1 - \sin\phi \cdot \sin\alpha)} \qquad (A4)$$

where

$$A = \frac{2V \cdot \cos\alpha}{4\pi\varepsilon_o \cdot R \cdot Z_1 \cdot c} = \frac{60V}{R \cdot Z_1} \cdot \cos\alpha \qquad (A5)$$

(A5) is a well known expression for vertical radiators. The vertical field E_θ is enhanced in the direction of current propagation by a factor:

$$G = \frac{1}{1 - \sin\phi \cdot \sin\alpha} \qquad (A6)$$

When the current arrives in the horizontal section, where $\alpha = 90°$, E_θ becomes zero. For an observer at a distance R from the source E_θ and E_ϕ are equal to zero. The radiation of the output taper is equal to that of the input taper, see (A1), only with opposite sign. Also the time interval of radiation is for both tapers the same:

$$\Delta t = \frac{l}{v} \cdot \frac{1}{G} \qquad (A7)$$

Because in this case the radiated pulse is rectangular in shape, the energy contained in each pulse is:

$$J = \frac{E_\theta^2}{120\pi} \cdot \Delta t \quad J/m^2 \qquad (A8)$$

or substituting (A5) and (A6)

$$J = \frac{(A \cdot G)^2}{377} \cdot \frac{l}{v} \cdot \frac{1}{G} = \frac{A^2 \cdot G \cdot l}{377v} \quad J/m^2 \qquad (A9)$$

A.2 Radiation from the 6m and 10m Simulator

In the case of the 6 m and 10 m line $\alpha = 78.7°$ and $71.6°$ respectively, $V = 450$ kV and $Z_l \sim 110\ \Omega$. The field strength at a distance R and at an angle $\phi = 0°$ or $180°$ is then:

$$A = \frac{48.1 \cdot 10^3}{R} \quad V/m \quad \text{for the 6m-line, and}$$

$$= \frac{77.6 \cdot 10^3}{R} \quad V/m \quad \text{for the 10m-line.}$$

The field pattern is given by equation (A6).

The energy in each pulse is:

$$J = \frac{0.61 \cdot G}{R^2} \quad J/m^2 \text{ for the 6m-line, and}$$

$$J = \frac{1.6 \cdot G}{R^2} \quad J/m^2 \text{ for the 10m-line.}$$

In table A1 the gain factor G is given for azimuth angles between +90° (direction of current flow), through 0° (broadside to simulator axis) to -90°. Also the pulse width Δt is tabulated.

The product $G \cdot \Delta t$ in (A7) has a constant value $l/v = 10^{-7}$ s, for the worst case $v = c$. In practice the velocity v along the taper is less than c, so Δt in (A7) is a little larger. In cases where Δt is smaller than the rise time t_r of the simulator (pulser and taper) only a part of the amplitude is built up. In our case $t_r = 5$ ns. A correction is made with a factor $\Delta t/5$. In figs. A3 and A4 the field patterns are plotted for the 6 m and 10 m simulator respectively, and in figs. A5 and A6 the corresponding energy density. The dashed lines are corrected for the rise time.

The width of the pulse observed at a distance R with an azimuth angle $\phi = 90°$ is very small because the velocity of the current in the taper is assumed to be the same as the velocity of the propagation of the radiated wave and because the difference in path length $\Delta\iota$ in fig. 23 is very small. In fig. A7 the timing of the pulses at several azimuth angles is given.

A.3 Examination of the Results

The radiation levels of the 6 m and 10 m lines were calculated by replacing the tapers with a single wire; by using a step function ($t_r = 0$); by assuming a perfectly conducting ground and no propagation loss ($E_\theta \propto 1/R$).

In practice measurements on scale models and on real EMP simulators have shown that the levels are smaller. At azimuth angles $\phi = -90°$ the calculated and measured peak values of the field strength are about the same, at $\phi = 0°$ the measured values may be a factor 2-3 smaller, and at $\phi = 90°$ even more than a factor of 10. That is because, particularly the high frequencies, are more than linearly attenuated with increasing distance R, in this manner increasing the rise time and reducing the radiation.

A.4 Radiation Levels

In UK and the Netherlands the following limits have been used for EMP Simulation (18):

- Pace makers, 400 V/m repetitive, 1 pps
- EED's, flash-over 1 kV/m,
  energy 12.5 $\mu J/m^2$.

The minimum distances to apply for safety reason can be assessed by interpolating or extrapolating the figs. A3 to A6.

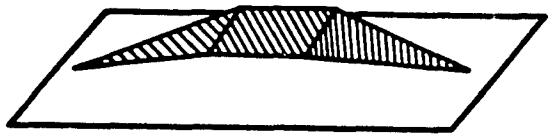

Parallel-plate Simulator, PPS

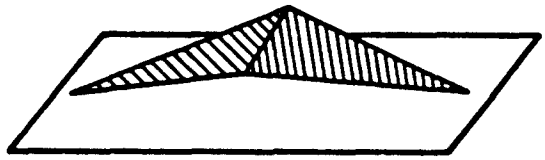

Triangular-plate Simulator, TPS

Rhombic-wire Simulator, RWS

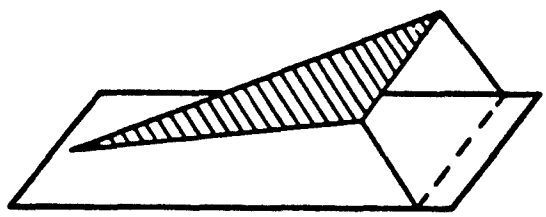

Conical-plate Simulator, CPS

Figure 1: Several types of bounded-wave simulators.

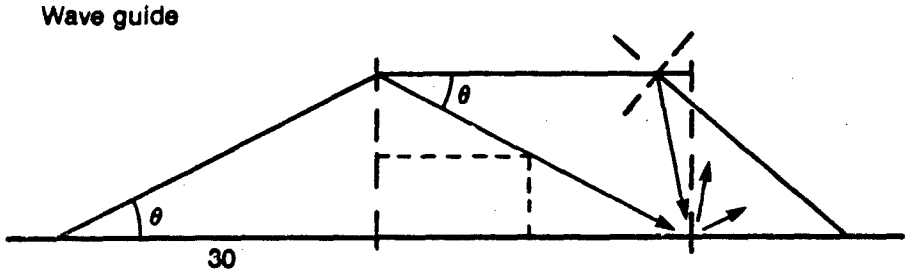

Reflections by changes in shape

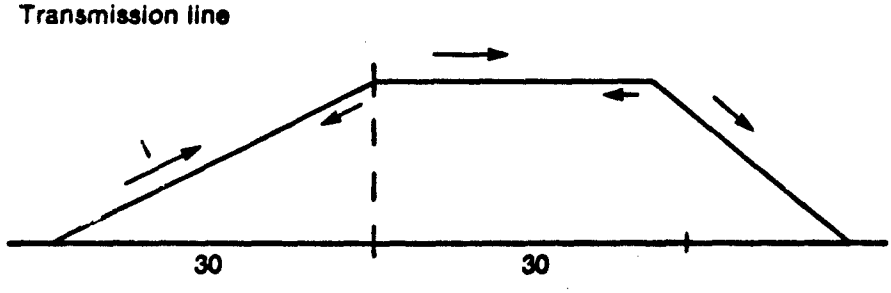

Reflections by local discontinuities of Z_1

Figure 2: Time-space concept for single pulse excitation (no SWR but clear times).

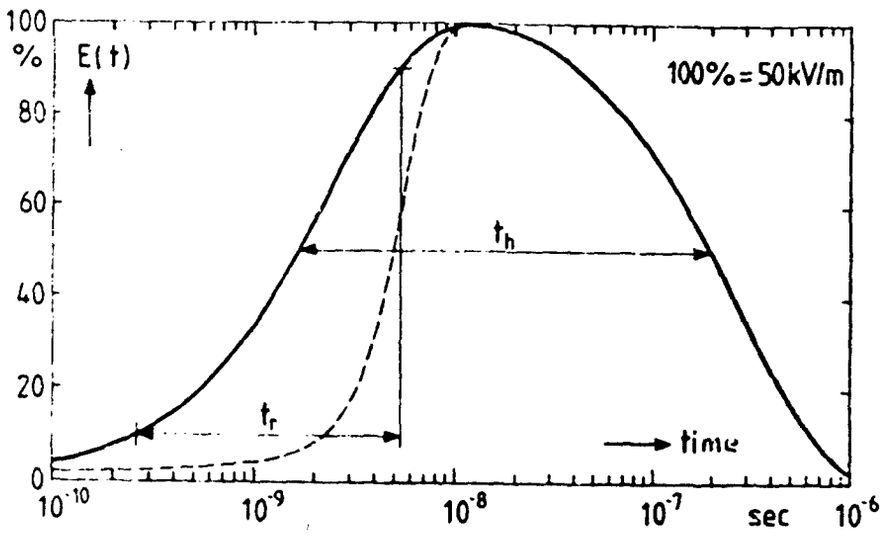

Figure 3: Model for exo-atmospheric EMP.

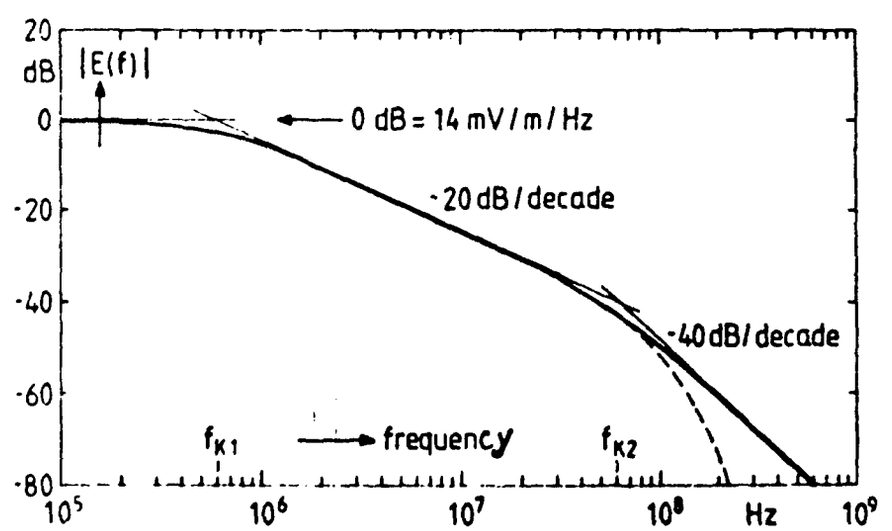

Figure 4: Spectrum of model in Figure 3.

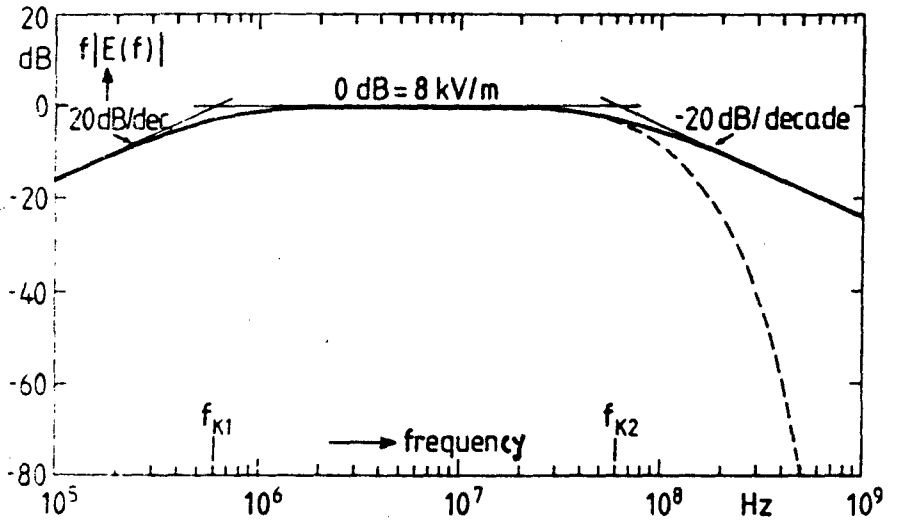

Figure 5: First derivative of spectrum Figure 4.

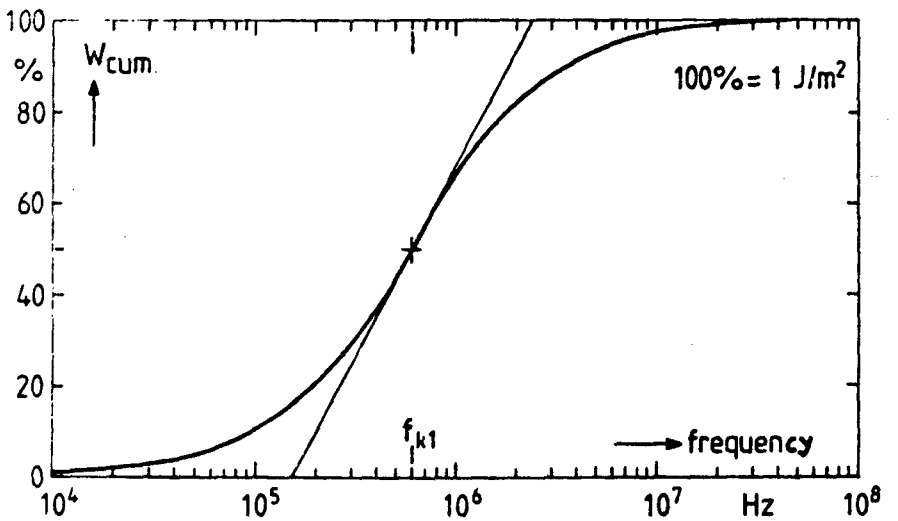

Figure 6: Cumulative energy density of model Figure 3.

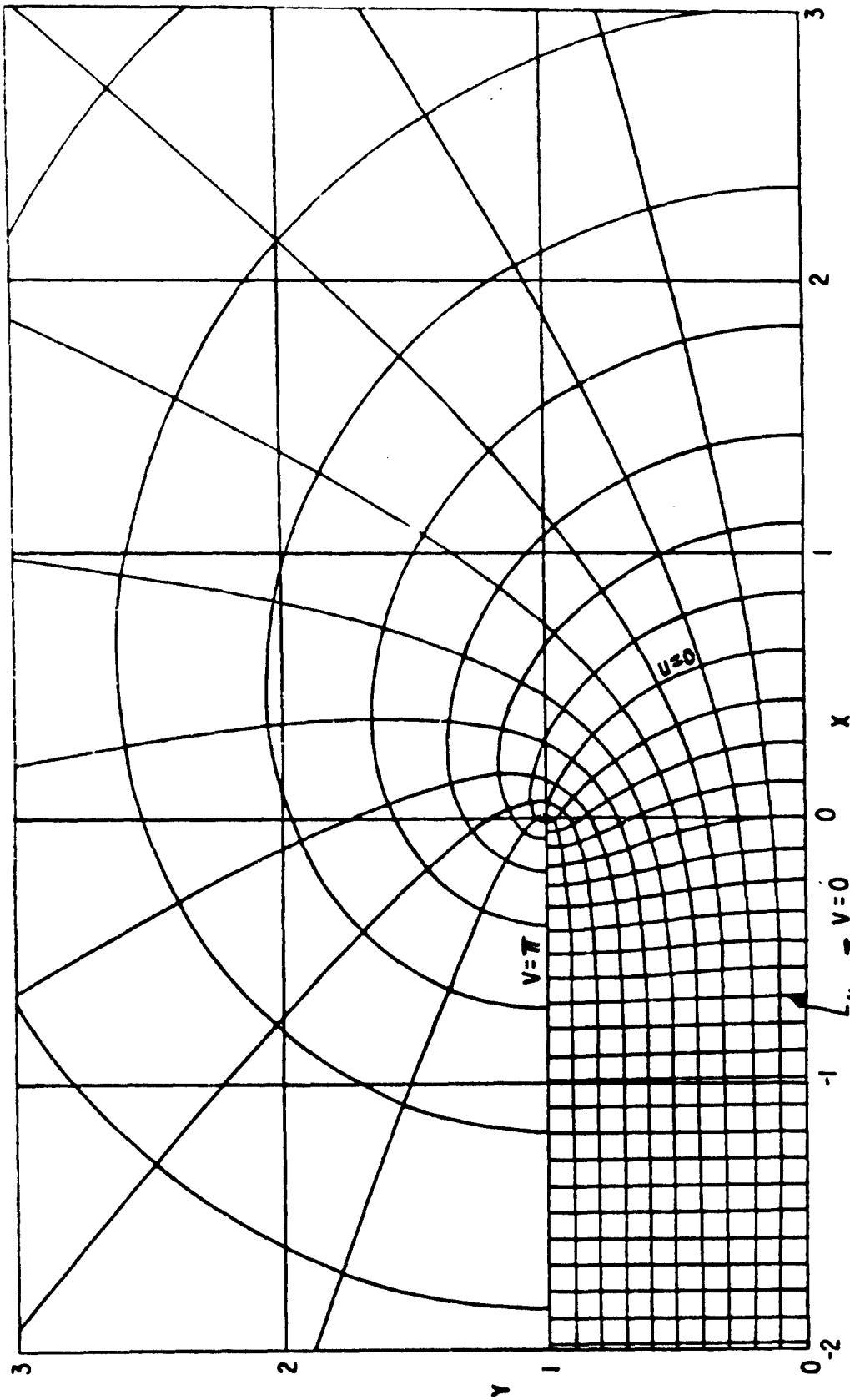

FIGURE 7: FIELD AND POTENTIAL DISTRIBUTION FOR SEMI-INFINITE, PARALLEL, TWO-PLATE TRANSMISSION LINE (UPPER HALF)

$Z = (W + 1 + e^{W})/\pi$ $\quad Z = x + jy$ and $W = u + jv$

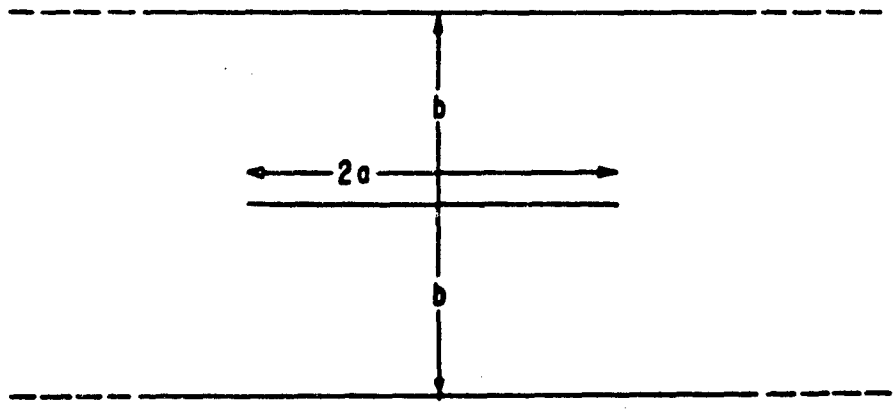

A. INFINITE OUTER PLATES, THREE CONDUCTOR, PARALLEL PLATE TRANSMISSION LINE

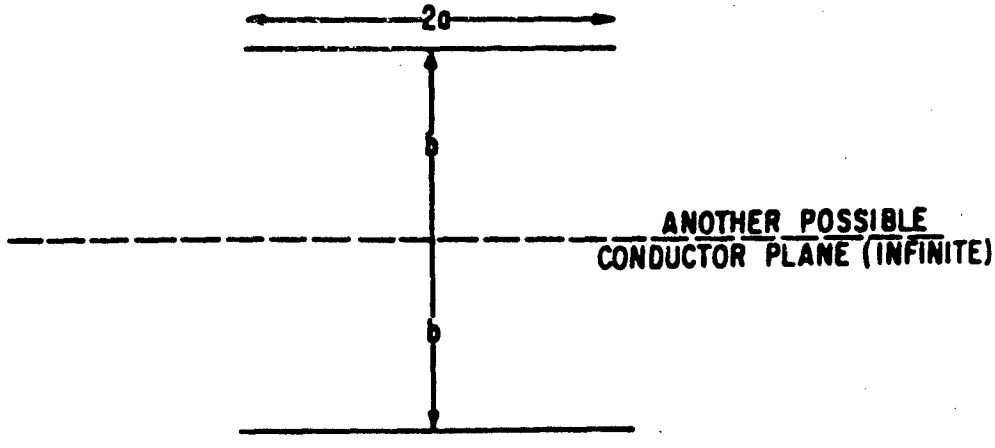

B. TWO CONDUCTOR, PARALLEL PLATE TRANSMISSION LINE

FIGURE 8: SYMMETRICAL, PARALLEL PLATE TRANSMISSION LINES

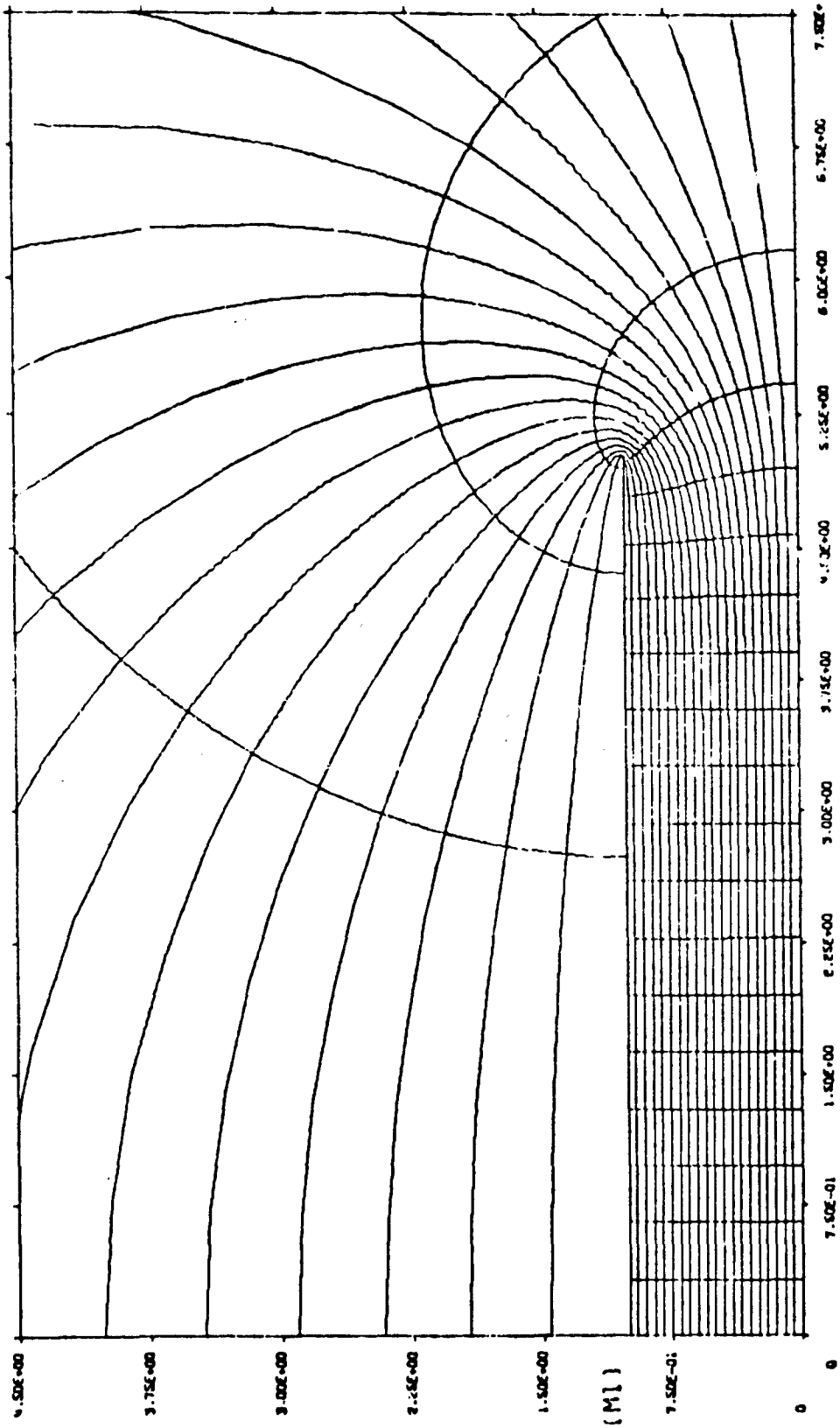

FIGURE 9: FIELD AND POTENTIAL DISTRIBUTION
FOR PARALLEL, TWO-PLATE TRANSMISSION LINE. 57.97 OHMS
B/A = .20

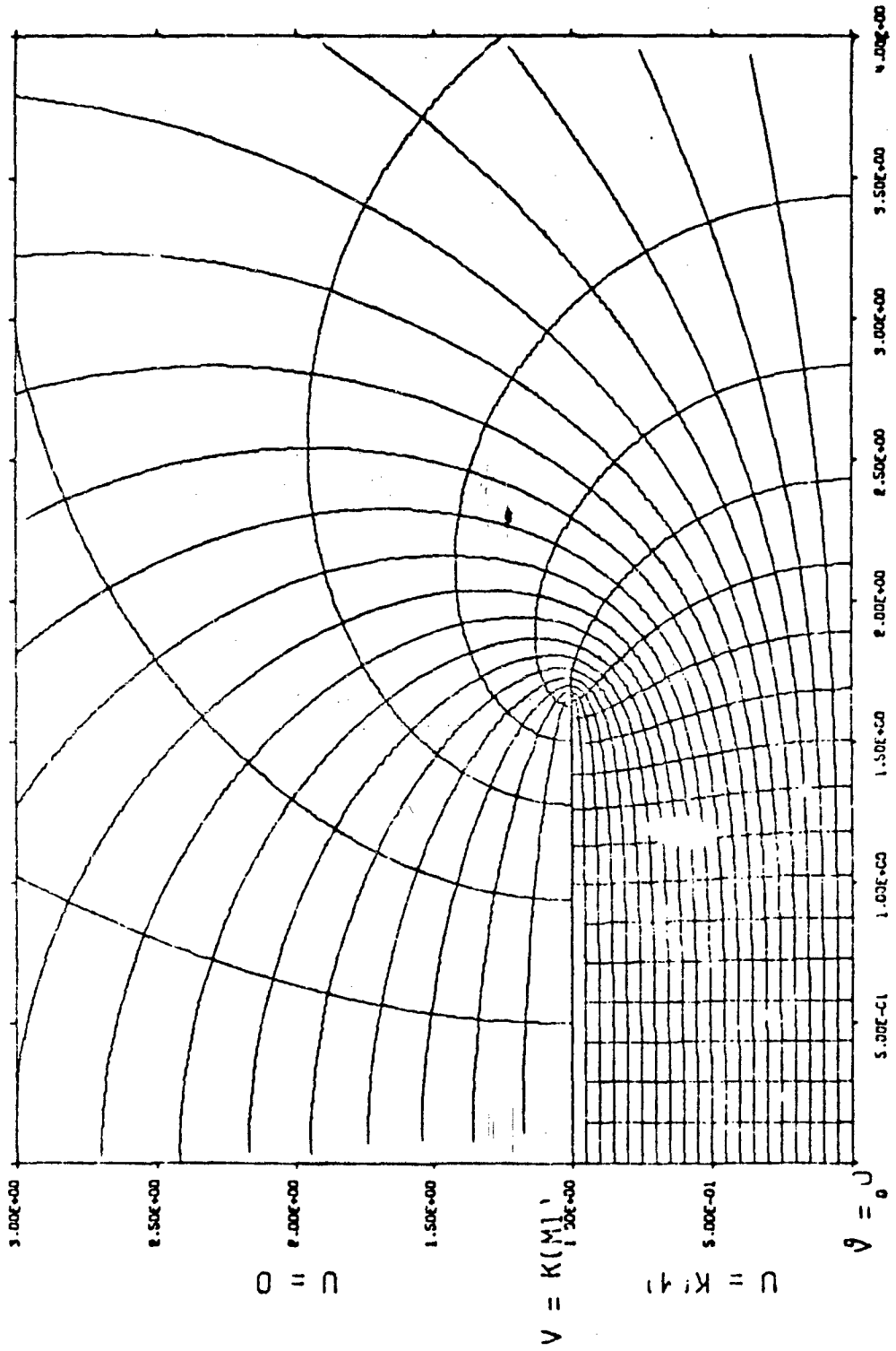

FIGURE 10: FIELD AND POTENTIAL DISTRIBUTION
FOR PARALLEL, TWO-PLATE TRANSMISSION LINE. 130.49 OHMS
B/A = .60

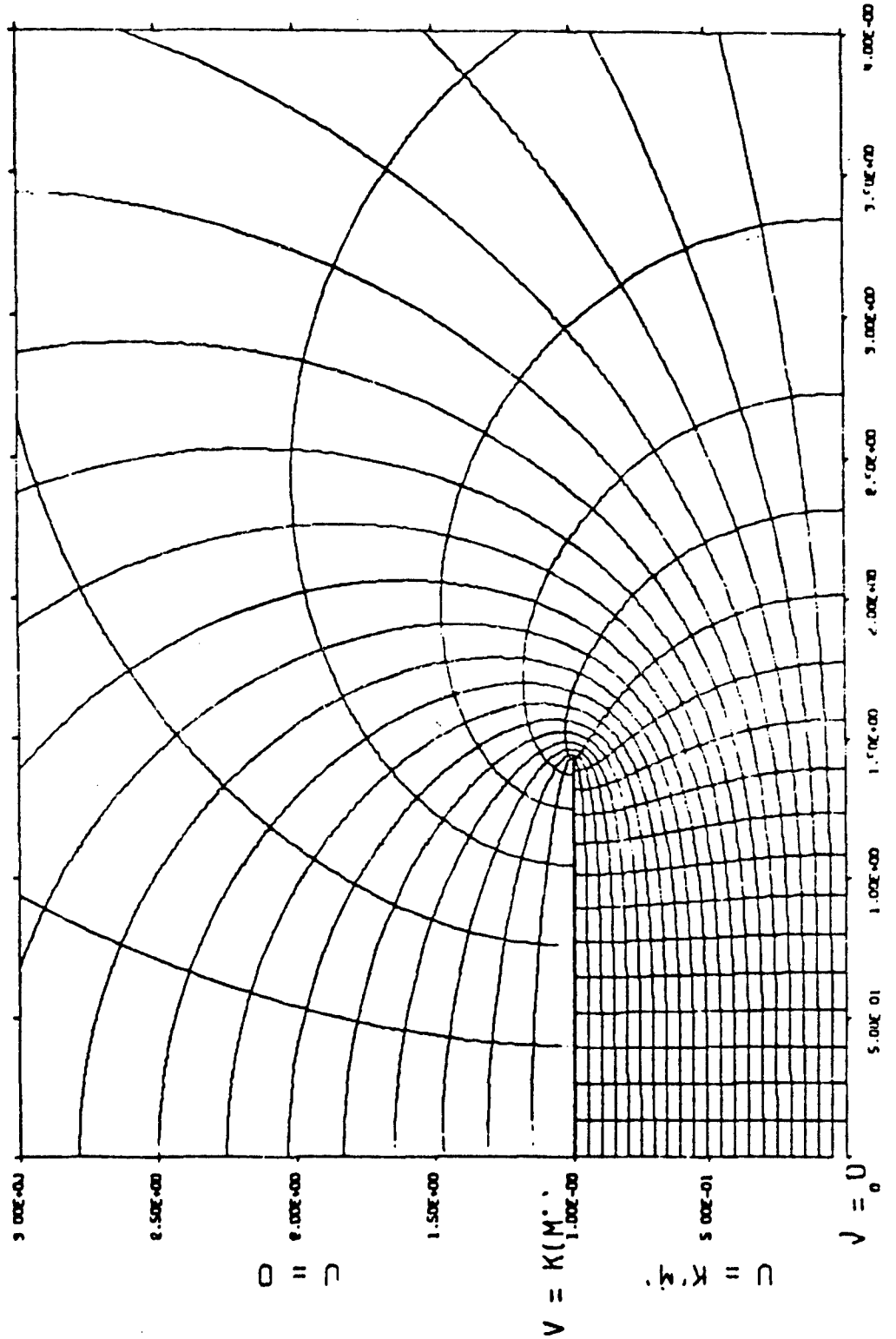

FIGURE 11: FIELD AND POTENTIAL DISTRIBUTION
FOR PARALLEL, TWO-PLATE TRANSMISSION LINE. 144.03 OHMS
B/A = .70

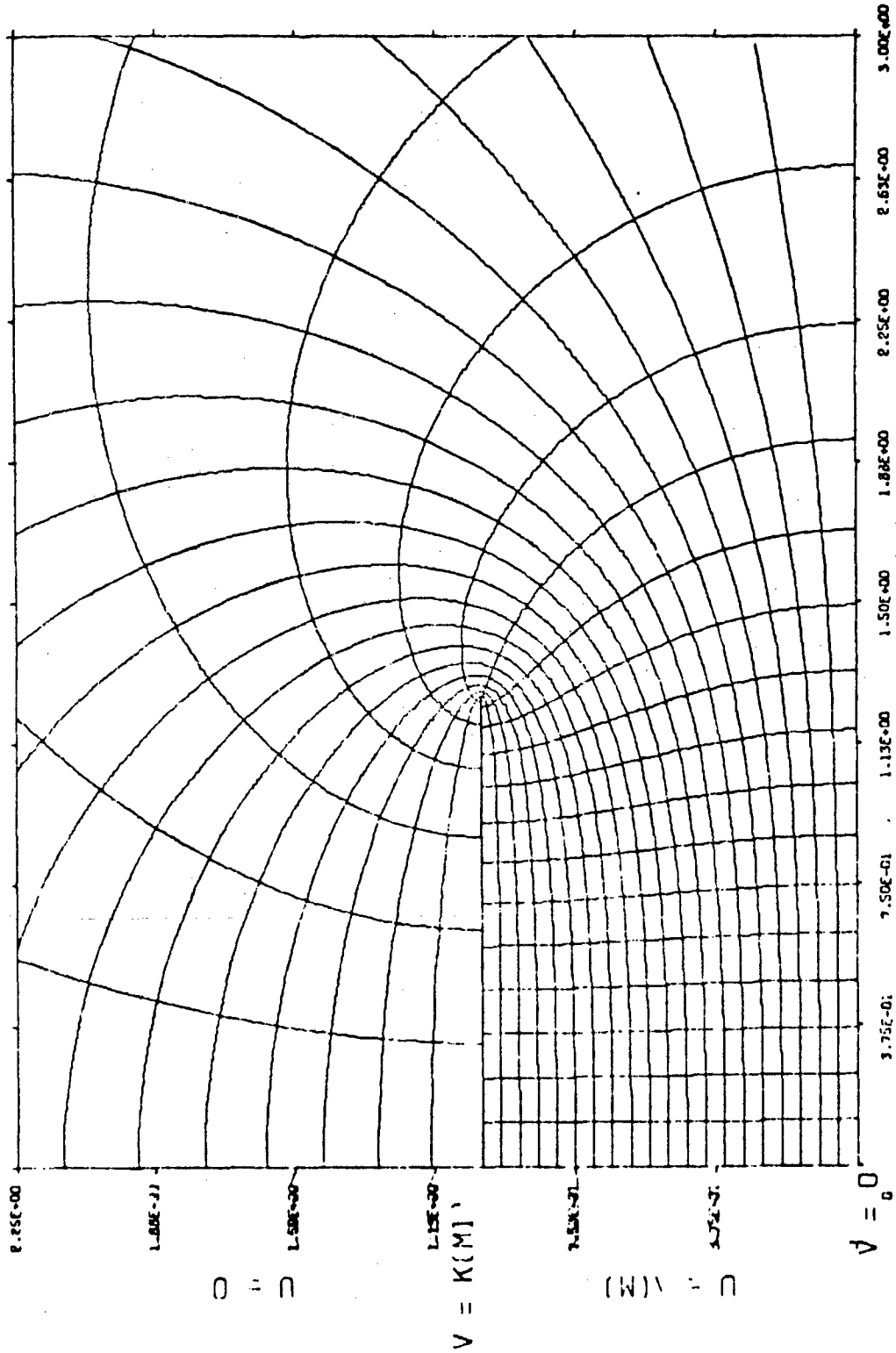
FIELD AND POTENTIAL DISTRIBUTION
FOR PARALLEL, TWO-PLATE TRANSMISSION LINE. 156.37 OHMS
B/A = .80
V = K(M)'
U = 0
U = K(M)
V = 0

FIGURE 12:

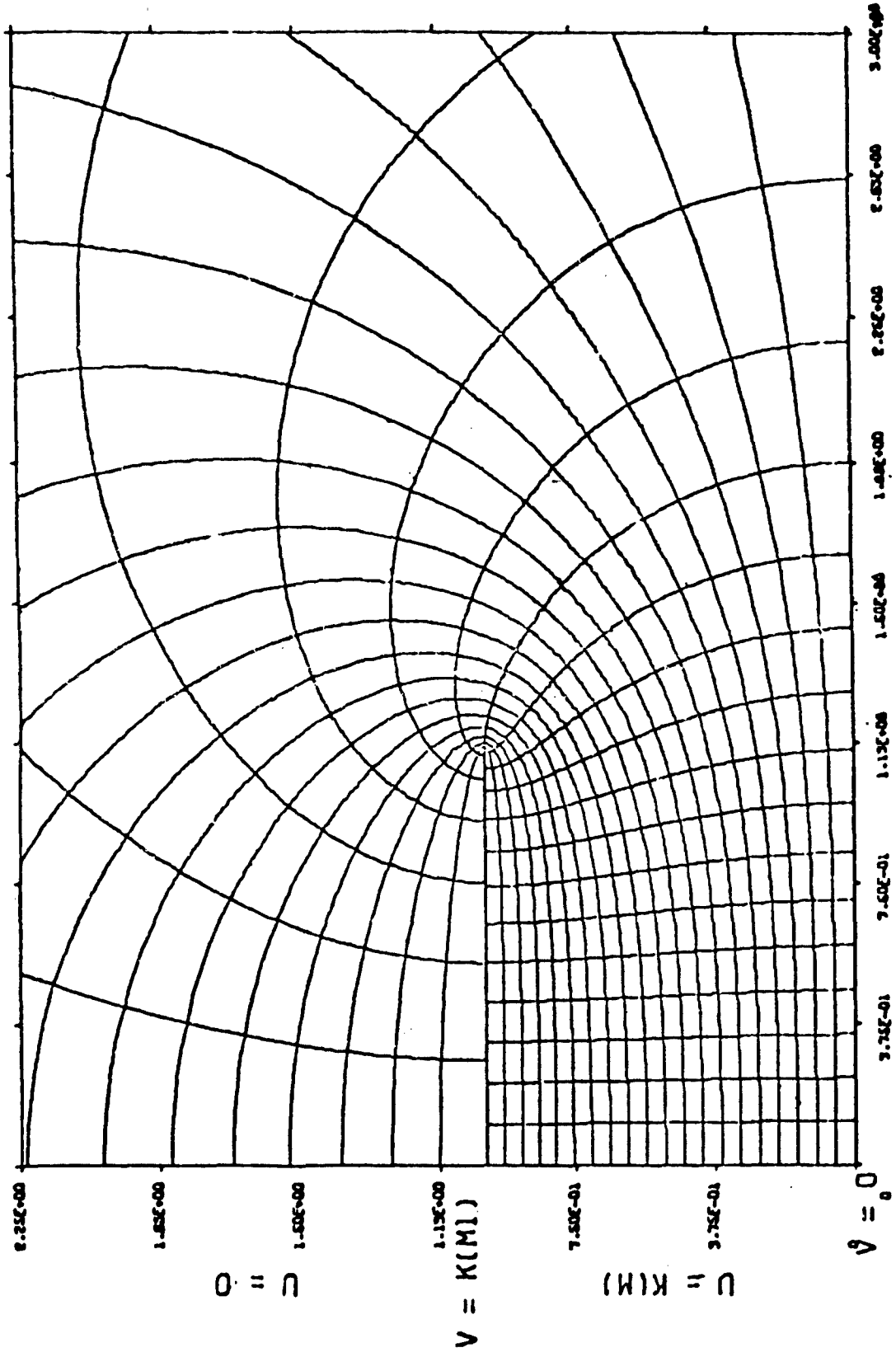

FIGURE 13: FIELD AND POTENTIAL DISTRIBUTION
FOR PARALLEL, TWO-PLATE TRANSMISSION LINE. 167.71 OHMS
B/A = .90

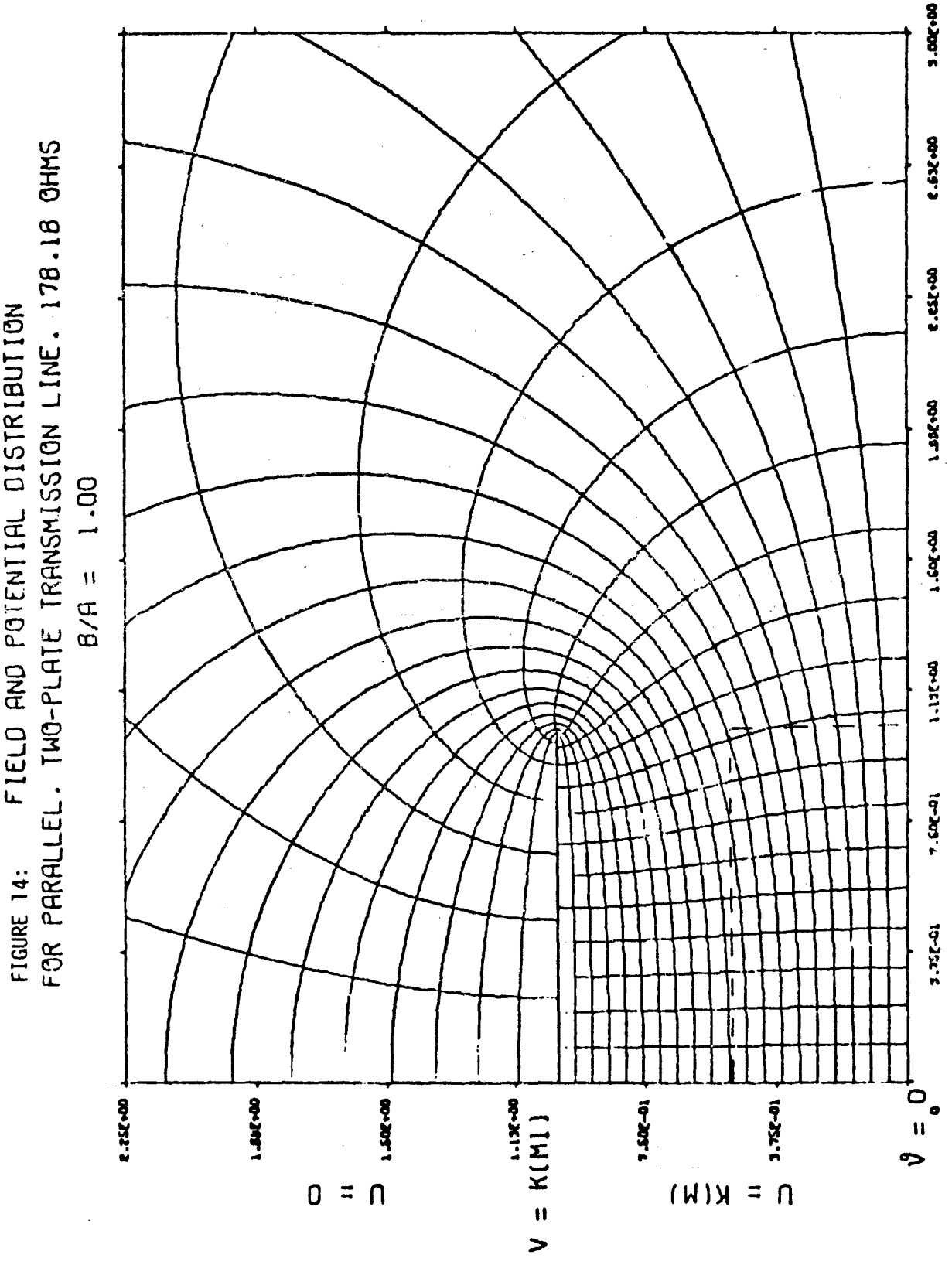

FIGURE 14: FIELD AND POTENTIAL DISTRIBUTION
FOR PARALLEL. TWO-PLATE TRANSMISSION LINE. 178.18 OHMS
B/A = 1.00

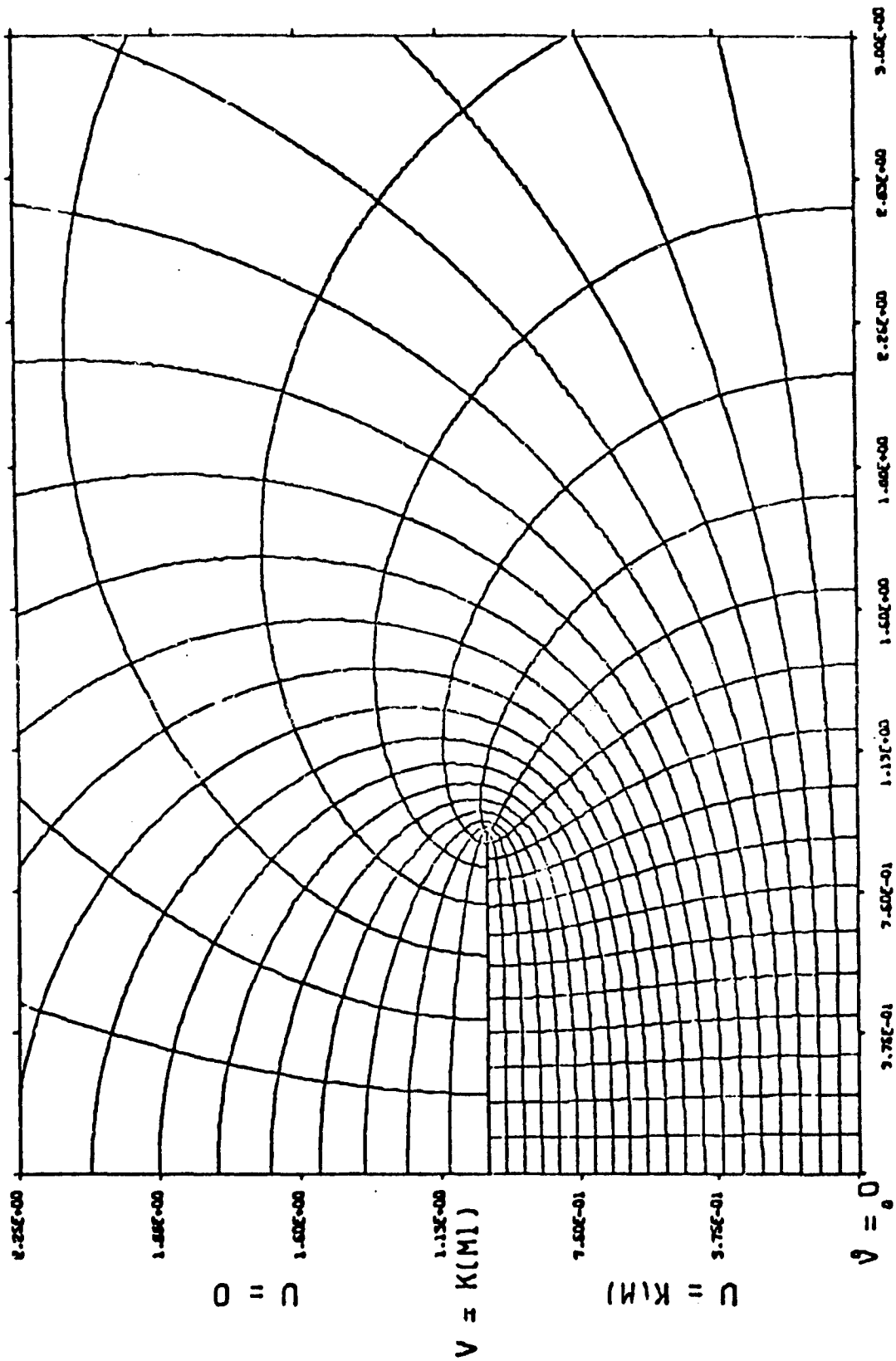

FIGURE 15: FIELD AND POTENTIAL DISTRIBUTION
FOR PARALLEL. TWO-PLATE TRANSMISSION LINE. 187.90 OHMS
B/A = 1.10

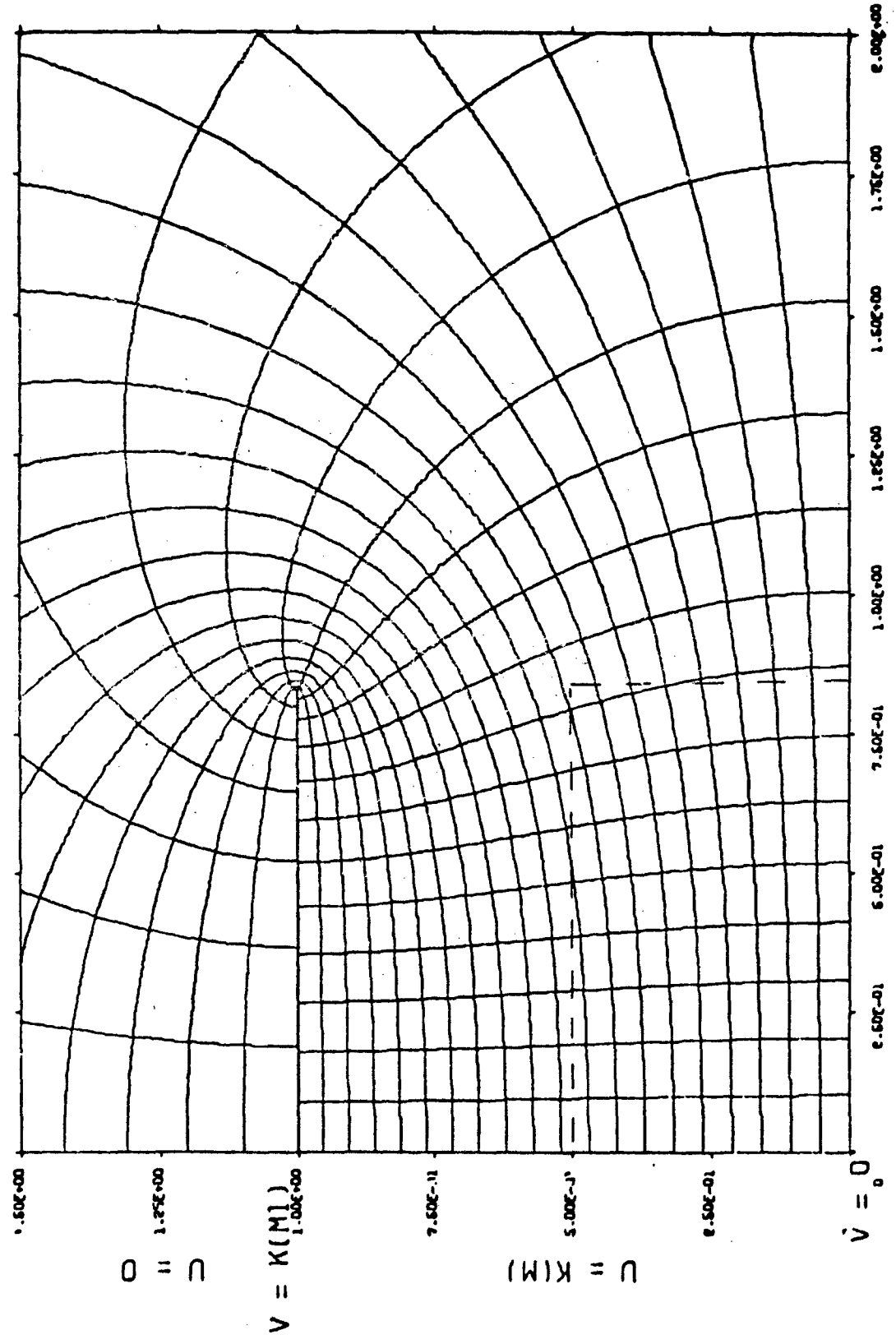

FIGURE 16: FIELD AND POTENTIAL DISTRIBUTION
FOR PARALLEL. TWO-PLATE TRANSMISSION LINE. 196.96 OHMS
B/A = 1.20

FIGURE 17: FIELD AND POTENTIAL DISTRIBUTION
FOR PARALLEL. TWO-PLATE TRANSMISSION LINE. 205.44 OHMS
B/A = 1.30

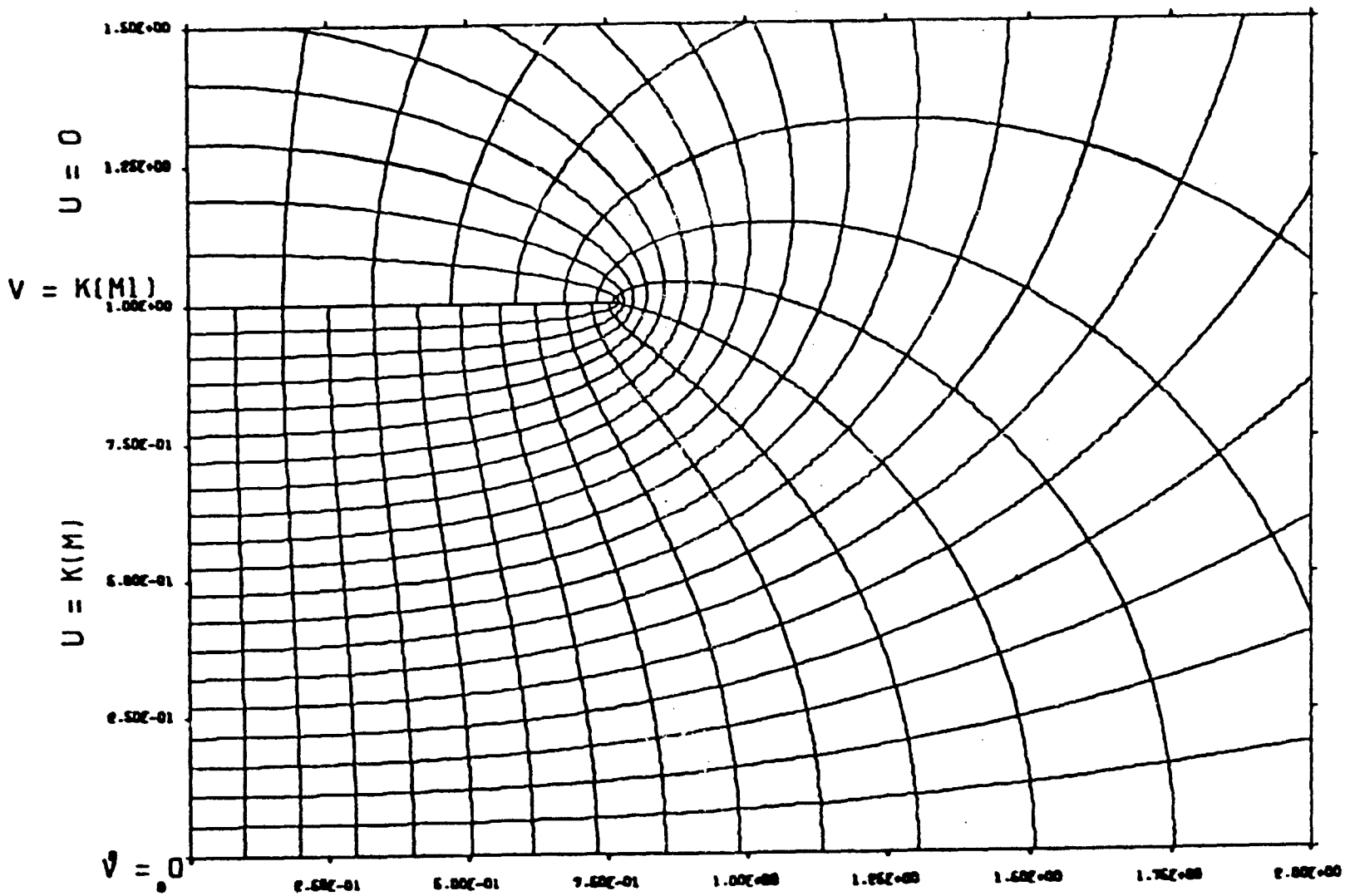

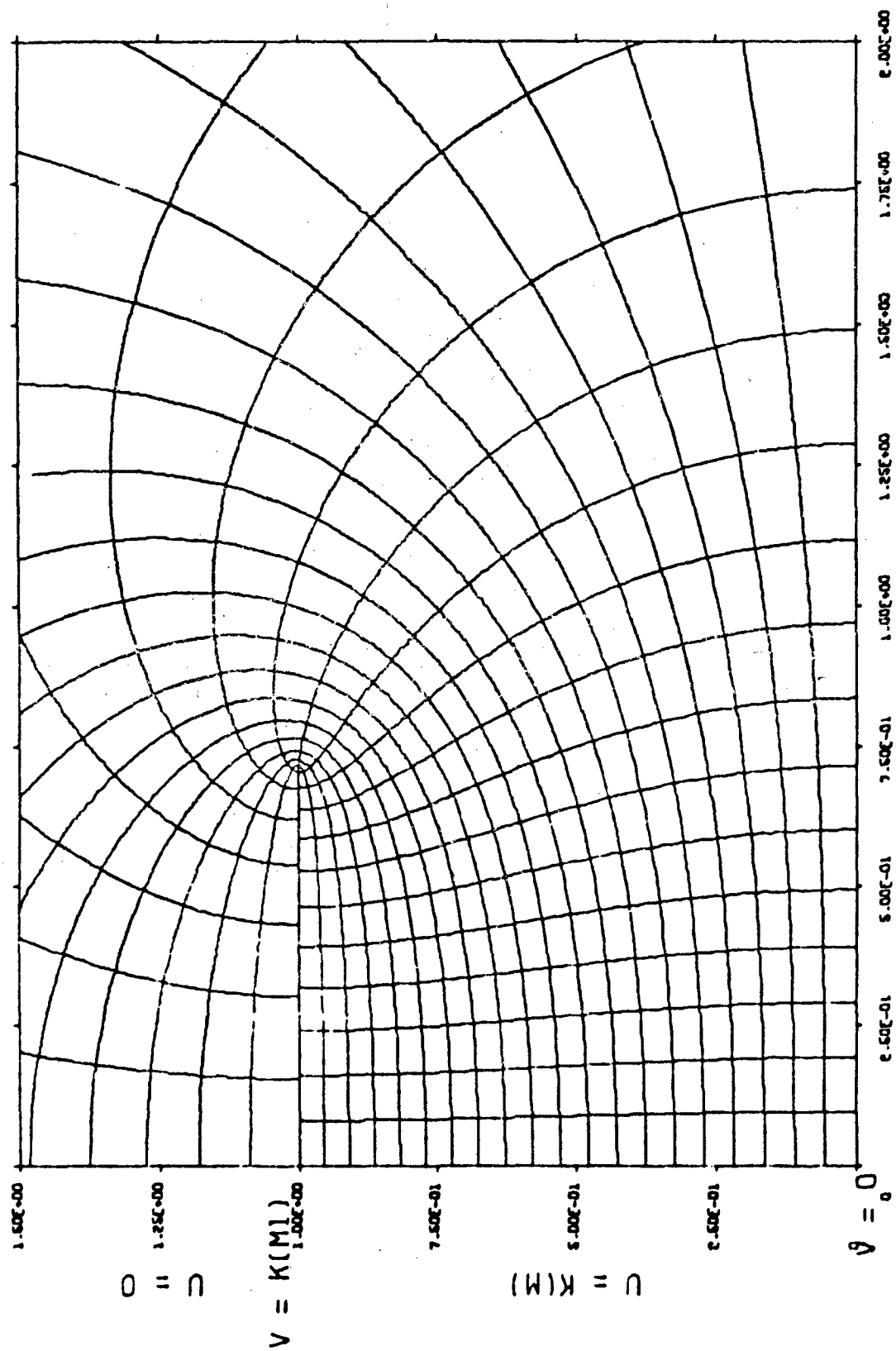

FIGURE 18: FIELD AND POTENTIAL DISTRIBUTION
FOR PARALLEL, TWO-PLATE TRANSMISSION LINE. 213.41 OHMS
B/A = 1.40

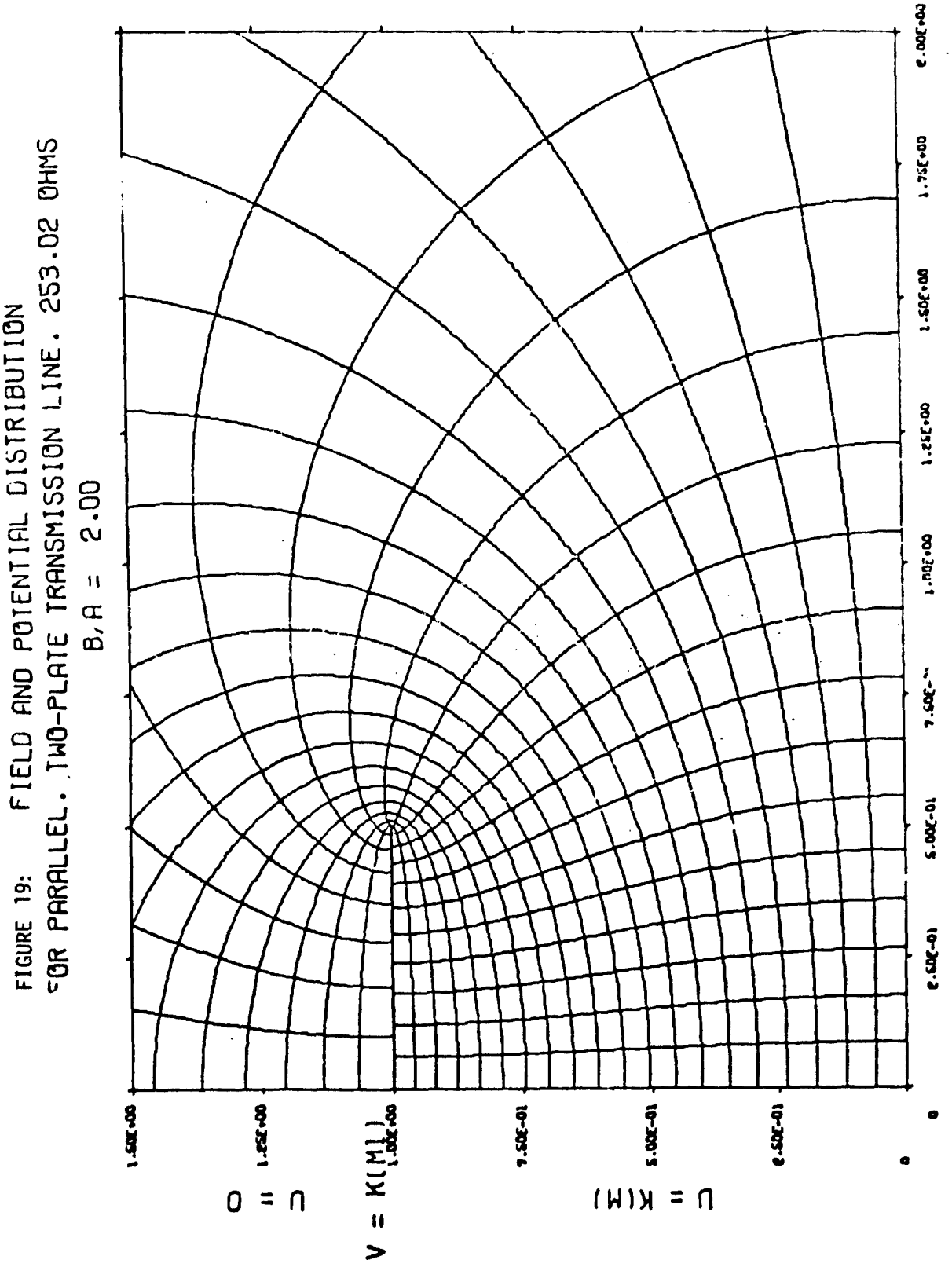

FIGURE 19: FIELD AND POTENTIAL DISTRIBUTION FOR PARALLEL. TWO-PLATE TRANSMISSION LINE. 253.02 OHMS B/A = 2.00

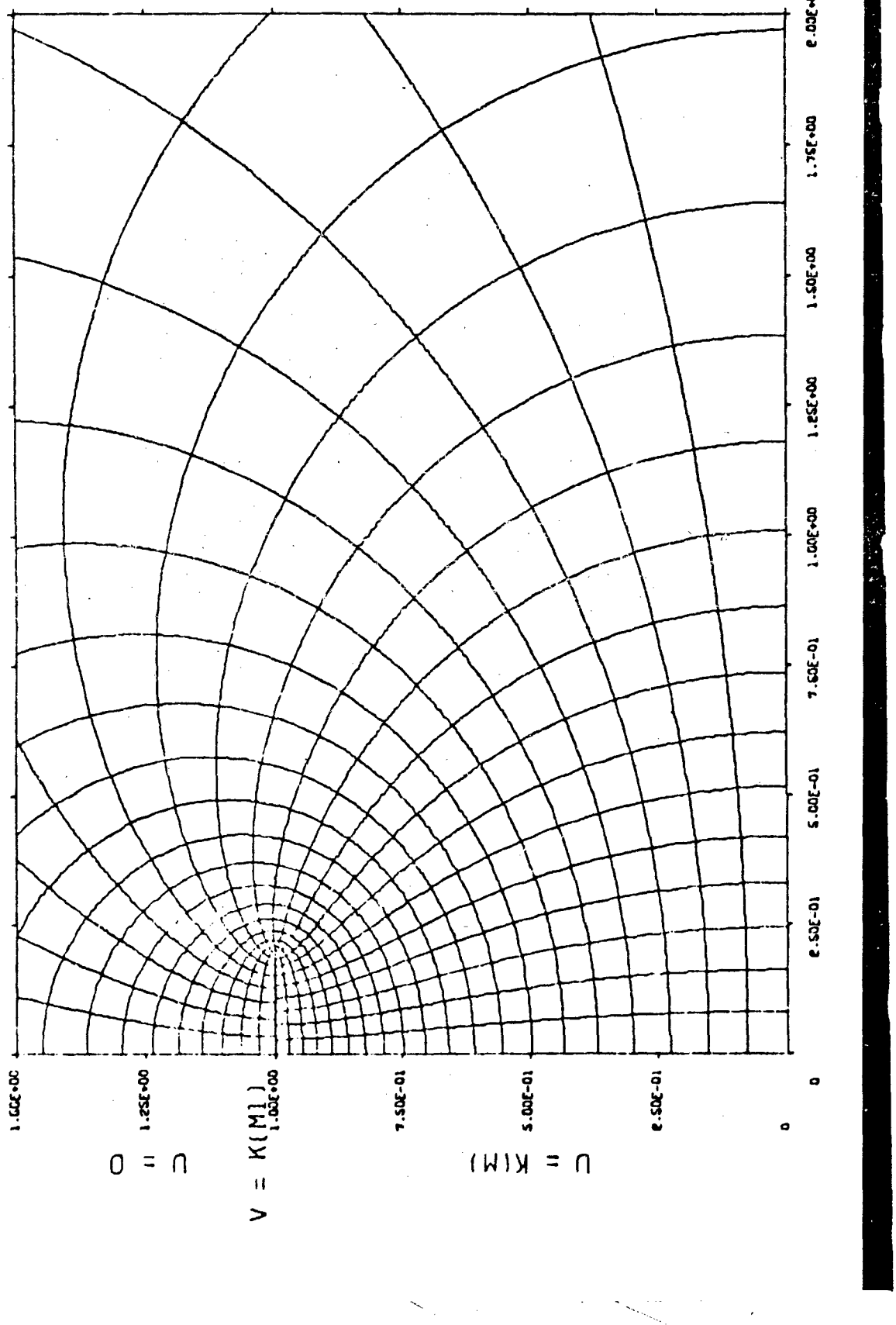

FIGURE 20: FIELD AND POTENTIAL DISTRIBUTION
FOR PARALLEL. TWO-PLATE TRANSMISSION LINE. 360.08.OHMS
B/A = 5.00

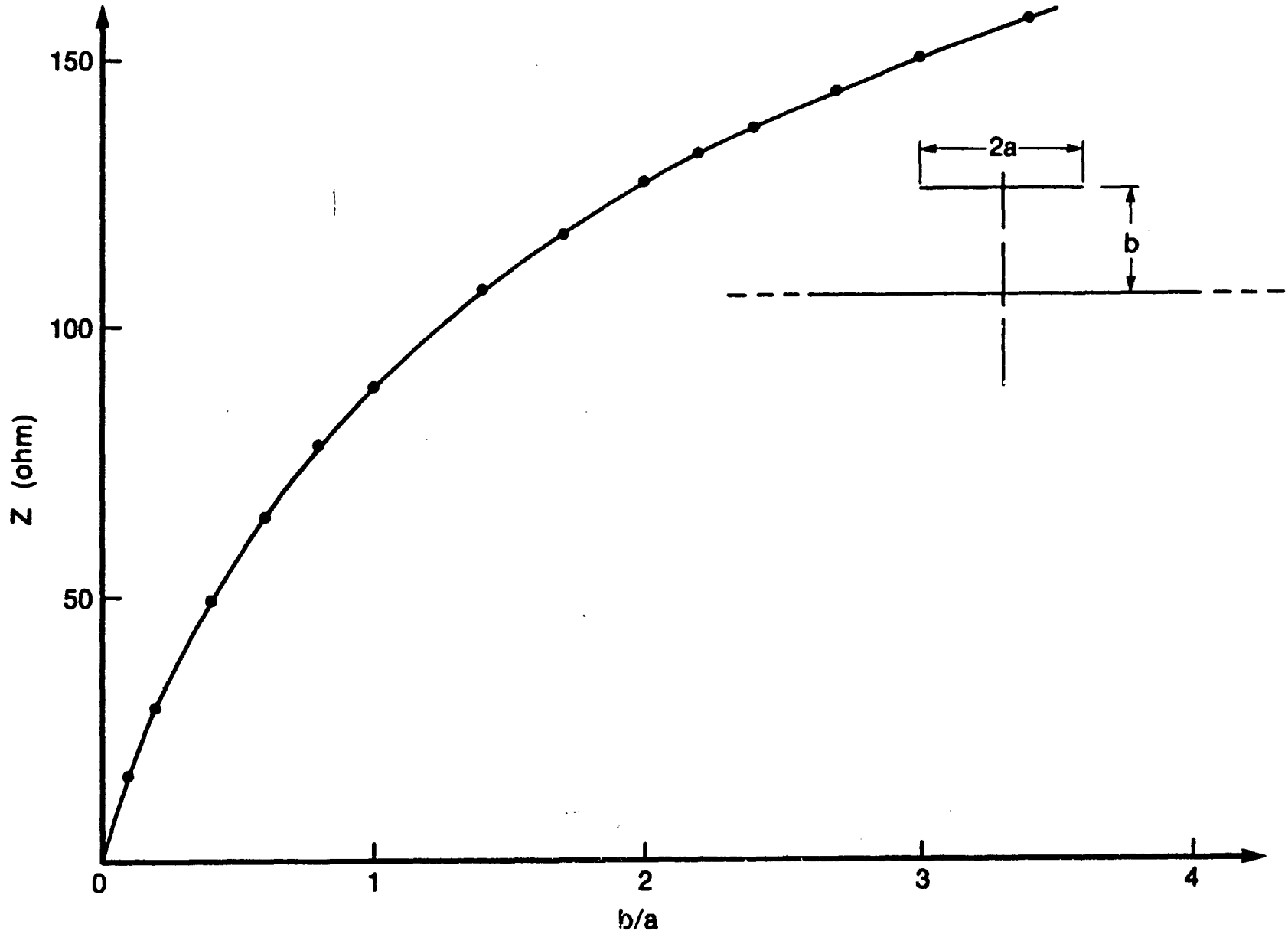

Figure 21: Impedance of asymmetric two plate lines.

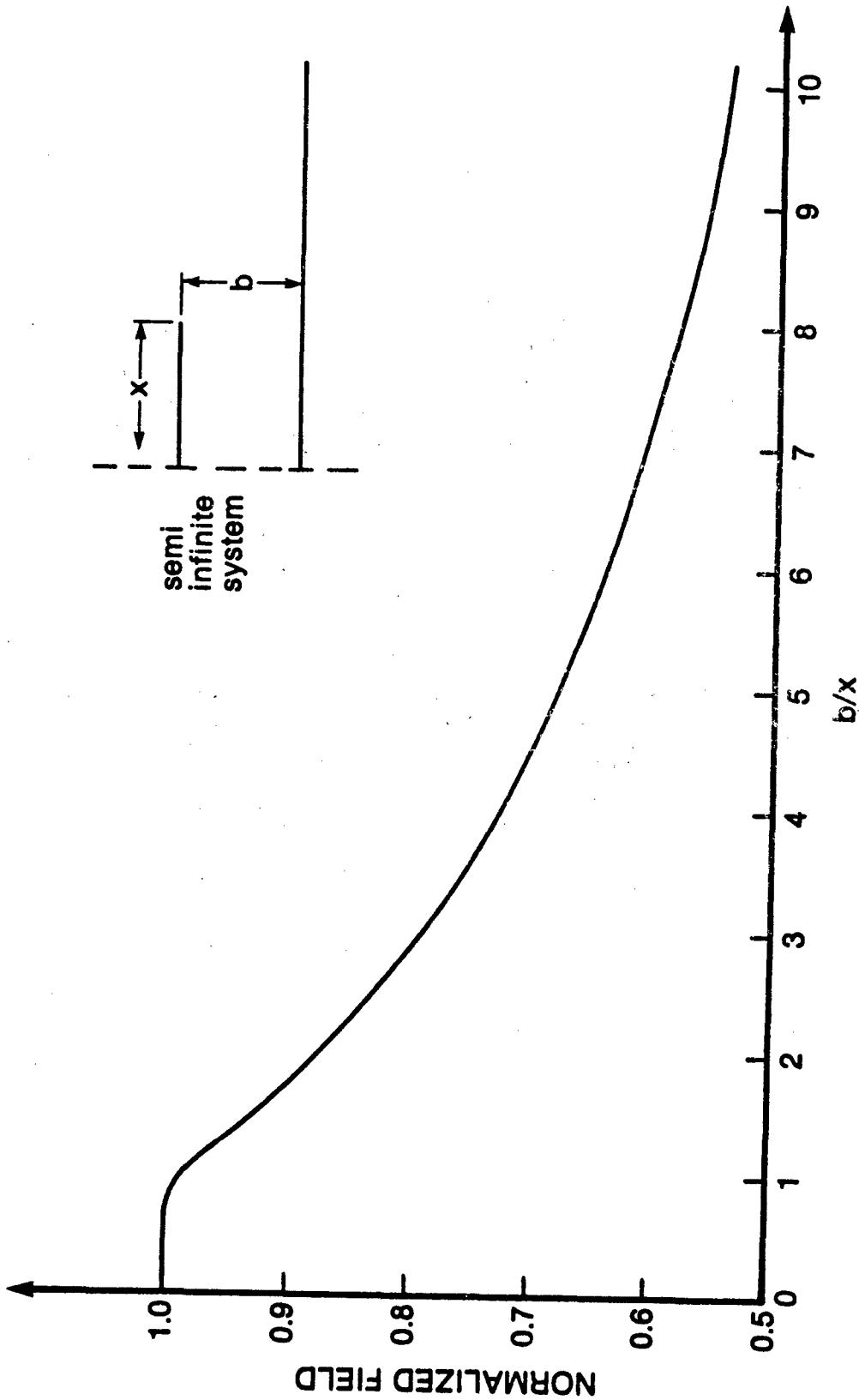

Figure 22: Field variations across a two plate transmission line.

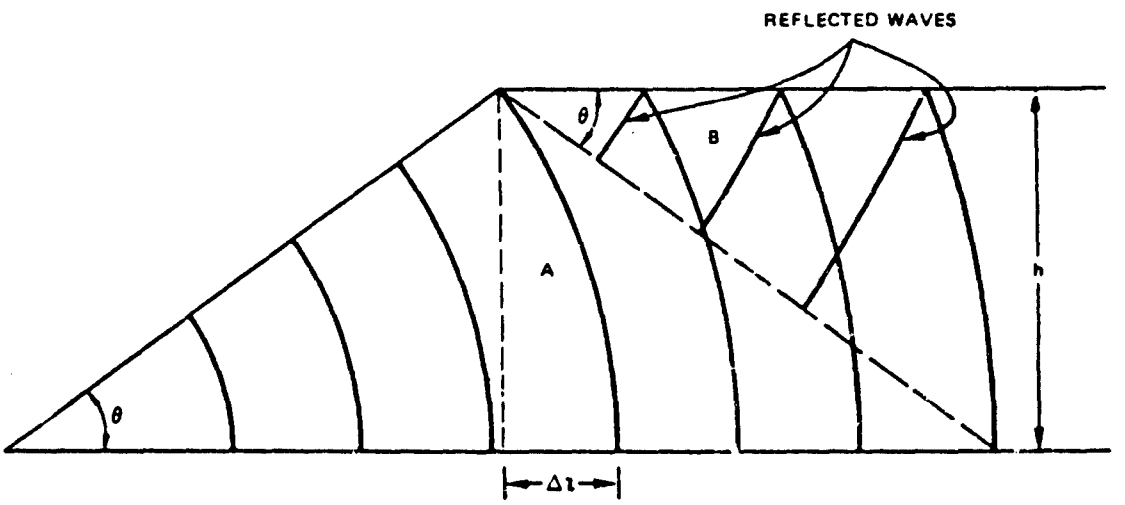

Figure 23: Wave front field structure in a transmission line simulator.

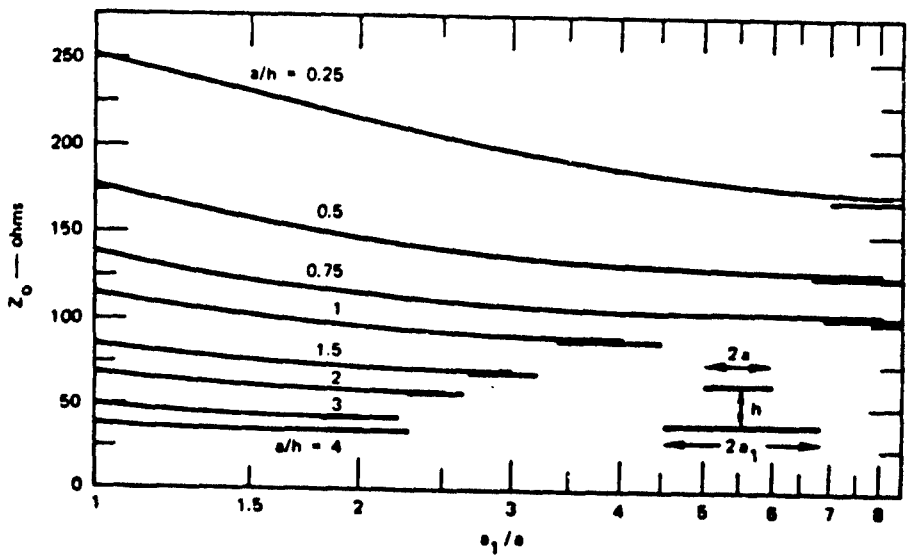

Figure 24: Transmission line impedance as a function of the lower plate width.

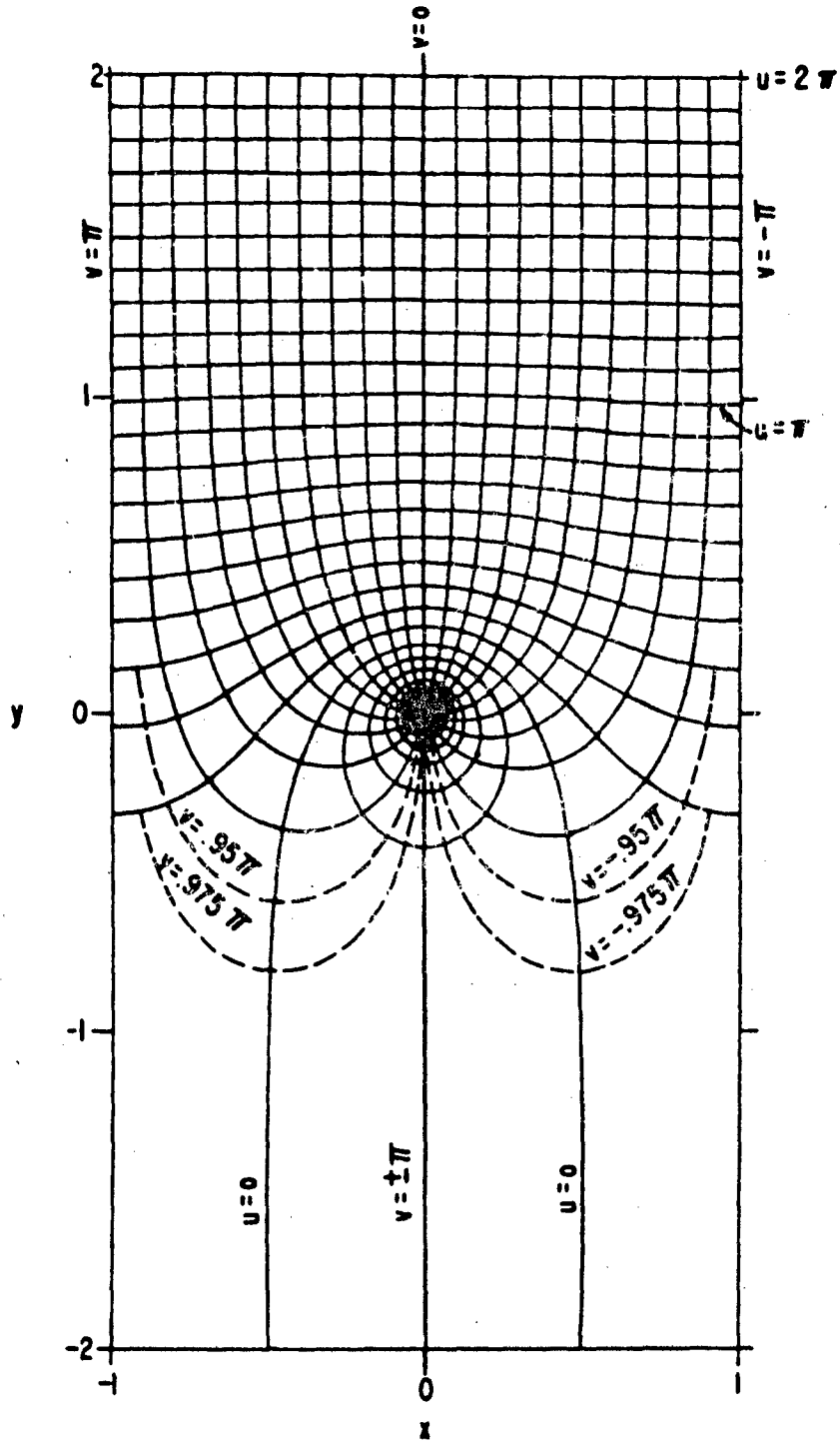

FIGURE 25: WIRE GRID (ONE CELL) TERMINATING UNIFORM FIELD ON ONE SIDE OF GRID

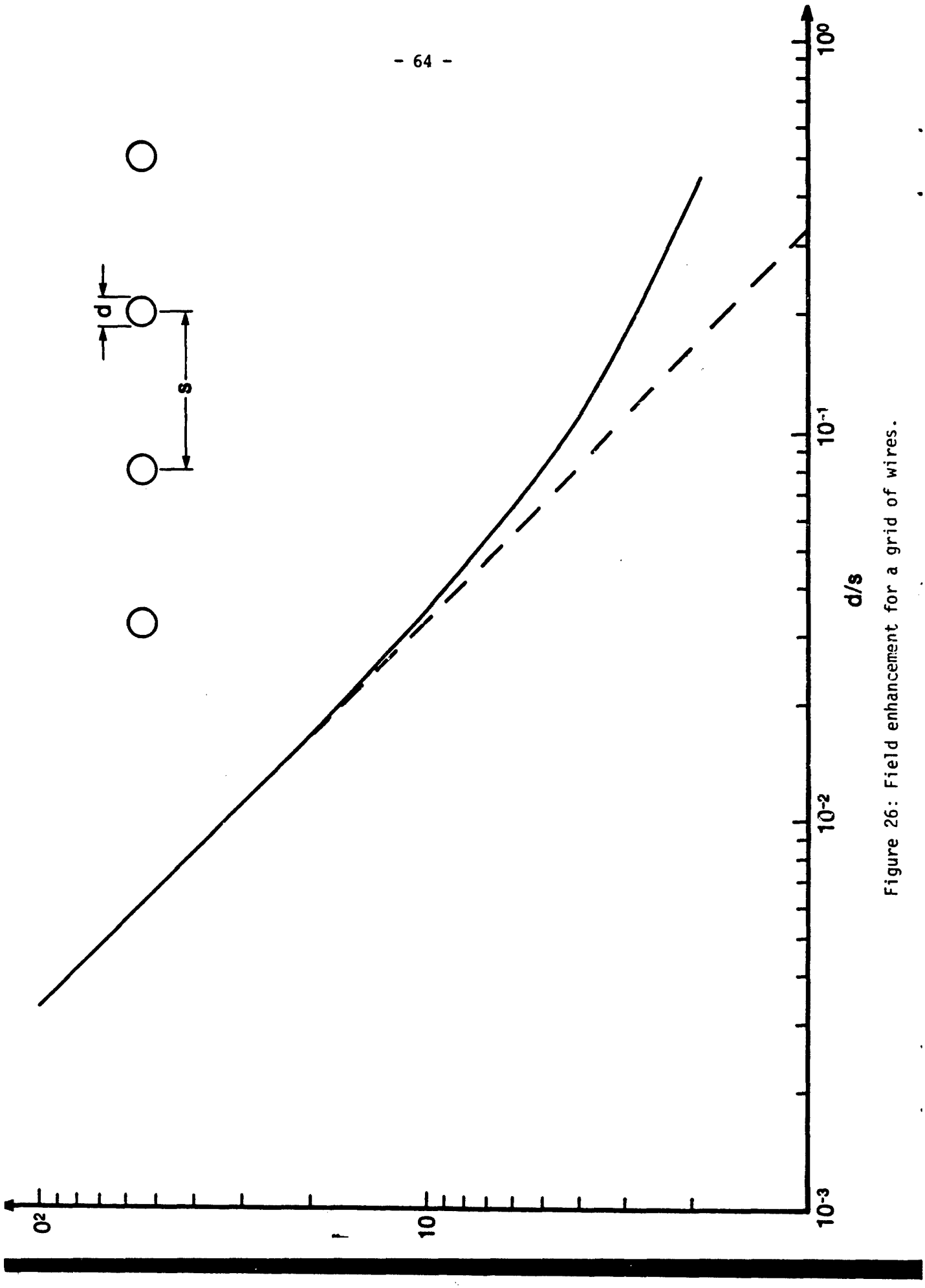

Figure 26: Field enhancement for a grid of wires.

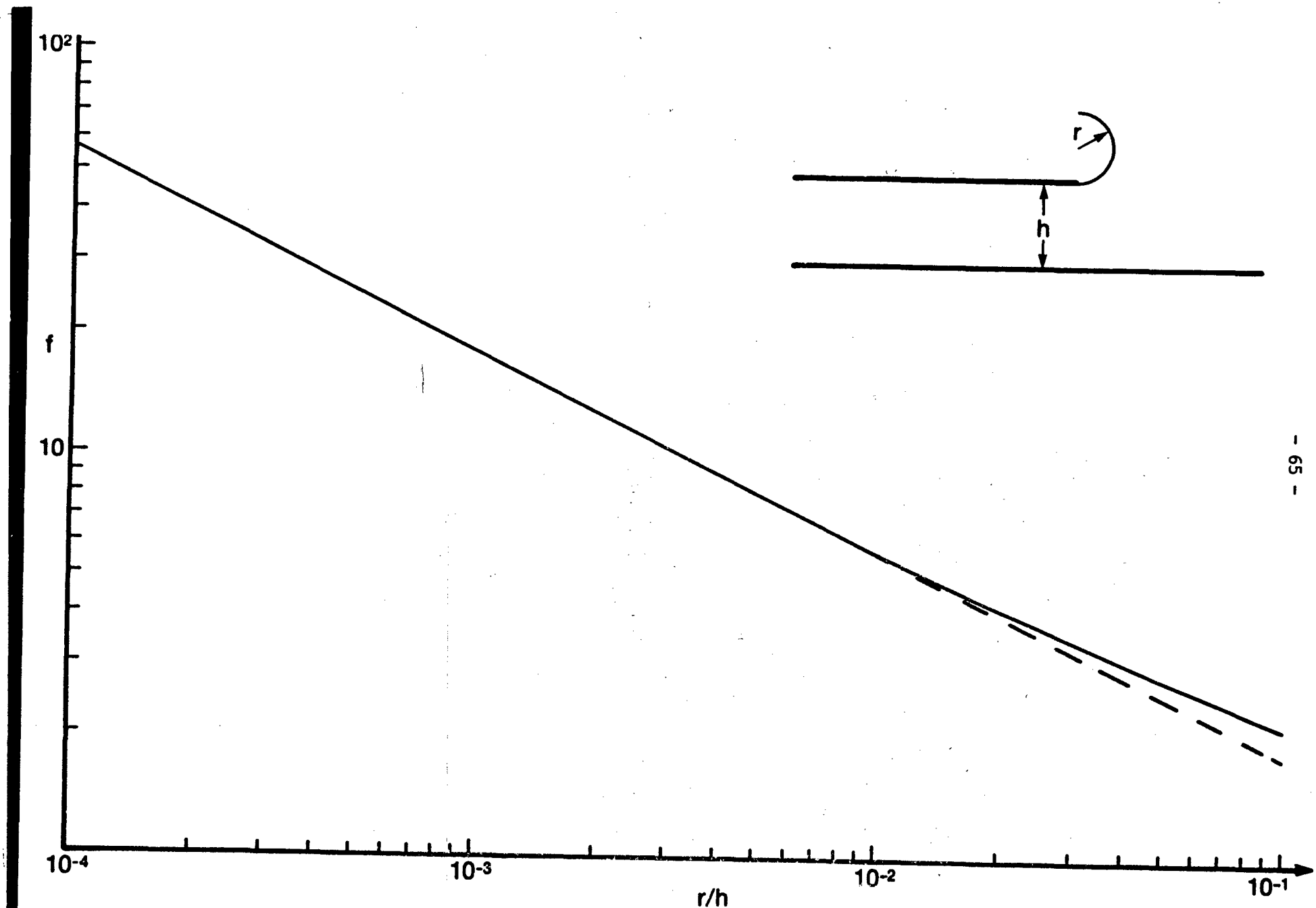

Figure 27: Field enhancement at edge of semi-infinite plate.

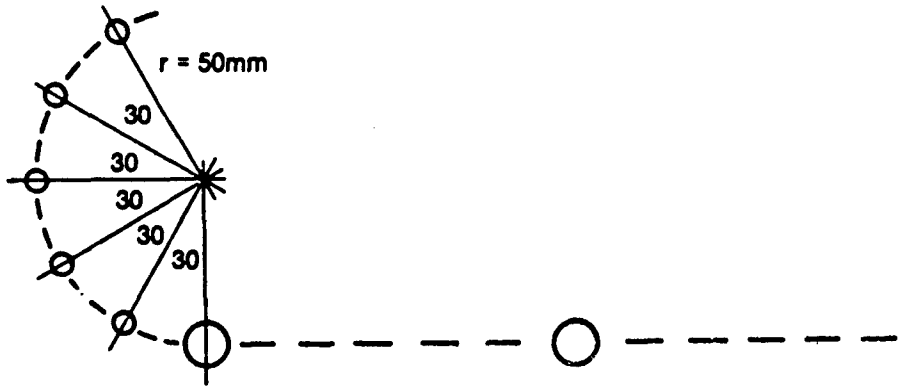

Figure 28: Rounding of the edges.

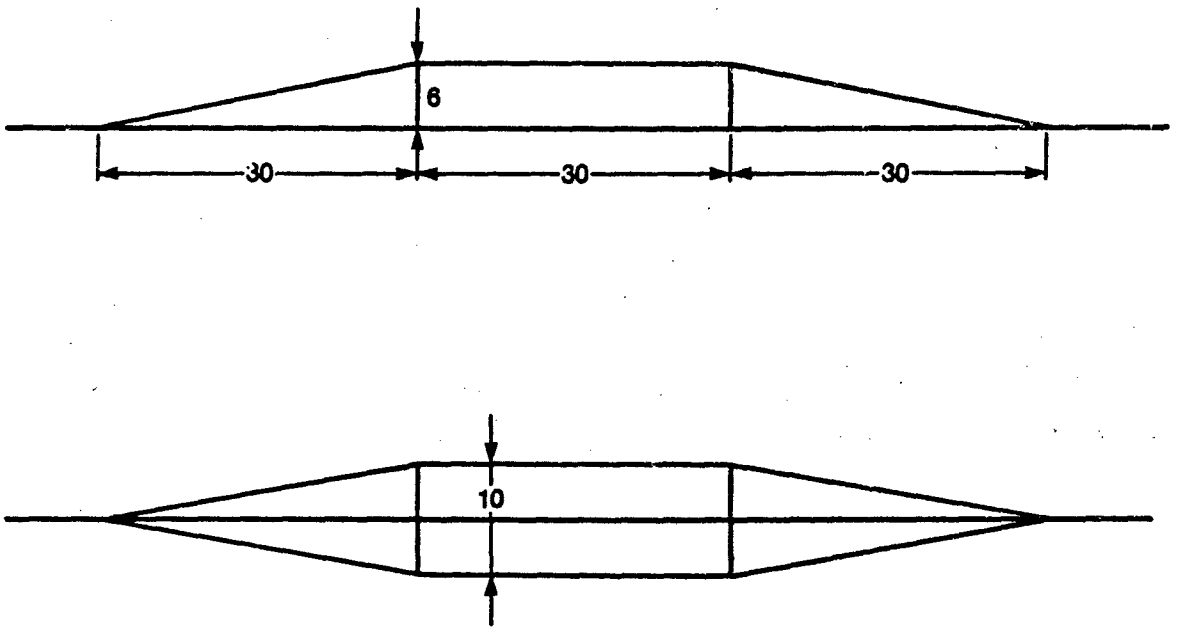

Figure 29: Dimensions of the 6 m-line.

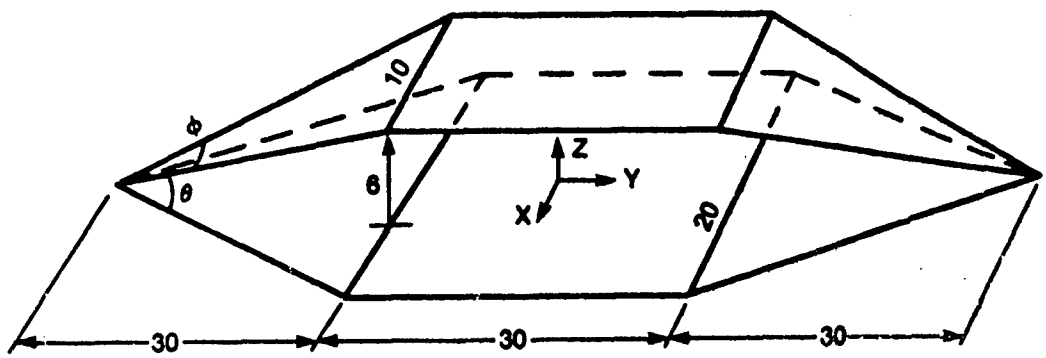

Elevation angle $\theta = 11.3°$
Apex angle $\phi = 18.6°$

Figure 30: Azimuth and elevation angle.

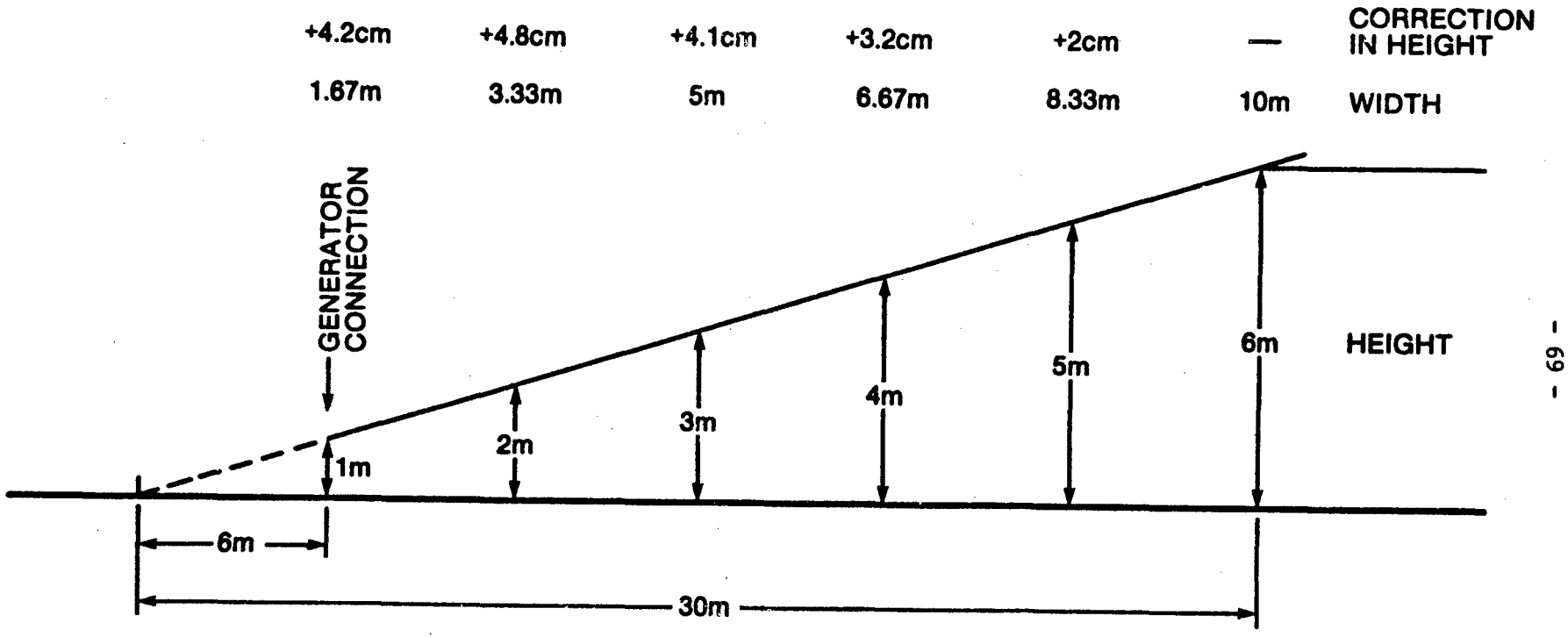

Figure 31: Correction for constant impedance of the launching taper.

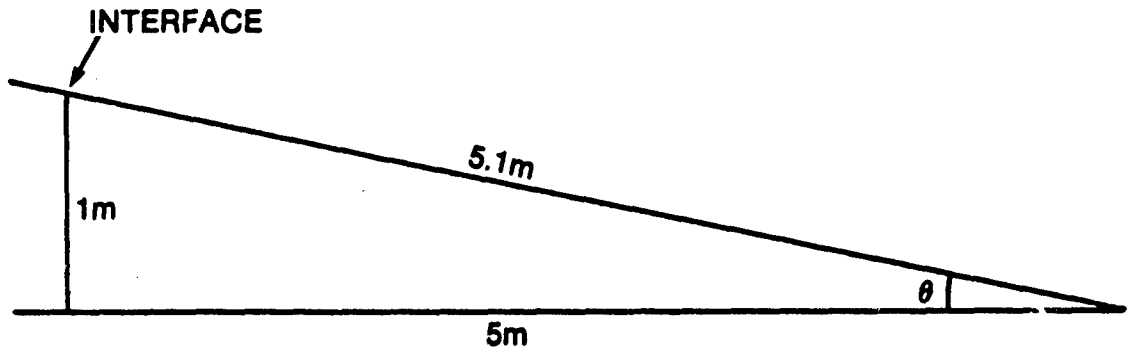

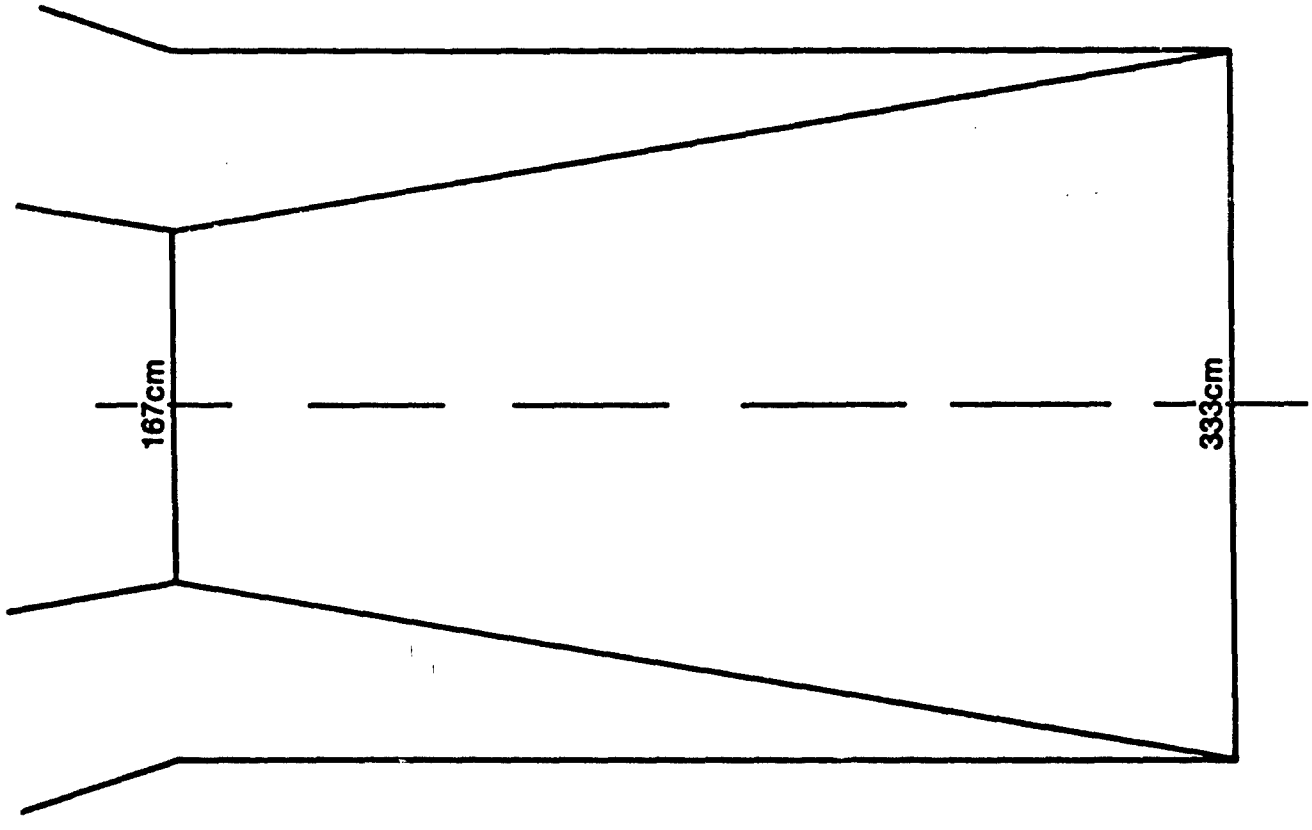

Figure 32: Dimensions of the terminating network.

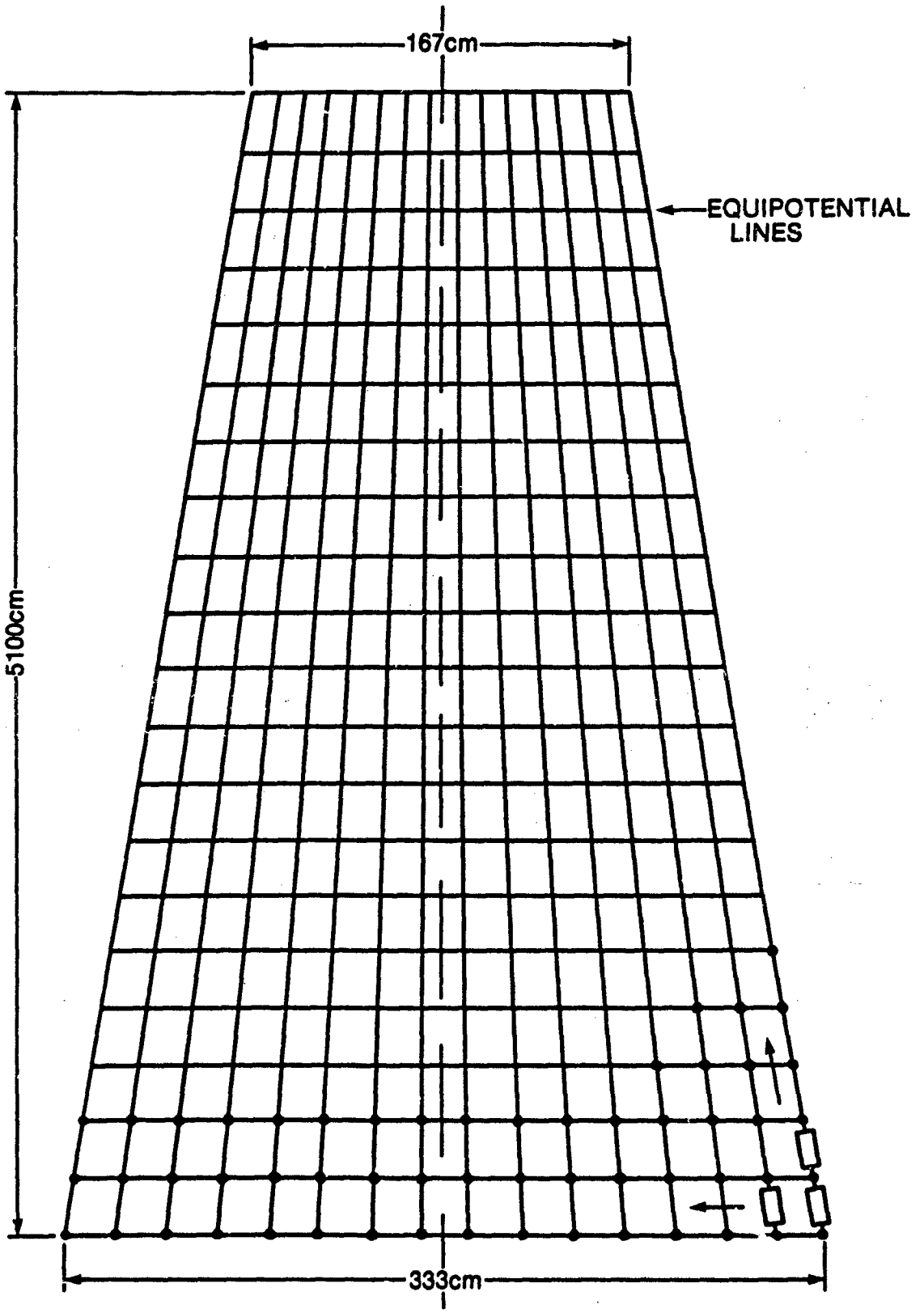

Figure 33: Terminating network 16 resistor-strings with 20 resistors each.

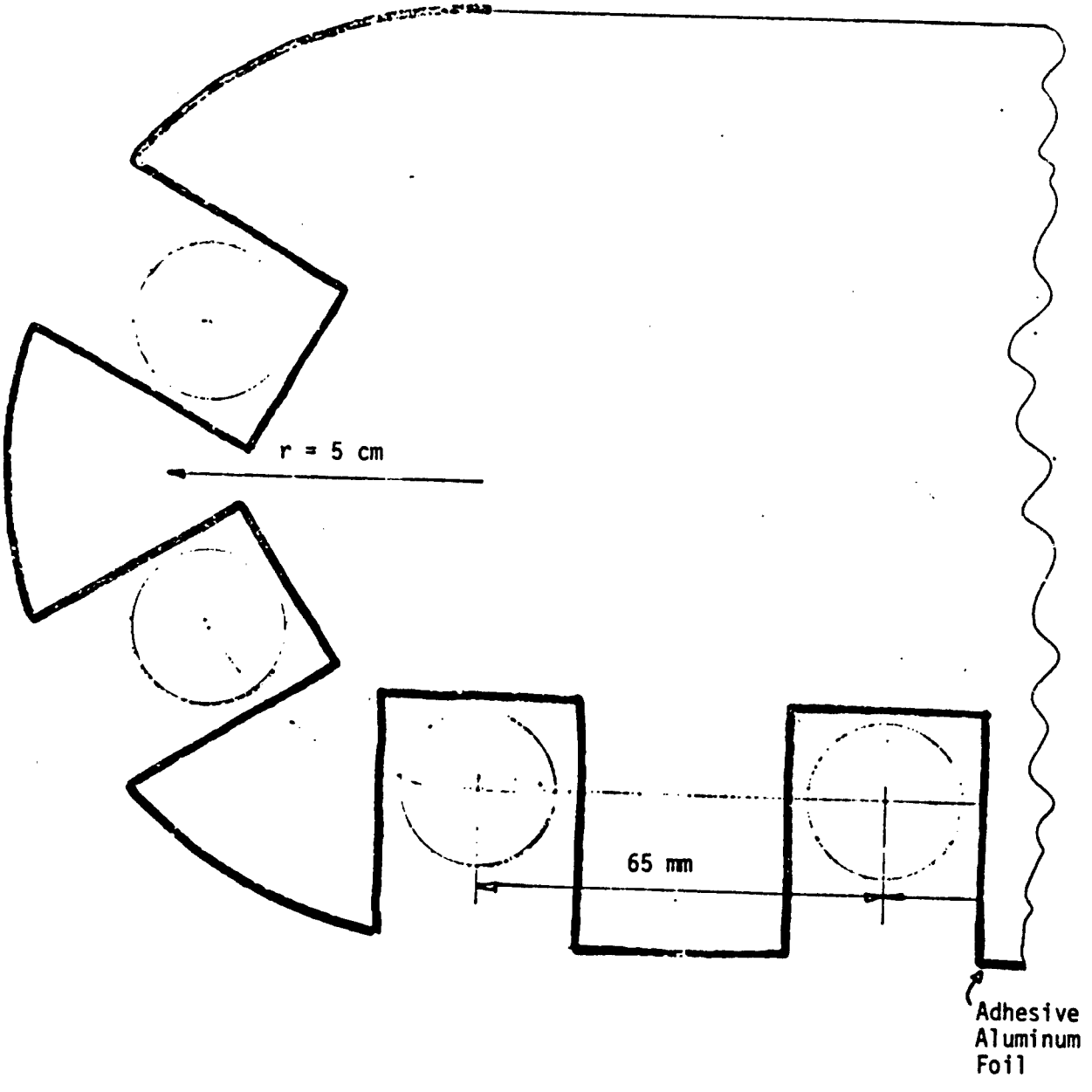

Figure 34: Detail of the edges of the wooden frame work.

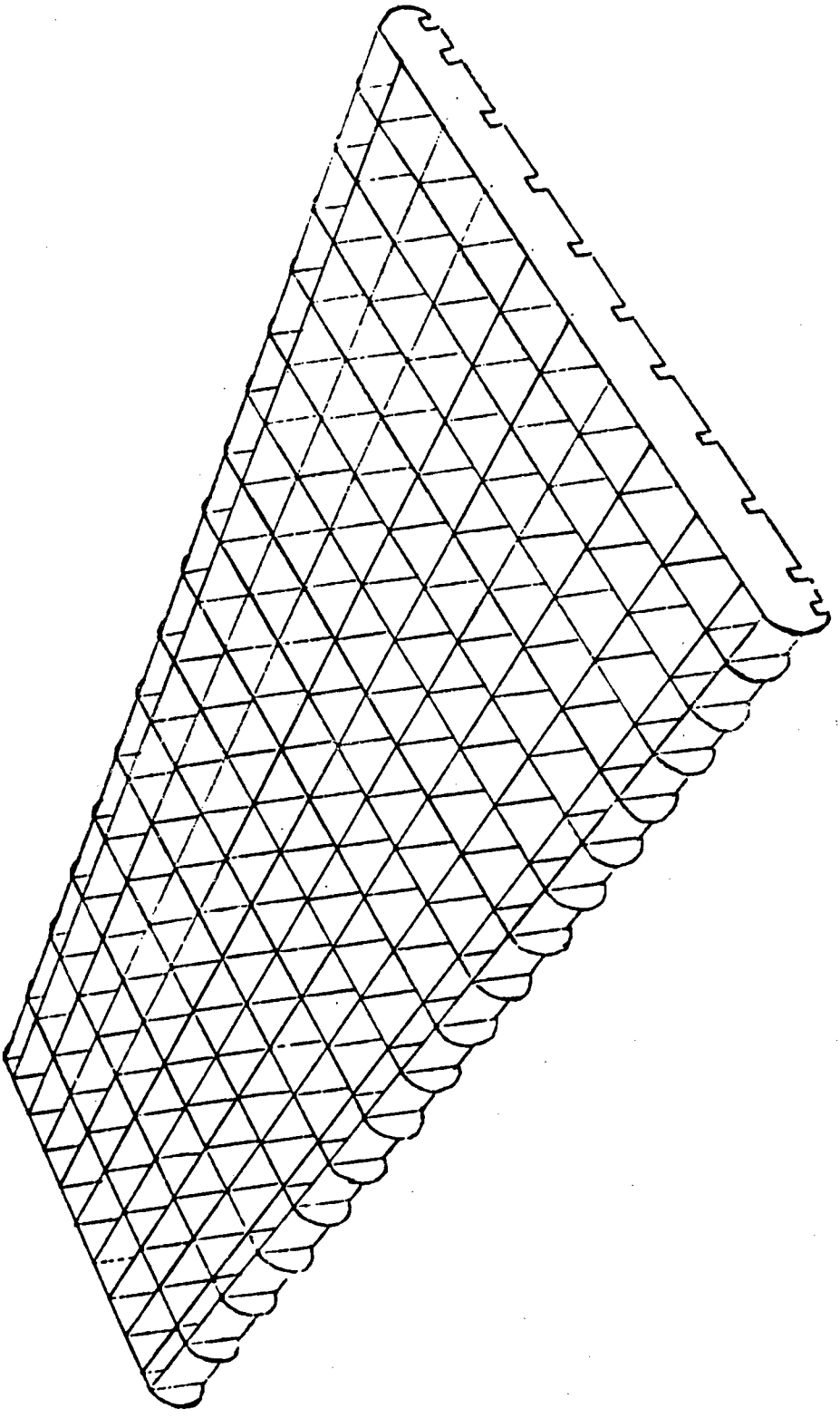

Figure 35: Example of a wood frame work (here 17 x 11 resistors).

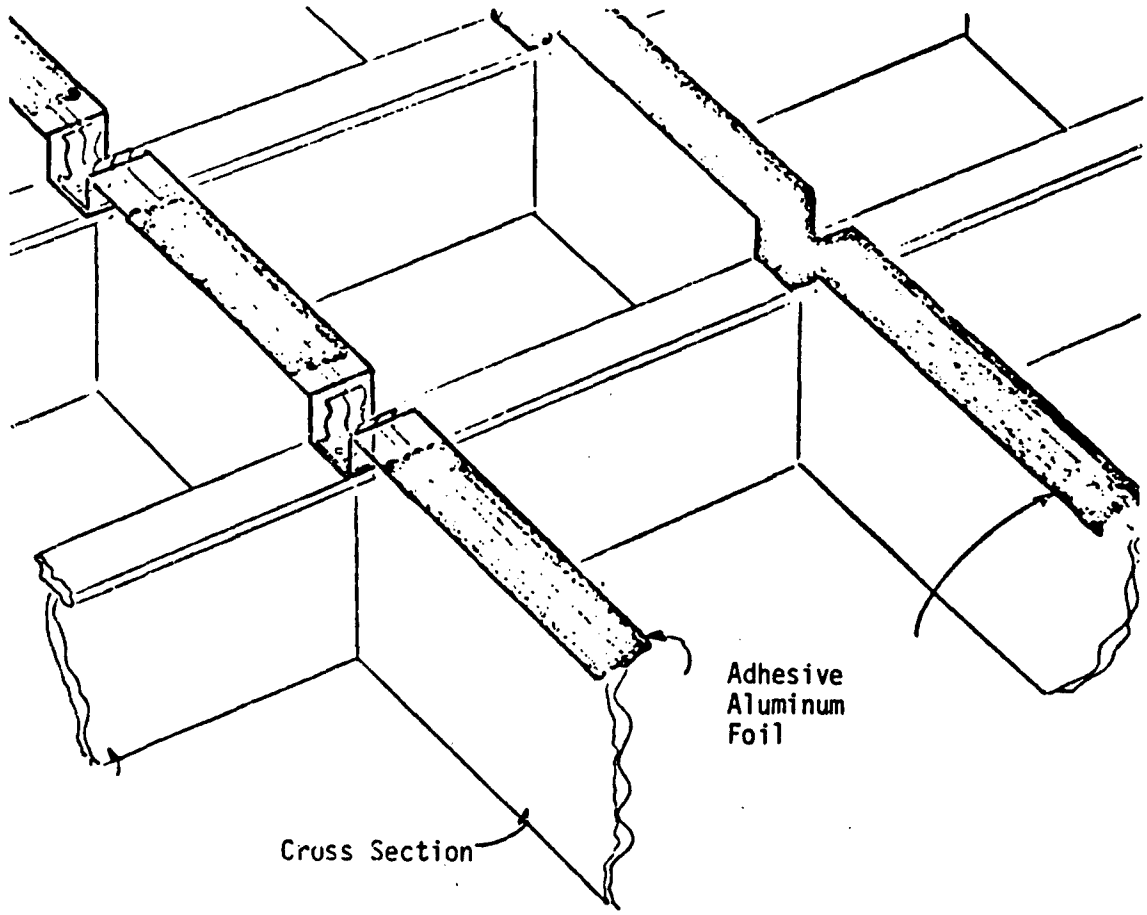

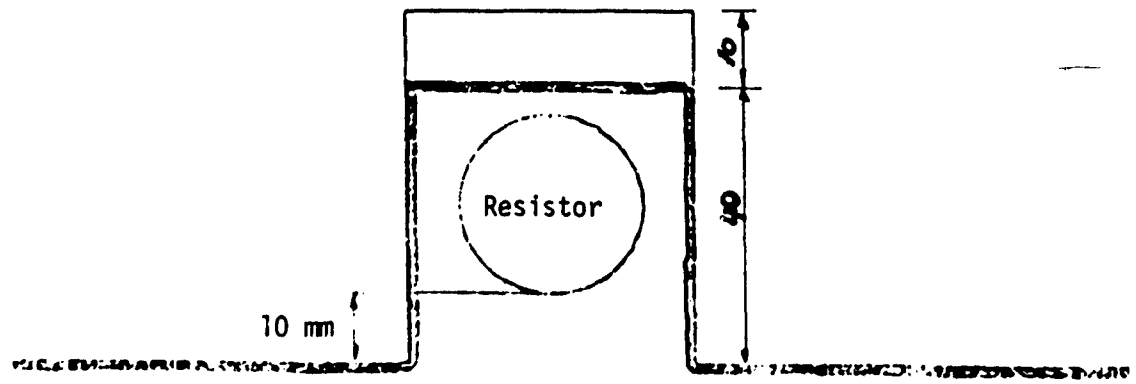

Figure 36: Some details of a wooden frame work.

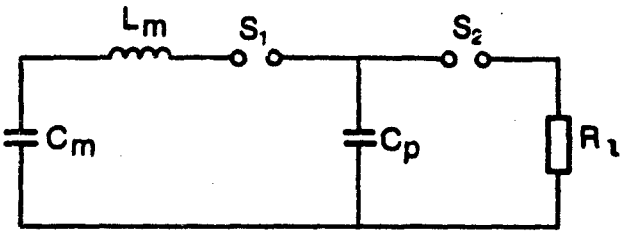

Figure 37: Peaking capacitor circuit.

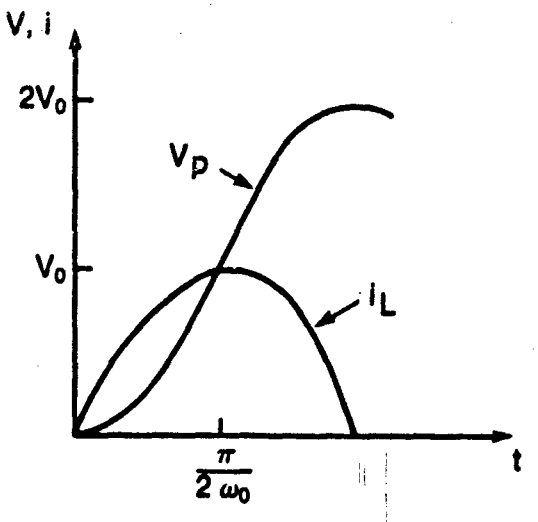

Figure 38: Current and voltage waveforms in peaking circuit.

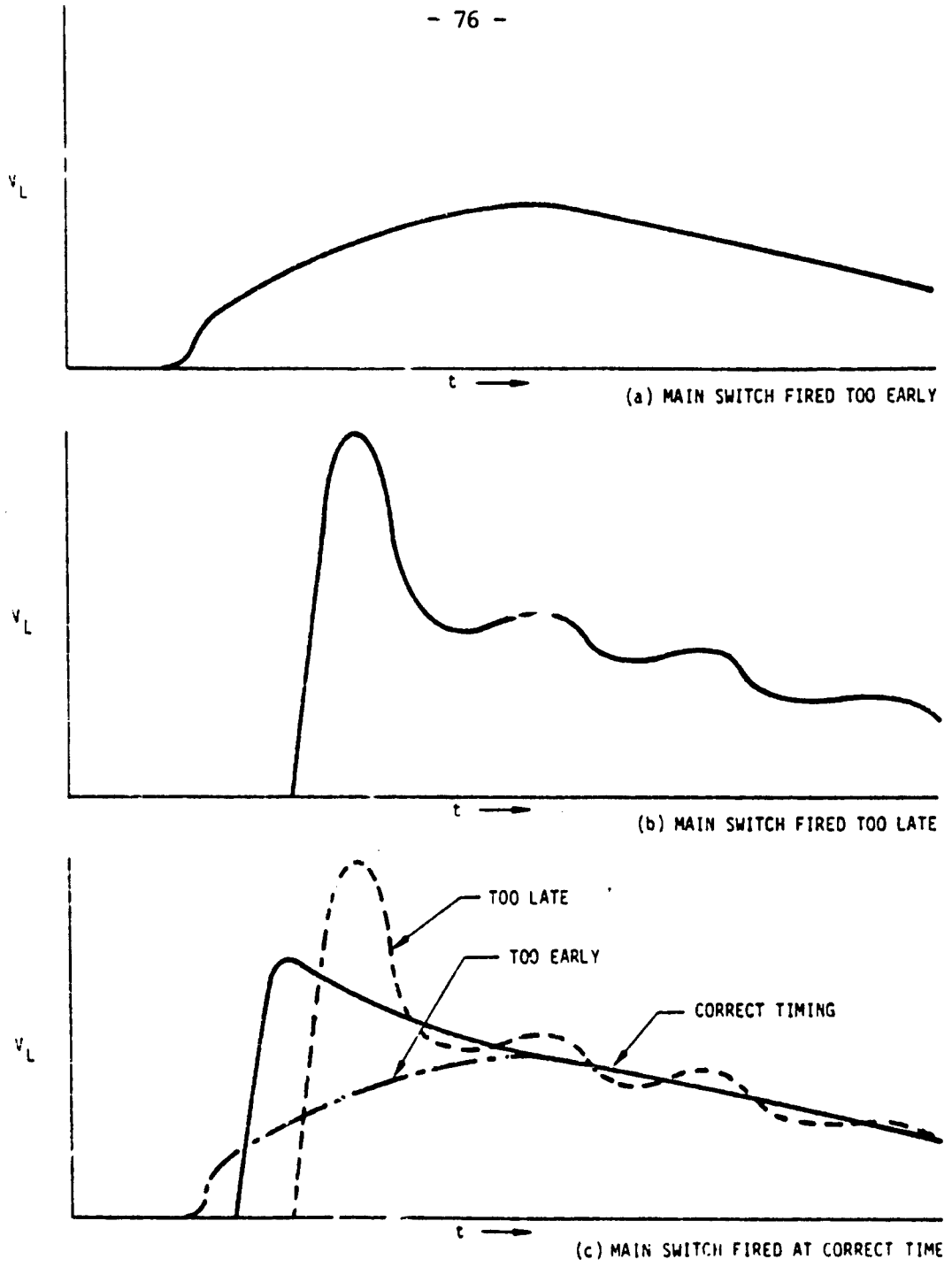

Figure 39: Effect of firing angle on peaking capacitor output pulse.

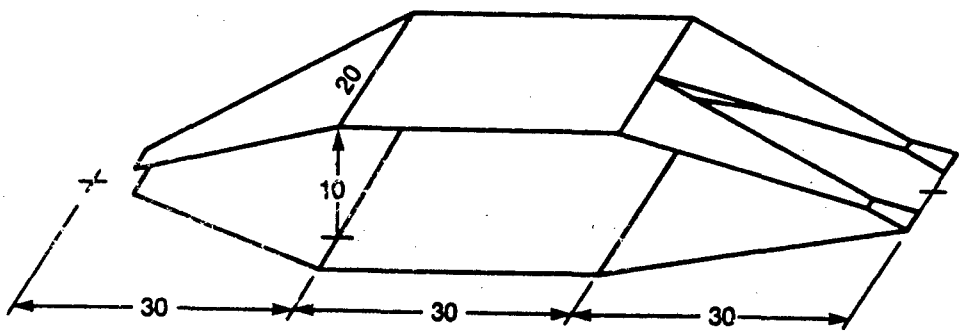

Width of ground plate at least 20m.

Figure 40: Dimensions of the 10 m-line.

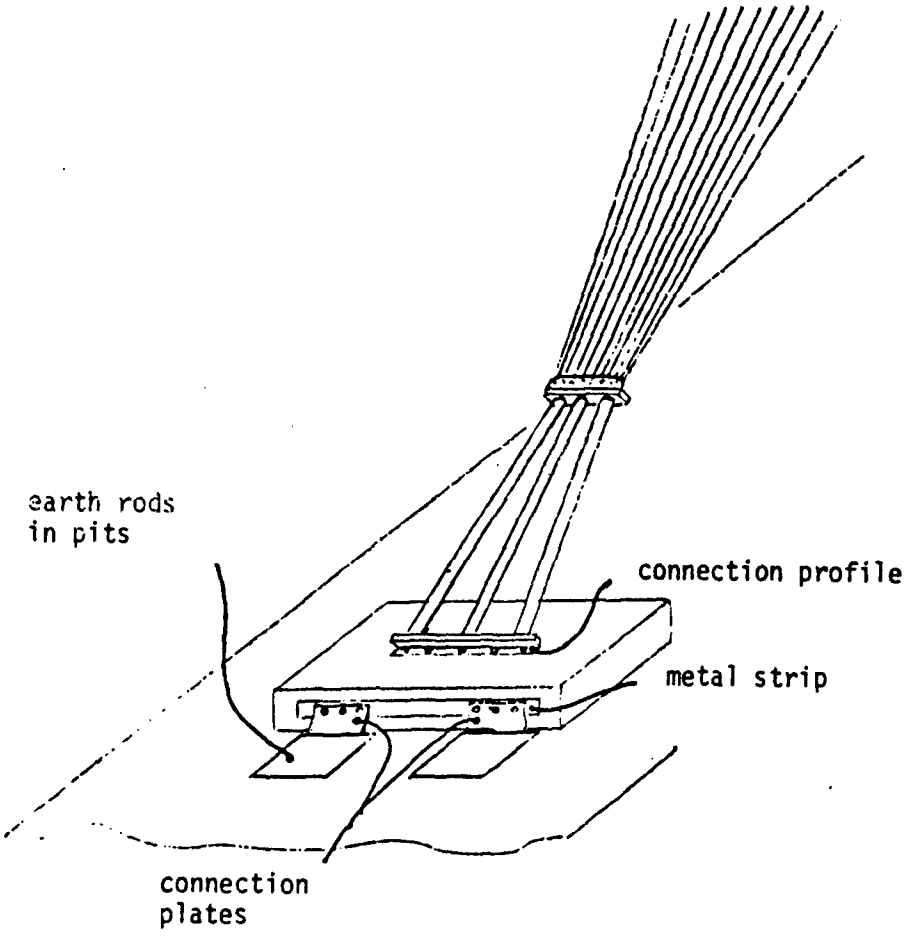

Figure 41: Terminating network in one of the tapers.

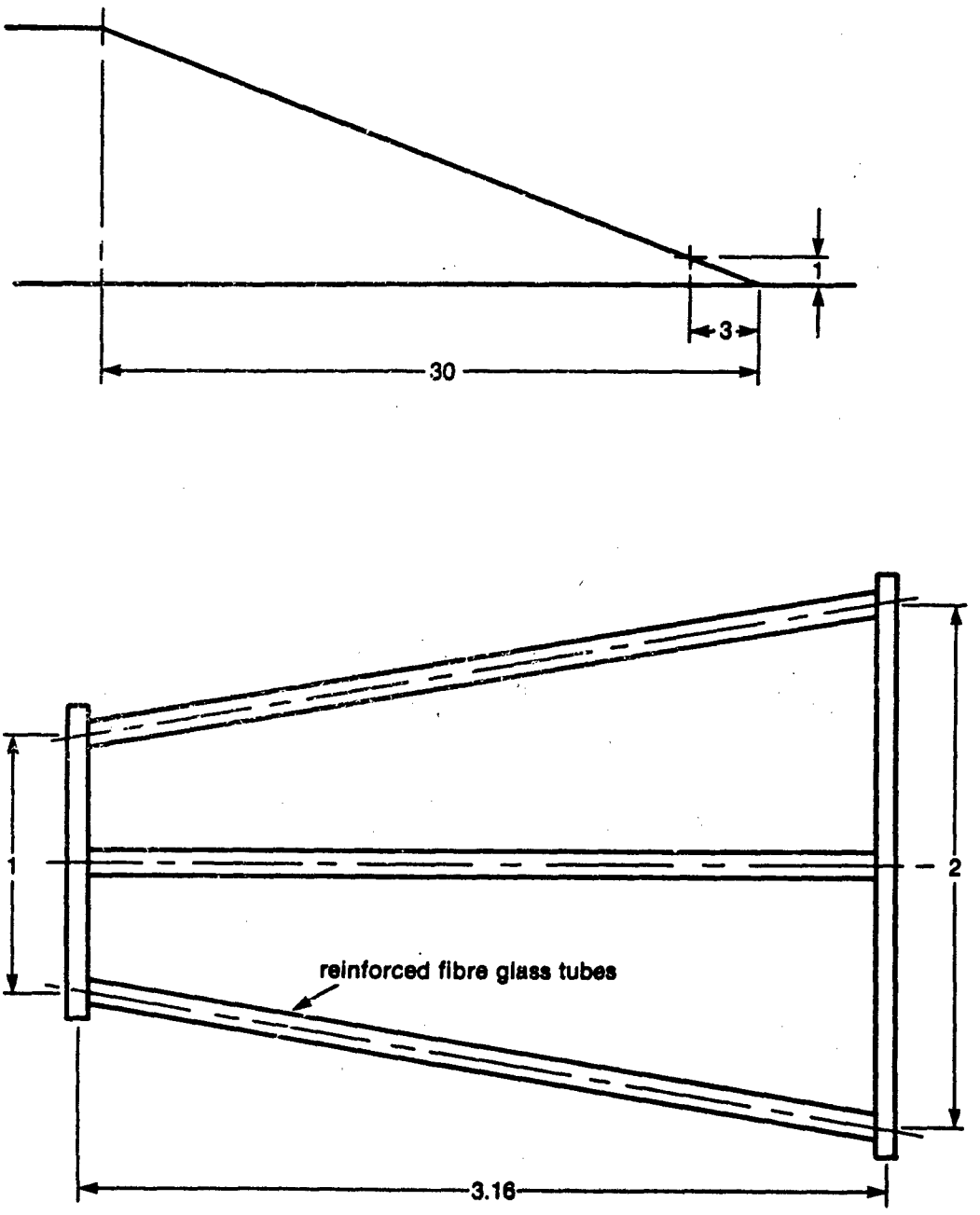

Figure 42: The place and dimensions of the terminating networks of the 10 m-line.

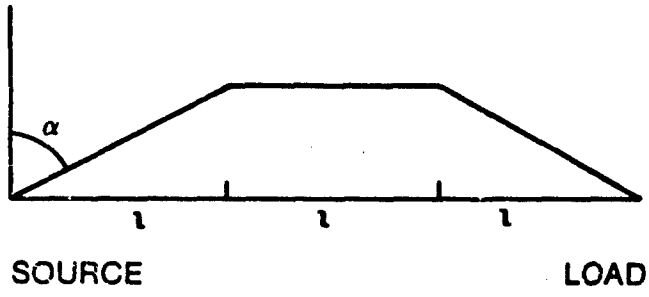

Figure A1: The parallel-plate structure.

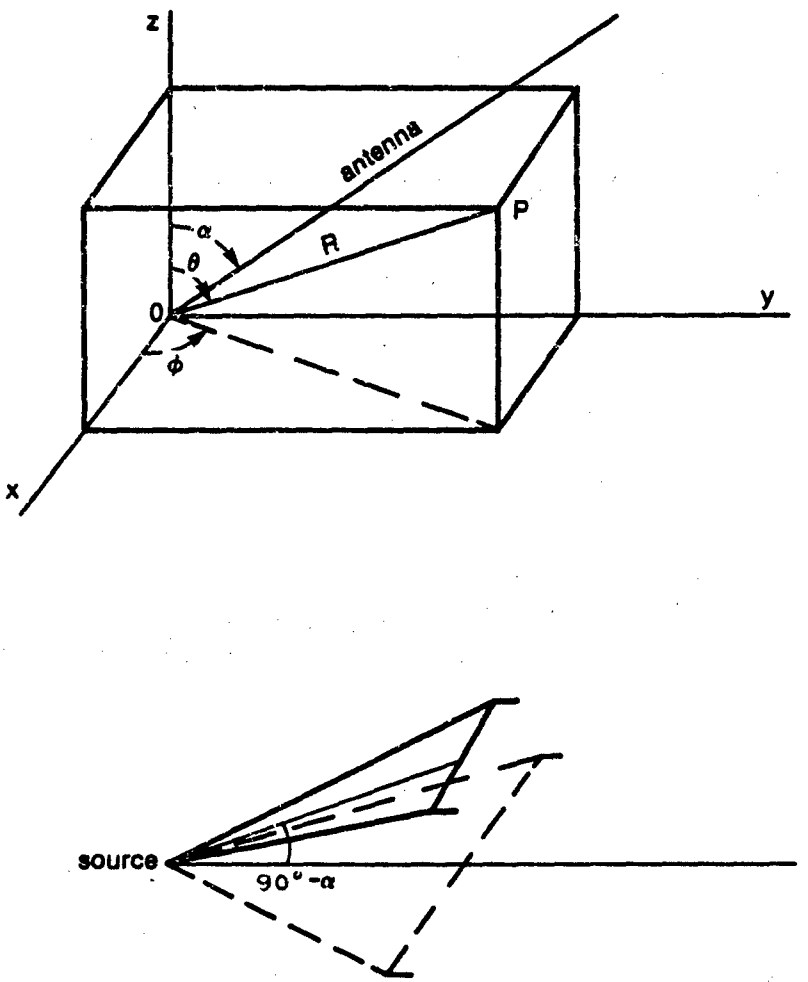

Figure A2: The co-ordinates of the observation point P.

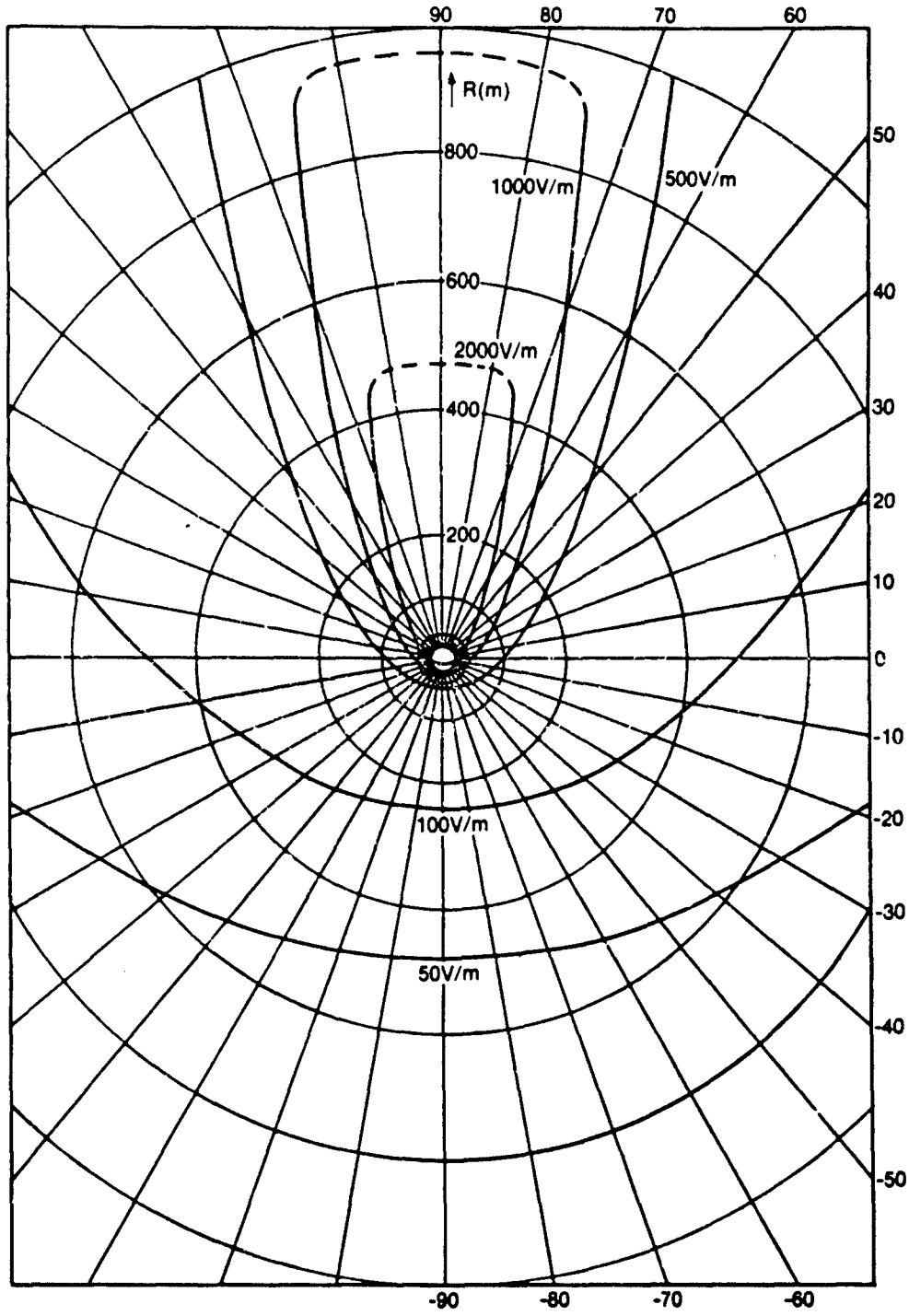

Figure A3: Field patter of E_θ from 6 m-line

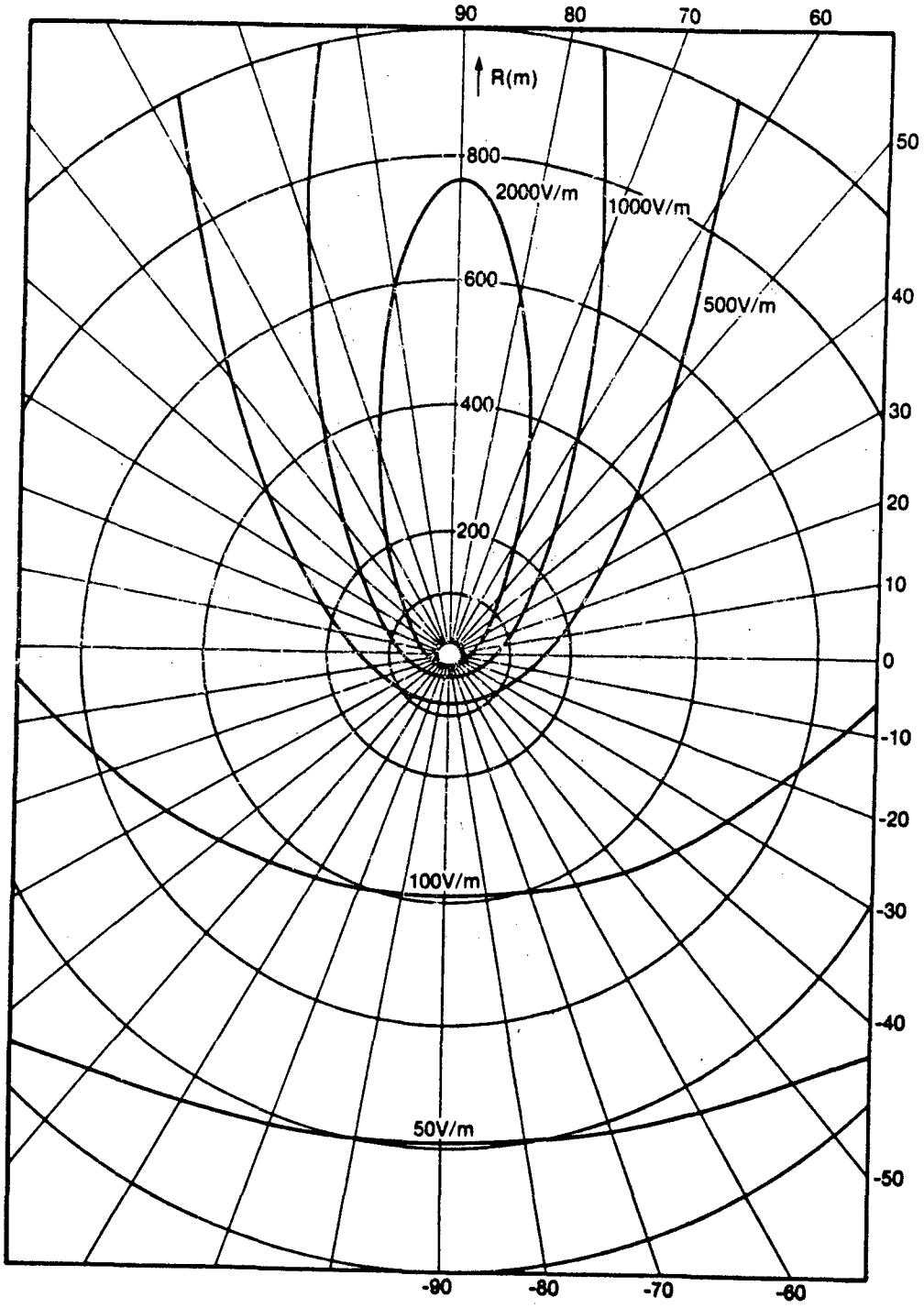

Figure A4: Field patterns of E_θ for 10 m-line

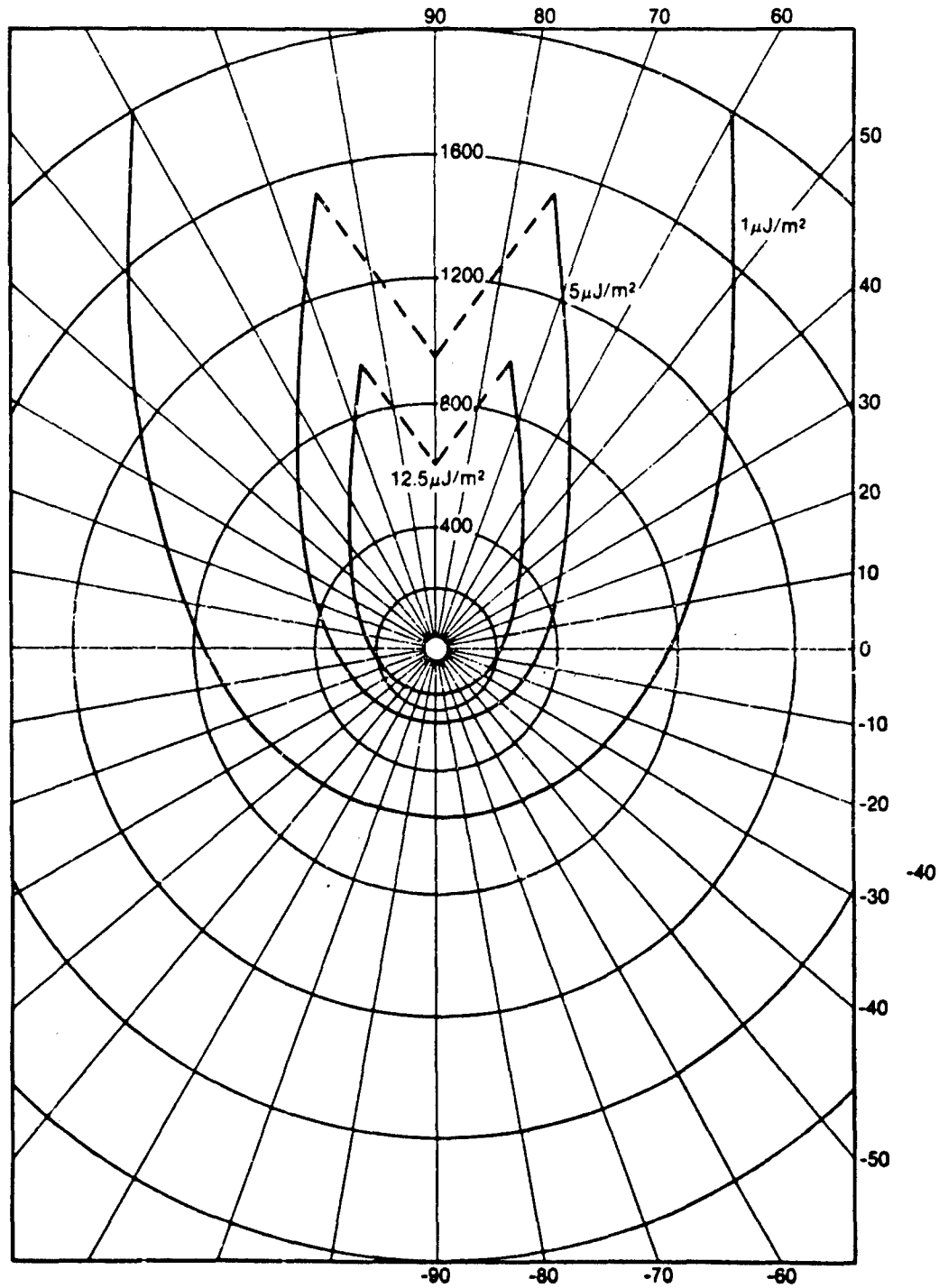

Figure A5: Energy density for
6 m-line

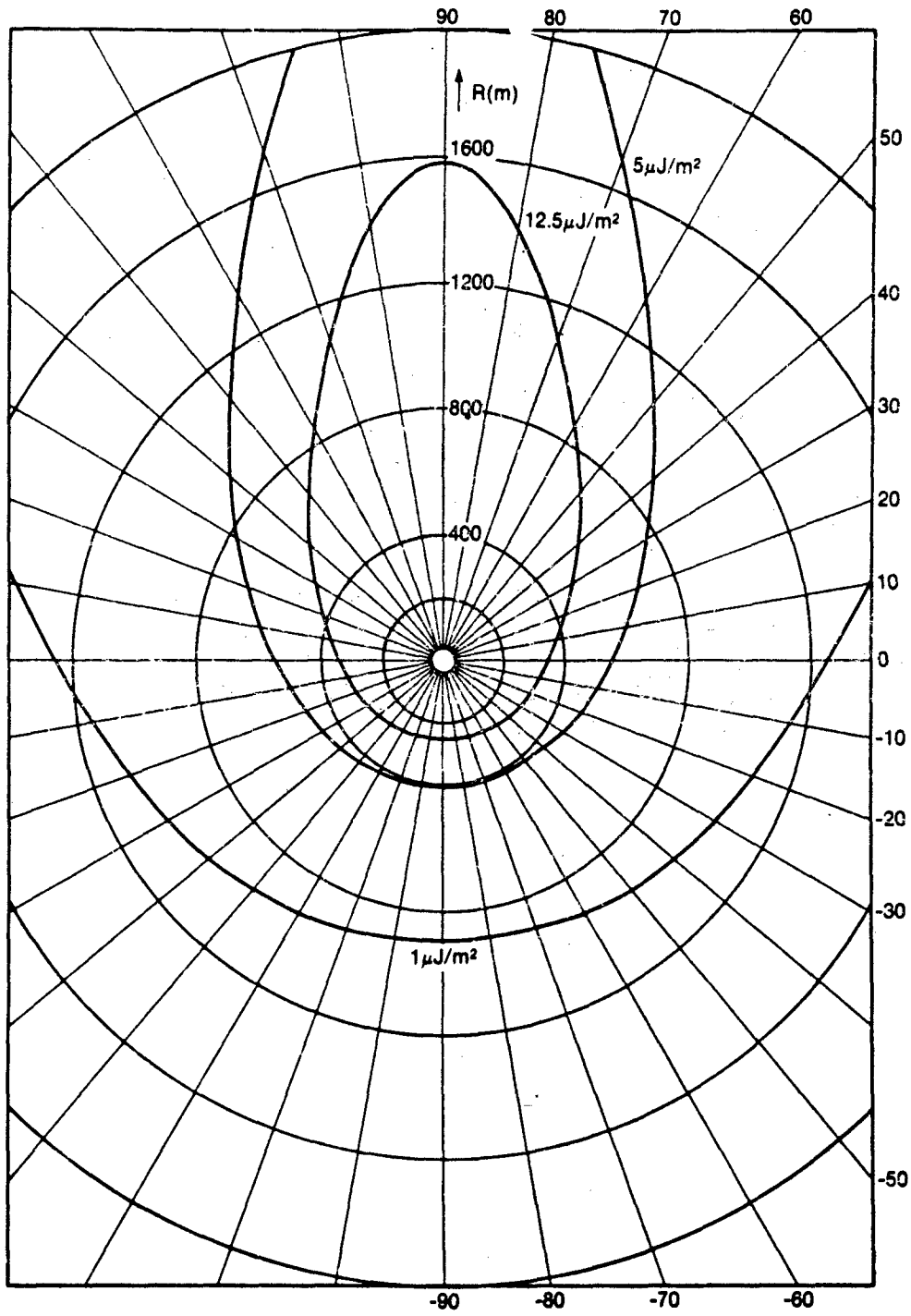

Figure A6: Energy density for 10 m-line

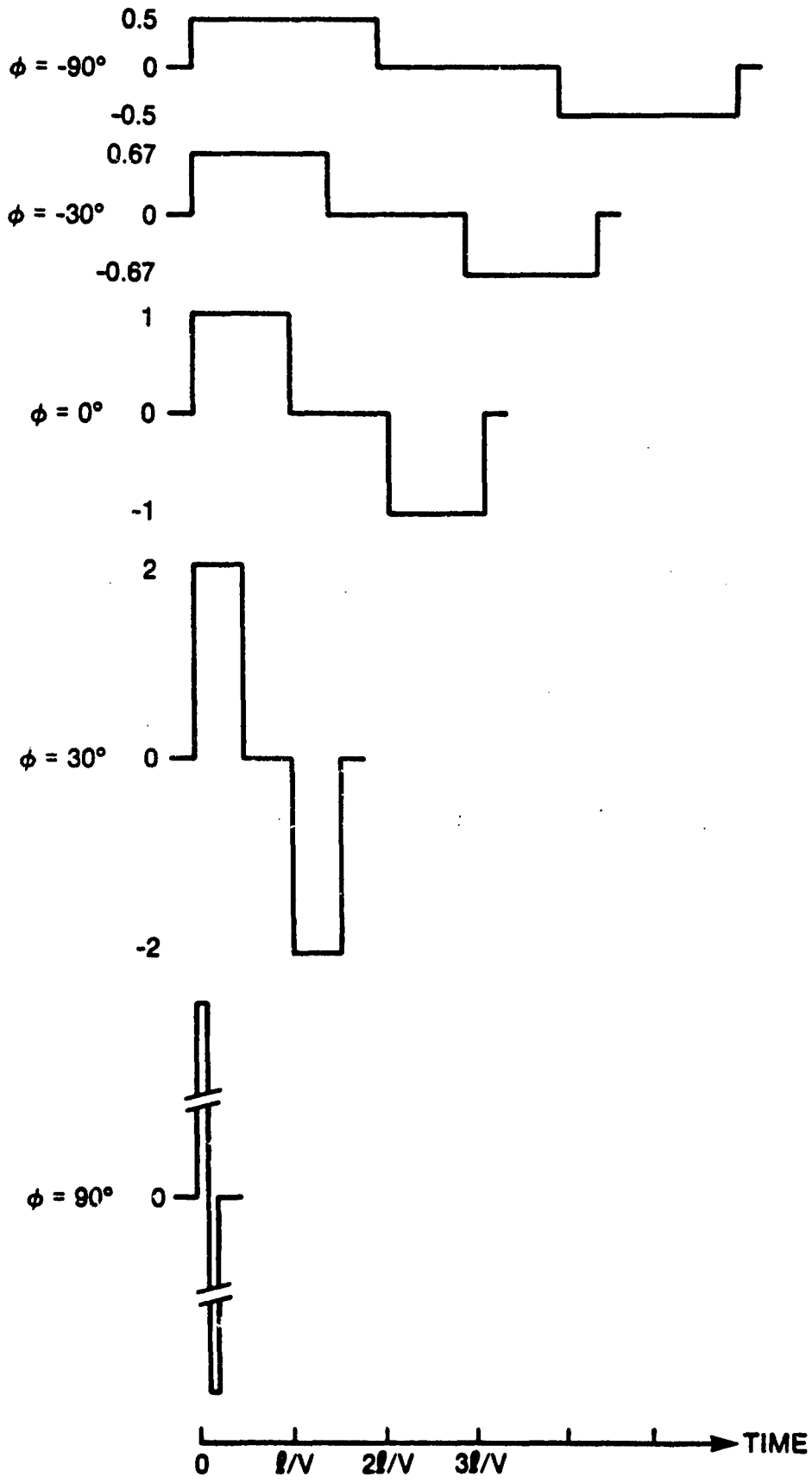

Figure A7: Timing and width of pulse versus azimuth angle ϕ.

b/a	f_g	(dif)	b/a	f_g	(dif)	b/a	f_g	(dif)
.010	0.009768		.040	0.037106		.070	0.062229	
		.000955			.000870			.000805
.011	0.010723		.041	0.037976		.071	0.063034	
		.000952			.000867			.000804
.012	0.011675		.042	0.038843		.072	0.063838	
		.000948			.000865			.000801
.013	0.012623		.043	0.039708		.073	0.064639	
		.000946			.000862			.000800
.014	0.013569		.044	0.040570		.074	0.065439	
		.000941			.000860			.000798
.015	0.014510		.045	0.041430		.075	0.066237	
		.000939			.000858			.000796
.016	0.015449		.046	0.042288		.076	0.067033	
		.000935			.000856			.000794
.017	0.016384		.047	0.043144		.077	0.067827	
		.000932			.000853			.000792
.018	0.017316		.048	0.043997		.078	0.068619	
		.000929			.000851			.000791
.019	0.018245		.049	0.044848		.079	0.069410	
		.000926			.000849			.000789
.020	0.019171		.050	0.045697		.080	0.070199	
		.000923			.000847			.000786
.021	0.020094		.051	0.046544		.081	0.070985	
		.000920			.000844			.000786
.022	0.021014		.052	0.047388		.082	0.071771	
		.000918			.000842			.000783
.023	0.021932		.053	0.048230		.083	0.072554	
		.000914			.000840			.000781
.024	0.022846		.054	0.049070		.084	0.073335	
		.000911			.000838			.000780
.025	0.023757		.055	0.049908		.085	0.074115	
		.000909			.000836			.000778
.026	0.024666		.056	0.050744		.086	0.074893	
		.000905			.000834			.000776
.027	0.025571		.057	0.051578		.087	0.075669	
		.000903			.000831			.000775
.028	0.026474		.058	0.052409		.088	0.076444	
		.000901			.000830			.000773
.029	0.027375		.059	0.053239		.089	0.077217	
		.000897			.000827			.000771
.030	0.028272		.060	0.054066		.090	0.077988	
		.000895			.000825			.000769
.031	0.029167		.061	0.054891		.091	0.078757	
		.000893			.000824			.000768
.032	0.030060		.062	0.055715		.092	0.079525	
		.000889			.000821			.000766
.033	0.030949		.063	0.056536		.093	0.080291	
		.000887			.000819			.000764
.034	0.031836		.064	0.057355		.094	0.081055	
		.000885			.000817			.000763
.035	0.032721		.065	0.058172		.095	0.081818	
		.000882			.000815			.000761
.036	0.033603		.066	0.058987		.096	0.082579	
		.000879			.000814			.000759
.037	0.034482		.067	0.059801		.097	0.083338	
		.000877			.000811			.000758
.038	0.035359		.068	0.060612		.098	0.084096	
		.000875			.000809			.000756
.039	0.036234		.069	0.061421		.099	0.084852	
		.000872			.000808			.000758

Table 1: Geometric factor f_g versus b/a = 0.01 - 0.1.

b/a	f_g	(dif)	b/a	f_g	(dif)	b/a	f_g	(dif)
0.10	0.08561		0.40	0.26207		0.70	0.38204	
		.00745			.00468			.00341
0.11	0.09306		0.41	0.26675		0.71	0.38545	
		.00731			.00462			.00338
0.12	0.10037		0.42	0.27137		0.72	0.38883	
		.00716			.00456			.00335
0.13	0.10753		0.43	0.27593		0.73	0.39218	
		.00702			.00451			.00331
0.14	0.11455		0.44	0.28044		0.74	0.39549	
		.00689			.00445			.00329
0.15	0.12144		0.45	0.28489		0.75	0.39878	
		.00676			.00441			.00326
0.16	0.12820		0.46	0.28930		0.76	0.40204	
		.00663			.00435			.00323
0.17	0.13483		0.47	0.29365		0.77	0.40527	
		.00653			.00431			.00320
0.18	0.14136		0.48	0.29796		0.78	0.40847	
		.00641			.00425			.00318
0.19	0.14777		0.49	0.30221		0.79	0.41165	
		.00630			.00421			.00314
0.20	0.15407		0.50	0.30642		0.80	0.41479	
		.00619			.00417			.00313
0.21	0.16026		0.51	0.31059		0.81	0.41792	
		.00610			.00411			.00309
0.22	0.16636		0.52	0.31470		0.82	0.42101	
		.00600			.00408			.00307
0.23	0.17236		0.53	0.31878		0.83	0.42408	
		.00591			.00403			.00304
0.24	0.17827		0.54	0.32281		0.84	0.42712	
		.00581			.00399			.00302
0.25	0.18408		0.55	0.32680		0.85	0.43014	
		.00573			.00394			.00299
0.26	0.18981		0.56	0.33074		0.86	0.43313	
		.00564			.00391			.00297
0.27	0.19545		0.57	0.33465		0.87	0.43610	
		.00556			.00386			.00295
0.28	0.20101		0.58	0.33851		0.88	0.43905	
		.00548			.00383			.00292
0.29	0.20649		0.59	0.34234		0.89	0.44197	
		.00540			.00379			.00290
0.30	0.21189		0.60	0.34613		0.90	0.44487	
		.00532			.00375			.00287
0.31	0.21721		0.61	0.34988		0.91	0.44774	
		.00526			.00371			.00285
0.32	0.22247		0.62	0.35359		0.92	0.45059	
		.00518			.00368			.00283
0.33	0.22765		0.63	0.35727		0.93	0.45342	
		.00511			.00364			.00281
0.34	0.23276		0.64	0.36091		0.94	0.45623	
		.00505			.00361			.00279
0.35	0.23781		0.65	0.36452		0.95	0.45902	
		.00497			.00357			.00276
0.36	0.24278		0.66	0.36809		0.96	0.46178	
		.00492			.00354			.00275
0.37	0.24770		0.67	0.37163		0.97	0.46453	
		.00485			.00350			.00272
0.38	0.25255		0.68	0.37513		0.98	0.46725	
		.00479			.00347			.00271
0.39	0.25734		0.69	0.37860		0.99	0.46996	
		.00473			.00344			.00268

Table 2: Geometric factor f_g versus b/a = 0.1 - 1.0.

b/a	f_g	(dif)	b/a	f_g	(dif)	b/a	f_g	(dif)
1.00	0.47264	.01312	2.50	0.73901	.00608	4.00	0.88498	.00390
1.05	0.48576	.01266	2.55	0.74509	.00596	4.05	0.88888	.00385
1.10	0.49842	.01222	2.60	0.75105	.00586	4.10	0.89273	.00380
1.15	0.51064	.01181	2.65	0.75691	.00576	4.15	0.89653	.00376
1.20	0.52245	.01143	2.70	0.76267	.00566	4.20	0.90029	.00372
1.25	0.53388	.01107	2.75	0.76833	.00556	4.25	0.90401	.00367
1.30	0.54495	.01073	2.80	0.77389	.00547	4.30	0.90768	.00363
1.35	0.55568	.01041	2.85	0.77936	.00538	4.35	0.91131	.00359
1.40	0.56609	.01010	2.90	0.78474	.00530	4.40	0.91490	.00356
1.45	0.57619	.00982	2.95	0.79004	.00521	4.45	0.91846	.00351
1.50	0.58601	.00954	3.00	0.79525	.00512	4.50	0.92197	.00347
1.55	0.59555	.00928	3.05	0.80037	.00505	4.55	0.92544	.00344
1.60	0.60483	.00904	3.10	0.80542	.00497	4.60	0.92888	.00341
1.65	0.61387	.00880	3.15	0.81039	.00490	4.65	0.93229	.00336
1.70	0.62267	.00859	3.20	0.81529	.00482	4.70	0.93565	.00333
1.75	0.63126	.00836	3.25	0.82011	.00475	4.75	0.93898	.00330
1.80	0.63962	.00817	3.30	0.82486	.00469	4.80	0.94228	.00327
1.85	0.64779	.00797	3.35	0.82955	.00461	4.85	0.94555	.00323
1.90	0.65576	.00779	3.40	0.83416	.00456	4.90	0.94878	.00320
1.95	0.66355	.00761	3.45	0.83872	.00449	4.95	0.95198	.00316
2.00	0.67116	.00745	3.50	0.84321	.00443	5.00	0.95514	.00314
2.05	0.67861	.00728	3.55	0.84764	.00436	5.05	0.95828	.00311
2.10	0.68589	.00712	3.60	0.85200	.00431	5.10	0.96139	.00307
2.15	0.69301	.00698	3.65	0.85631	.00426	5.15	0.96446	.00305
2.20	0.69999	.00683	3.70	0.86057	.00420	5.20	0.96751	.00302
2.25	0.70682	.00669	3.75	0.86477	.00414	5.25	0.97053	.00299
2.30	0.71351	.00656	3.80	0.86891	.00410	5.30	0.97352	.00296
2.35	0.72007	.00643	3.85	0.87301	.00404	5.35	0.97648	.00294
2.40	0.72650	.00632	3.90	0.87705	.00399	5.40	0.97942	.00291
2.45	0.73282	.00619	3.95	0.88104	.00394	5.45	0.98233	.00287

Table 3: Geometric factor f_g versus b/a = 1.0 - 5.5.

b/a	f_g	(dif)	b/a	f_g	(dif)	b/a	f_g	(dif)
5.50	0.9852		7.00	1.0615		8.50	1.1230	
		.0029			.0022			.0019
5.55	0.9881		7.05	1.0637		8.55	1.1249	
		.0028			.0023			.0018
5.60	0.9909		7.10	1.0660		8.60	1.1267	
		.0028			.0022			.0019
5.65	0.9937		7.15	1.0682		8.65	1.1286	
		.0028			.0022			.0018
5.70	0.9965		7.20	1.0704		8.70	1.1304	
		.0028			.0022			.0018
5.75	0.9993		7.25	1.0726		8.75	1.1322	
		.0027			.0022			.0018
5.80	1.0020		7.30	1.0748		8.80	1.1340	
		.0027			.0021			.0018
5.85	1.0047		7.35	1.0769		8.85	1.1358	
		.0027			.0022			.0018
5.90	1.0074		7.40	1.0791		8.90	1.1376	
		.0027			.0021			.0018
5.95	1.0101		7.45	1.0812		8.95	1.1394	
		.0026			.0021			.0018
6.00	1.0127		7.50	1.0833		9.00	1.1412	
		.0026			.0021			.0017
6.05	1.0153		7.55	1.0854		9.05	1.1429	
		.0026			.0021			.0018
6.10	1.0179		7.60	1.0875		9.10	1.1447	
		.0026			.0021			.0017
6.15	1.0205		7.65	1.0896		9.15	1.1464	
		.0026			.0021			.0017
6.20	1.0231		7.70	1.0917		9.20	1.1481	
		.0025			.0020			.0018
6.25	1.0256		7.75	1.0937		9.25	1.1499	
		.0025			.0021			.0017
6.30	1.0281		7.80	1.0958		9.30	1.1516	
		.0025			.0020			.0017
6.35	1.0306		7.85	1.0978		9.35	1.1533	
		.0025			.0020			.0017
6.40	1.0331		7.90	1.0998		9.40	1.1550	
		.0025			.0020			.0016
6.45	1.0356		7.95	1.1018		9.45	1.1566	
		.0024			.0020			.0017
6.50	1.0380		8.00	1.1038		9.50	1.1583	
		.0024			.0020			.0017
6.55	1.0404		8.05	1.1058		9.55	1.1600	
		.0025			.0019			.0016
6.60	1.0429		8.10	1.1077		9.60	1.1616	
		.0023			.0020			.0017
6.65	1.0452		8.15	1.1097		9.65	1.1633	
		.0024			.0019			.0016
6.70	1.0476		8.20	1.1116		9.70	1.1649	
		.0024			.0020			.0017
6.75	1.0500		8.25	1.1136		9.75	1.1666	
		.0023			.0019			.0016
6.80	1.0523		8.30	1.1155		9.80	1.1682	
		.0023			.0019			.0016
6.85	1.0546		8.35	1.1174		9.85	1.1698	
		.0023			.0019			.0016
6.90	1.0569		8.40	1.1193		9.90	1.1714	
		.0023			.0019			.0016
6.95	1.0592		8.45	1.1212		9.95	1.1730	
		.0023			.0018			.0016

Table 4: Geometric factor f_g versus b/a = 5.5 - 10

b/a	f_g	(dif)	b/a	f_g	(dif)	b/a	f_g	(dif)
10.0	1.1746		40.0	1.6155		70.0	1.7936	
		.0303			.0079			.0045
11.0	1.2049		41.0	1.6234		71.0	1.7981	
		.0276			.0076			.0045
12.0	1.2325		42.0	1.6310		72.0	1.8026	
		.0255			.0075			.0044
13.0	1.2580		43.0	1.6385		73.0	1.8070	
		.0235			.0073			.0043
14.0	1.2815		44.0	1.6458		74.0	1.8113	
		.0219			.0072			.0043
15.0	1.3034		45.0	1.6530		75.0	1.8156	
		.0206			.0070			.0042
16.0	1.3240		46.0	1.6600		76.0	1.8198	
		.0192			.0068			.0042
17.0	1.3432		47.0	1.6668		77.0	1.8240	
		.0182			.0067			.0041
18.0	1.3614		48.0	1.6735		78.0	1.8281	
		.0172			.0066			.0040
19.0	1.3786		49.0	1.6801		79.0	1.8321	
		.0163			.0064			.0040
20.0	1.3949		50.0	1.6865		80.0	1.8361	
		.0156			.0063			.0040
21.0	1.4105		51.0	1.6928		81.0	1.8401	
		.0148			.0062			.0039
22.0	1.4253		52.0	1.6990		82.0	1.8440	
		.0141			.0061			.0038
23.0	1.4394		53.0	1.7051		83.0	1.8478	
		.0135			.0059			.0038
24.0	1.4529		54.0	1.7110		84.0	1.8516	
		.0130			.0059			.0038
25.0	1.4659		55.0	1.7169		85.0	1.8554	
		.0125			.0057			.0037
26.0	1.4784		56.0	1.7226		86.0	1.8591	
		.0120			.0055			.0037
27.0	1.4904		57.0	1.7282		87.0	1.8628	
		.0116			.0056			.0037
28.0	1.5020		58.0	1.7338		88.0	1.8665	
		.0112			.0054			.0036
29.0	1.5132		59.0	1.7392		89.0	1.8701	
		.0107			.0054			.0035
30.0	1.5239		60.0	1.7446		90.0	1.8736	
		.0105			.0052			.0035
31.0	1.5344		61.0	1.7498		91.0	1.8771	
		.0101			.0052			.0035
32.0	1.5445		62.0	1.7550		92.0	1.8806	
		.0098			.0051			.0034
33.0	1.5543		63.0	1.7601		93.0	1.8840	
		.0095			.0050			.0035
34.0	1.5638		64.0	1.7651		94.0	1.8875	
		.0092			.0049			.0033
35.0	1.5730		65.0	1.7700		95.0	1.8908	
		.0090			.0049			.0034
36.0	1.5820		66.0	1.7749		96.0	1.8942	
		.0087			.0048			.0033
37.0	1.5907		67.0	1.7797		97.0	1.8975	
		.0085			.0047			.0032
38.0	1.5992		68.0	1.7844		98.0	1.9007	
		.0082			.0046			.0032
39.0	1.6074		69.0	1.7890		99.0	1.9039	
		.0081			.0046			

Table 5: Geometric factor f_g versus b/a = 10 - 100.

TABLE 6

h (m)	r/h	f	E_f (kV/cm)	E_e (kV/cm)
6	$6.7 \cdot 10^{-4}$	22	0.75	16.5
5	$8 \cdot 10^{-4}$	20	0.9	18
4	$1 \cdot 10^{-4}$	18	1.13	20.3
3	$1.3 \cdot 10^{-3}$	15.5	1.5	23.3
2	$2 \cdot 10^{-3}$	12.5	2.25	28.1
1	$4 \cdot 10^{-3}$	9	4.5	40.5

Table 6: The edge enhanced field E_e of the taper (wire radius r = 4 mm).

TABLE 7

h (m)	E_f (kV/cm)	r/h	f	E_e (kV/cm)	s (cm)	d/s	f	E_w (kV/cm)
6	0.75	$8.33 \cdot 10^{-3}$	6.2	4.65	40	$2 \cdot 10^{-2}$	17	12.75
5	0.9	$1 \cdot 10^{-2}$	5.6	5.04	33.3	$2.4 \cdot 10^{-2}$	14	12.6
4	1.13	$1.25 \cdot 10^{-2}$	5.2	5.88	26.7	$3 \cdot 10^{-2}$	11.5	13
3	1.5	$1.67 \cdot 10^{-2}$	4.6	6.9	20	$4 \cdot 10^{-2}$	9	13.5
2	2.25	$2.5 \cdot 10^{-2}$	3.9	8.8	13.3	$6 \cdot 10^{-2}$	6.3	14.2
1	4.5	$5 \cdot 10^{-2}$	2.9	13	6.67	$12 \cdot 10^{-2}$	3.8	17.1

Table 7. Enhanced field at the edge E_e and between the wires E_w (edge radius is 5 cm, wire radius is 4 mm).

TABLE 8

height h(m)	spacing s(cm)	a(m)	Δh(cm)	h'(m)	h'/a	f_g	$Z_l(\Omega)$	correction Δb(cm)
6	40	5	17.6	6.352	1.27	0.5383	101.5	-
5	33.3	4.17	13.7	5.274	1.265	0.5372	101.26	2.0
4	26.7	3.33	10	4.2	1.26	0.5361	101.05	3.2
3	20	2.5	6.6	3.132	1.253	0.5345	100.7	4.1
2	13.3	1.67	3.53	2.07	1.24	0.5316	100.2	4.8
1	6.67	0.83	1.04	1.02	1.23	0.5293	99.8	3.2 + 1*

Table 8. Correction of the taper height for constant impedance $Z_l = 101.5\ \Omega$ (*dependent on wire-wiremesh-solid parts) of the 6m-line.

TABLE 9

h (m)	E_f (kV/cm)	r/h	f	E_e (kV/cm)	s (cm)	d/s	f	E_w (kV/cm)
10	0.5	$1.5 \cdot 10^{-4}$	46	23	50	$6 \cdot 10^{-3}$	55	27.5
8	0.625	$1.88 \cdot 10^{-4}$	41	25.6	40	$7.5 \cdot 10^{-3}$	44	27.5
6	0.833	$2.5 \cdot 10^{-4}$	36	30	30	$1 \cdot 10^{-2}$	33	27.5
4	1.25	$3.75 \cdot 10^{-4}$	29	36	20	$1.5 \cdot 10^{-2}$	22	27.5
2	2.5	$7.5 \cdot 10^{-4}$	21	53	10	$3 \cdot 10^{-2}$	11.5	28.8
1	5.0	$1.5 \cdot 10^{-3}$	14.5	73	5	$6 \cdot 10^{-2}$	6.3	31.5

Table 9. Enhanced field E_e at the edge and E_w between the wires of the 10m-line.

TABLE 10

h (m)	s (cm)	Δh (cm)	h' (m)	a (m)	a' (m)	h'/a'	f_g	Z_l (Ω)	correction (cm)
10	50	31.6	10.32	10	10	1.032	0.481	90.67	-
8	40	23.9	8.24	8	8	1.03			1.6
6	30	16.5	6.17	6	6	1.028			2.3
4	20	9.7	4.10	4	4.005	1.024			3.1
2	10	3.76	2.04	2	2.01	1.015			3.3
1	5	1.33	1.01	1	1.015	0.995			3.7

Table 10. Correction of height of the taper for constant Z_l = 90.7 Ω of the 10m-line.

Table 11

Specifications	6m-line	10m-line
dimensions l × w × h	90 × 10 × 6 m	90 × 20 × 10 m
working volume	(15-30) × 10 × 3 m^3	(15-30) × 20 × 5 m^3
ground plate	wires, w = 20 m	wire mesh, 20 m
line impedance	101.5 Ω + 14 Ω	90.7 Ω + 24 Ω
rise time	elevation 2 ns azimuth 1.4 ns	5.4 ns 5.4 ns
field magnitude	75 kV/m	25-50 kV/m
field distortion field variation	50%	50%
field uniformity field orientation	fig. 16	fig. 14

Table 11. Summary of the specifications of the 6m and 10m line.

TABLE A1

	6m-line		10m-line	
angle ϕ (°)	G	Δt(ns)	G	Δt(ns)
-90	0.5	198	0.51	195
-75			0.522	192
-60	0.54	185	0.55	182
-45			0.6	167
-30	0.67	149	0.68	147
-15			0.8	125
0	1	100	1	100
15	1.34	74.6	1.33	75
30	1.96	51	1.9	53
50	4.02	24.9	3.66	27.3
60	6.63	15.1	5.6	17.8
65	8.99	11.1		
70	12.7	7.9	9.23	10.8
75	18.9	5.3	12	8.34
80	19.6	3.4	15.3	6.6
85			18.3	5.47
90	19.6	1.9	19.6	5.1

Table A1. The gain factor G and pulse width Δt for the 6m and 10m line with rise time t_r = 2 ns and 5.4 ns respectively

DOCUMENT CONTROL DATA

(Security classification of title, body of abstract and indexing annotation must be entered when the overall document is classified)

1. ORIGINATOR (the name and address of the organization preparing the document. Organizations for whom the document was prepared, e.g. Establishment sponsoring a contractor's report, or tasking agency, are entered in section 8.)

Defence Research Establishment Ottawa
Ottawa, Ontario
Canada, K1A 0R8

2. SECURITY CLASSIFICATION (overall security classification of the document. including special warning terms if applicable)

UNCLASSIFIED

3. TITLE (the complete document title as indicated on the title page. Its classification should be indicated by the appropriate abbreviation (S,C,R or U) in parentheses after the title.)

Design of a Bounded Wave EMP Simulator (U)

4. AUTHORS (Last name, first name, middle initial)

P.A.A. Sevat

5. DATE OF PUBLICATION (month and year of publication of document)

January 1989

6a. NO. OF PAGES (total containing information. Include Annexes, Appendices, etc.)

98

6b. NO. OF REFS (total cited in document)

22

7. DESCRIPTIVE NOTES (the category of the document, e.g. technical report, technical note or memorandum. If appropriate, enter the type of report, e.g. interim, progress, summary, annual or final. Give the inclusive dates when a specific reporting period is covered.)

DREO REPORT

8. SPONSORING ACTIVITY (the name of the department project office or laboratory sponsoring the research and development. Include the address.)

9a. PROJECT OR GRANT NO. (if appropriate, the applicable research and development project or grant number under which the document was written. Please specify whether project or grant)

041LT

9b. CONTRACT NO. (if appropriate, the applicable number under which the document was written)

10a. ORIGINATOR'S DOCUMENT NUMBER (the official document number by which the document is identified by the originating activity. This number must be unique to this document.)

10b. OTHER DOCUMENT NOS. (Any other numbers which may be assigned this document either by the originator or by the sponsor)

11. DOCUMENT AVAILABILITY (any limitations on further dissemination of the document, other than those imposed by security classification)

(X) Unlimited distribution
( ) Distribution limited to defence departments and defence contractors; further distribution only as approved
( ) Distribution limited to defence departments and Canadian defence contractors; further distribution only as approved
( ) Distribution limited to government departments and agencies; further distribution only as approved
( ) Distribution limited to defence departments; further distribution only as approved
( ) Other (please specify):

12. DOCUMENT ANNOUNCEMENT (any limitation to the bibliographic announcement of this document. This will normally correspond to the Document Availability (11). However, where further distribution (beyond the audience specified in 11) is possible, a wider announcement audience may be selected.)

FULL UNLIMITED ANNOUNCEMENT

UNCLASSIFIED

SECURITY CLASSIFICATION OF FORM

13. ABSTRACT (a brief and factual summary of the document. It may also appear elsewhere in the body of the document itself. It is highly desirable that the abstract of classified documents be unclassified. Each paragraph of the abstract shall begin with an indication of the security classification of the information in the paragraph (unless the document itself is unclassified) represented as (S), (C), (R), or (U). It is not necessary to include here abstracts in both offical languages unless the text is bilingual).

This report is concerned with the design of a bounded wave Electromagnetic Pulse (EMP) simulator. Different types of simulators are described and their pros and cons are discussed. A detailed design is given for a wire grid parallel plate type simulator. The fields inside the simulator as well as the radiated fields around the simulator are also computed.

14. KEYWORDS, DESCRIPTORS or IDENTIFIERS (technically meaningful terms or short phrases that characterize a document and could be helpful in cataloguing the document. They should be selected so that no security classification is required. Identifiers, such as equipment model designation, trade name, military project code name, geographic location may also be included. If possible keywords should be selected from a published thesaurus, e.g. Thesaurus of Engineering and Scientific Terms (TEST) and that thesaurus-identified. If it is not possible to select indexing terms which are Unclassified, the classification of each should be indicated as with the title.)

Electromagnetic Pulse
Simulator
Parallel Plate
Electromagnetic Fields

UNCLASSIFIED

SECURITY CLASSIFICATION OF FORM